Title
Spontaneous emission and optical control of spins in quantum dots

Permalink
https://escholarship.org/uc/item/5sq9f9fp

Author
Economou, Sophia E.

Publication Date
2006

Peer reviewed|Thesis/dissertation

UNIVERSITY OF CALIFORNIA, SAN DIEGO

Spontaneous Emission and Optical Control of Spins in Quantum Dots

A dissertation submitted in partial satisfaction of the

requirements for the degree Doctor of Philosophy

in

Physics

by

Sophia E. Economou

Committee in charge:

> Professor Lu J. Sham, Chair
> Professor Massimiliano Di Ventra
> Professor John M. Goodkind
> Professor David A. Meyer
> Professor George C. Papen

2006

The dissertation of Sophia E. Economou is approved, and it is acceptable in quality and form for publication on microfilm:

_____

_____

_____

_____

_____
Chair

University of California, San Diego

2006

To my Parents

TABLE OF CONTENTS

LIST OF FIGURES

ACKNOWLEDGEMENTS

grateful to both Stefanos Trachanas and Nikos Papanicolaou for introducing me to the transitionless hyperbolic secant pulses, which form the basis of the work presented in Chapter VII.

I would also like to thank Professor Peter Lambropoulos for the great Advanced Quantum Mechanics course he gave during my last months in the University of Crete and for his willingness to answer my Quantum Optics questions in lengthy emails.

I cannot thank enough my father for teaching me a great deal of the physics I know, for passing on to me his enthusiasm for clarity in explanation and understanding of physics, and for his subtle balance of approval and expectations.

The text of Chapters V and VI is in part a reprint of the material as it appears in Sophia E. Economou, Ren-Bao Liu, L. J. Sham, and D. G. Steel, "Unified theory of consequences of spontaneous emission in a Lambda system," Phys. Rev. B 71, 195327 (2005). "Copyright (2005) by the American Physical Society." The dissertation author was the primary researcher and author and the co-authors listed in this publication, directed and supervised the research which forms the basis for this chapter. The text of Chapter V. is in part a reprint of the material as it appears in M. V. Gurudev Dutt, Jun Cheng, Bo Li, Xiaodong Xu, Xiaoqin Li, P. R. Berman, D. G. Steel, A. S. Bracker, D. Gammon, Sophia E. Economou, Ren-Bao Liu, and L. J. Sham, "Stimulated and Spontaneous Optical Generation of Electron Spin Coherence in Charged GaAs Quantum Dots," Phys. Rev. Lett. 94, 227403 (2005). "Copyright (2005) by the American Physical Society." The dissertation author was a coauthor listed in this publication.

VITA

2000	B.S. in Physics University of Crete, Iraklion, Crete, Greece
2000–2001	Teaching Assistant, Department of Physics, University of Crete, Greece
2001–2002	Teaching Assistant, Department of Physics, University of California, San Diego
2002–2006	Research Assistant, Department of Physics, University of California, San Diego
2006	Ph.D. in Physics University of California, San Diego

PUBLICATIONS

M. V. Gurudev Dutt, Jun Cheng, Bo Li, Xiaodong Xu, Xiaoqin Li, P. R. Berman, D. G. Steel, A. S. Bracker, D. Gammon, Sophia E. Economou, Ren-Bao Liu, and L. J. Sham, "Stimulated and Spontaneous Optical Generation of Electron Spin Coherence in Charged GaAs Quantum Dots," Phys. Rev. Lett. 94, 227403 (2005)

Sophia E. Economou, Ren-Bao Liu, L. J. Sham, and D. G. Steel, "Unified theory of consequences of spontaneous emission in a Lambda system," Phys. Rev. B 71, 195327 (2005)

Sophia E. Economou, Renbao Liu, L. J. Sham, "Theory of spontaneously generated spin coherence in nanodots", Quantum Electronics and Laser Science Conference 2005, Vol. 1, P. 258-259.

Sophia E. Economou, L. J. Sham, Yanwen Wu, and D. G. Steel, "Theory proposal of electron spin rotation in a quantum dot", Quantum Electronics and Laser Science Conference 2006, to be published.

ABSTRACT OF THE DISSERTATION

Spontaneous Emission and Optical Control of Spins in Quantum Dots

by

Sophia E. Economou

Doctor of Philosophy in Physics

University of California, San Diego, 2006

Professor Lu J. Sham, Chair

Quantum dots are attractive due to their potential technological applications and the opportunity they provide for study of fundamental physics in the mesoscopic scale. This dissertation studies optically controlled spins in quantum dots in connection to quantum information processing.

The physical realization of the quantum bit (qubit) consists of the two spin states of an extra electron confined in a quantum dot. Spin rotations are performed optically, by use of an intermediate charged exciton (trion) state. The two spin states and the trion form a Λ-type system. The merits of this system

for quantum information processing include integrability into a solid-state device, long spin coherence time, and fast and focused optical control.

In this dissertation, we study the optical decay mechanisms of the trion state in the quantum dot. Using a master-equation approach, we derive microscopically the optical decay of the three-level system and find a novel term, the so-called spontaneously generated coherence (SGC). The latter, though predicted more than a decade ago for atomic Λ-systems satisfying certain conditions, had not been detected yet in any system. We found that in quantum dots, these conditions can be satisfied. We present the experiment which, in collaboration with our theory, constituted the first measurement of SGC.

We establish the unification of SGC, polarization entanglement, and two-pathway decay. By keeping track of the spontaneously emitted photon dynamics, we find the conditions on the couplings that determine which effect will take place. We have thus placed SGC in a more quantum informational framework, characterizing it as lack of entanglement between the emitted photon and the three-level system.

We develop a theory of ultrafast optical single-qubit rotations by use of 2π pulses, which have the two-fold advantage of minimal trion excitation and negligible spin precession. The analytically solvable hyperbolic secant pulses of Rosen and Zener for the two-level system are investigated in the context of the three-level system. Ultrafast rotations about the quantum dot growth direction are designed, the angle of spin rotation is expressed analytically, and the fidelity is studied by simulations. Adaptive feedback loops are employed to correct for unintended dynamics.

I.

Introduction

Quantum dots (QDs) are semiconductor nanostructures ranging in size from several nanometers to about 100 nanometers and grown on a substrate of different semiconductor material. Their formation is due to lattice mismatch between the two semiconductors, or due to fluctuations of quantum wells, or it is achieved via gates on a quantum well. QDs confine electrons and holes in all three-dimensions owing to their small direct band gap compared to the host material. Due to the confinement, they have sharp, atomic-like energy levels and so they are sometimes termed artificial atoms. However, quite contrary to atoms, the particles in a quantum-dot are subject to the potential created by a large number of atoms. An extra electron in the QD is subject to the periodic crystal potential of the bulk semiconductor plus the confining potential of the QD. Since the characteristic length scale of the latter is much larger than the lattice constant of the crystal, we can still use concepts like the effective mass and the band structure, including valence and conduction bands; however, due to the confining QD potential the boundary conditions are strongly altered and the properties of the quantum dot strongly depend on its geometry. As a result, the continuous bands of the bulk become quantized. It must be stressed that the concept of effective mass of an extra electron added to the ground state of an insulator or semiconductor and moving under the action of a slowly varying external potential (such as the one

due to the quantum dot) is valid not only within the independent-particle approximation, but in the presence of the many body interactions as well [71, 125]. To incorporate both the underlying semiconductor characteristics and the quantum dot geometry, the so-called envelope function method is employed. The main idea is that the wavefunction of the trapped particle can be decomposed into a product of an envelope, with a characteristic length comparable to the dot dimensions, and a Bloch function, originating from the semiconductor nature of the structure. This will be further explained in Chapter II.

As was mentioned before, the quantum dot semiconductor material has a smaller band gap than the host material, so that it is energetically favorable for the electrons and holes in addition to the electrons in the ground state to be confined in the dot. To calculate analytically the electronic structure of QDs we use the effective masses of the trapped particles, as determined in the bulk, and model the dot potential by a simple harmonic oscillator or a particle-in-a-box. Then, Coulomb corrections are taken into account, i.e. direct repulsion (attraction) between electron and electron (hole), and exchange interaction. With the electronic structure available, either from theoretical calculations or from experimental data, one can study the dynamics of the electrons in the dots.

Quantum dots are interesting, both due to their potential technological applications and due to the opportunity they open up for studying fundamental physics in the mesoscopic scale, in man-made materials. Among their suggested applications, quantum dots play a prominent role as candidates in physically realizing quantum information units and thus being used as the basic element of quantum computing. Besides quantum computing, which is the main motivation of the research in this dissertation, the significance of optics in semiconductor quantum-dot systems extends to other tasks of quantum information processing as well; it is a field of intense research in the context of quantum network interfaces, single-photon generation, and entangled-photon sources.

Quantum computing is a multidisciplinary field of research. It is of tech-

nological relevance because it will speed up computations intractable by usual (classical) computers. Quantum information processing makes use of counterintuitive features of quantum mechanics, such as superposition and entanglement. Numerous physical schemes have been proposed for implementing quantum information units (qubits); out of these, the solid state ones based on semiconductor QDs are particularly promising, as they should be readily integrable with the existing semiconductor technology.

This dissertation adopts the suggestion that the spin of an excess electron in a quantum dot can acts as a quantum bit (qubit) of information in quantum computation implementation schemes [79, 61]. The single-qubit control can be carried out directly via transitions between the two spin states by use of a pulsed magnetic field [79], or optically by use of an auxiliary optically excited state that lies outside the computational subspace [61]. This excited state is a bound state of the electron and the exciton created by the laser. Optical manipulation of quantum dots exploits the advanced laser technology and employs features of the laser such as speed and focusing. The operations can therefore be fast compared to the dephasing time and each dot can be addressed separately with near-field techniques [17].

One of the challenges of implementing schemes of quantum computing is the compromise between long coherence times–which implies weak coupling to the environment–and the need for fast and robust quantum control of the system–which suggests strong coupling to a classical system, the controlling system (e.g. the laser). Any realistic proposal however has to account for the deteriorating mechanisms of coupling to the environment.

The research described in this dissertation heads towards the implementation of quantum computing with all-optically manipulated spins in quantum dots.

In Chapter II we briefly review the electronic structure and optical properties (selection rules) of quantum dots. We employ the effective mass approximation

for the semiconductor, and the envelope function approach for the dot. We account also for electron-electron and electron-hole direct and electron-electron exchange Coulomb interactions. Optical quantum computing schemes in quantum dots are discussed.

Chapter III introduces basic concepts of optics and interaction between the electromagnetic field and quantum systems, such as atoms and quantum dots. The stress is towards the optics of quantum dots, mostly in relation to the research in this dissertation. A broader overview of current research activities in the field of optics in quantum dots is also briefly given.

In Chapter IV we develop the theory underlying a nonlinear pump-probe experiment in quantum dots using a density-matrix formalism. This gives an explicit expression to compute and to test the theory against experiments. We explain why the acousto-optical modulation of the pump and probe followed by a homodyne measurement at the difference of the modulation frequencies measures the differential nonlinear signal. An analysis of the experimental initialization, control and measurement of the spin is also given.

In Chapter V we address the issue of optical decay during the optical pulse, out of which we find occurrence of intriguing physics, namely spin coherence generated through spontaneous emission of the optically excited state. We derive this term by employing a master-equation approach. Once this term is accounted for in the decay equations, we show how it alters the nonlinear signal in a pump-probe experiment in a quantum dot. We also show experimental results, obtained by the experimental group of Professor Steel, which are interpreted by our theory as spontaneously generated coherence.

In Chapter VI we examine the spontaneously generated coherence in a more quantum information theoretical context. We show that it can be understood as lack of entanglement between the system (spin) and the bath (spontaneously emitted photon). A unified theory is developed which shows how these effects naturally emerge when spontaneous emission is viewed as unitary evolution of a

single whole ('system'+bath), much in the spirit of Weisskopf-Wigner theory of spontaneous emission [141]. We also propose a scheme to create and measure entanglement between the spin states in a quantum dot and the spontaneously emitted photon from a light-hole trion state.

In Chapter VII, after briefly reviewing existing proposals, we develop a new scheme for ultrafast single-qubit operations, which reduces the three-level system to a two-level system during the fast duration of the pulse. The exactly solvable hyperbolic secant pulses of Rosen and Zener [117] are employed, such that the angle of rotation has an analytical form as a function of the pulse parameters. We also design an experiment to measure spin rotation about the quantum-dot growth direction by use of the aforementioned pulses. We address experimental issues, such as uncertainty in the laser parameters and issues related to incomplete characterization of the quantum dot, such as valence-band mixing. Feedback loops are used to select the ideal pulses, based on known pulse envelopes but without assumption of knowledge of pulse parameters.

II.

Electronic Structure and Selection Rules of the III-V Semiconductor: From Bulk to the Quantum Dot

In this chapter, after briefly reviewing the electronic structure of the zinc-blend semiconductors, we review the electronic structure of the quantum dot in the envelope-function approximation and particularly the optically excited spectra and selection rules. As mentioned already, the quantum dots retain partially the underlying symmetry of the semiconductor.

The most important property of a crystal is invariance under specific translations. Most crystals additionally possess rotational and reflection symmetries. Most semiconductors have high rotational symmetries, which greatly facilitate band structure calculations.

When a particle moves in a periodic potential its energy eigenfunctions can be expressed in the form of Bloch functions, which are plane waves modulated by a function with the same periodicity as the crystal potential, $V(\mathbf{r})$. They have the form

$$\Phi_{\mathbf{k}}(\mathbf{r}) = u_{\mathbf{k}}(\mathbf{r})e^{i\mathbf{k}\cdot\mathbf{r}}, \tag{II.1}$$

with $u_{\mathbf{k}}(\mathbf{r} + \mathbf{R}_\ell) = u_{\mathbf{k}}(\mathbf{r})$, where $\mathbf{R}_\ell$ is a lattice vector of the crystal: $\mathbf{R}_\ell = \ell_1 \alpha_1 +$

$\ell_2\alpha_2 + \ell_3\alpha_3$; in the latter ℓ_i are integers and $\alpha_1, \alpha_2, \alpha_3$ are three non-coplanar vectors. The quantum number $\mathbf{k}$ is called the wave vector and $\hbar\mathbf{k}$ is the crystal momentum.

Schrödinger's equation, $H\Phi = E\Phi$, where $H = \mathbf{p}^2/2m + V(\mathbf{r})$, leads to the following equation for the periodic part $u_{\mathbf{k}}(\mathbf{r})$:

$$\left(\frac{p^2}{2m} + \frac{\hbar\mathbf{k}\cdot\mathbf{p}}{m} + \frac{\hbar^2 k^2}{2m} + V\right)u_{n\mathbf{k}}(\mathbf{r}) = E_{n\mathbf{k}}u_{n\mathbf{k}}(\mathbf{r}), \qquad (\text{II}.2)$$

where $\mathbf{p} = -i\hbar\nabla$, and the additional index $n = 1, 2, 3, ...$ is called band index and indicates the various solutions of Eq. (II.2) for a given $\mathbf{k}$.

The electron eigenenergy, $E_{n\mathbf{k}}$, as a function of $\mathbf{k}$ (dispersion relation) and the band index n is known as the electronic band structure.

The Bloch functions are eigenstates of the translation operator T_R. Since the latter commutes with the total Hamiltonian H, the Bloch functions satisfying Eq.(II.2) are eigenfunctions of both T_R and the total Hamiltonian. Eigenfunction of H with eigenvalue E is also any sum $\sum'_{\mathbf{k},n} c_{\mathbf{k},n}\Phi_{\mathbf{k},n}$, where the prime denotes that the summation must be restricted to all n's and $\mathbf{k}$'s for which $E_{n\mathbf{k}} = E$.

Because of the relation $\mathbf{R}_\ell \cdot \mathbf{G}_m \equiv 2\pi q$, defining the reciprocal lattice $\mathbf{G}_m = m_1\mathbf{b}_1 + m_2\mathbf{b}_2 + m_3\mathbf{b}_3$, where q and m_1, m_2, m_3 are an integers, and $\mathbf{R}_\ell$ is any vector of the lattice, the solution $\Phi_{\mathbf{k},n}(\mathbf{r})$ is identical with $\Phi_{\mathbf{k}+\mathbf{G},n}(\mathbf{r})$. Hence, it is enough to restrict $\mathbf{k}$ within the so-called first Brillouin zone (1BZ), which is a polyhedron in $\mathbf{k}$-space, with the following property: The distance of any point of the 1BZ from the origin ($\mathbf{k} = 0$) is less than its distance from any other point $\mathbf{G}_m \neq 0$ of the reciprocal lattice. In a one-dimensional lattice, the 1BZ is the region $-\pi/\alpha < k < \pi/\alpha$, where α is the period of the direct lattice.

A. Diamond and Zinc-Blend Basics

The III-V compounds crystalize in zinc-blend structure. The direct lattice consists of two interpenetrating fcc lattices–each with its own type of atoms–

displaced relatively to one another by a quarter of the body diagonal along the [111] direction. The reciprocal lattice of an fcc is a body-centered cubic (bcc). The III-V semiconductors have a direct band gap, i.e., the top of the valence band occurs at the same k-value as the bottom of the conduction band.

The space group of the zinc-blend structure is denoted by T_d^2. Its point group has 24 elements and is identical to the elements of the point group of a tetrahedron. Here we sketch the procedure of using group theory to group the wavefunctions by their degeneracy. We start from a nearly free electron characterized by a plane wave, with $\mathbf{k} = (2\pi/a)(1,1,1)$. By applying the C_3 symmetry of zinc-blend, the eight points $(2\pi/a)(\pm 1, \pm 1, \pm 1)$ are shown to be equivalent, and by the previous discussion they can all be projected back to the center of the Brillouin zone ($k = 0$ or Γ point), which possesses the maximal possible symmetry, i.e., its group is isomorphic to the point group of the lattice. The eight plane waves formed by the wavevectors corresponding to these symmetry points form an eight-dimensional representation, which is reducible. They can be shown to reduce to two one-dimensional Γ_1 and two three-dimensional Γ_4 representations. From group theoretical considerations we can deduce the selection rules between these states. Optical transitions are allowed between Γ_4 states and states belonging to the $\Gamma_1, \Gamma_3, \Gamma_4, \Gamma_5$ representations. When the spin is included, the states are regrouped (the inclusion of the spin leads to the so-called double group). The new representations are of Γ_8 symmetry (four states) and two Γ_7 states, and the lowest conduction band states are now of Γ_6 symmetry.

Thus far, we have assumed a nearly free electron. The crystal potential has been assumed infinitely weak, and has entered through symmetry considerations on the wavefunctions. The extreme opposite approach is to start from the atomic states comprising the solid and use atomic or atomic-like wavefunctions as a basis for the electron wavefunctions in the solid, and calculate the electronic structure usually by numerical diagonalization of the Hamiltonian (LCAO method). Here, we will just show how basic information about the band structure can be

found based on this line of thought.

The atomic structure of the III elements of the periodic table has filled shells plus three valence electrons in the s^2p configuration. The V have also filled shells plus five valence electrons in the s^2p^3 configuration.[1] When two atoms, one of each species, are brought together there is attraction between them because the electrons can rearrange and spread their wavefunctions over both atoms and lower their energy. There is a total of eight basis states, four from each atom.

The four atomic orbitals, one s and three p's in each atom form sp^3 hybrids diected either along the $(1, 1, 1), (1, \bar{1}, \bar{1}), (\bar{1}, 1, \bar{1}), (\bar{1}, \bar{1}, 1)$ or the $(\bar{1}, \bar{1}, \bar{1})$, $(\bar{1}, 1, 1), (1, \bar{1}, 1), (1, 1, \bar{1})$ directions. Each pair of opposite pointing hybrids belonging to the nearest neighbor atoms form one bonding (lower energy compared with every sp^3 hybridized atomic state) and one antibonding (higher energy compared with every sp^3 hybridized atomic state) molecular orbital. When there is a macroscopic number of the constituent atoms, the energy levels broaden into bands. Around the bonding (antibonding) energy level the valence (conduction) band is formed. At $T = 0K$, the valence band (which is actually split into two subbands) is fully occupied by electrons while the conduction band is completely empty. The two bands are separated by a gap, the magnitude of which is denoted by E_g. This is schematically shown in Fig. II.1.

The higher valence band states are p-like, originating from the bonding states. The lowest conduction band states are s-like. Including the spin, the total degeneracy of the p-like top valence band states is 6 when spin-orbit coupling is neglected. However, spin-orbit interaction, represented by a contribution $H_{SO} = \lambda \mathbf{l} \cdot \mathbf{s}$ in the Hamiltonian, scales with the atomic number and is thus an important effect, especially for semiconductors containing heavier elements such as Ga, In and As. When included, the eigenstates are eigenstates of the total angular momentum $\mathbf{j} = \mathbf{l} + \mathbf{s}$ and the projection m_j along a quantization axis. Addition of angular momenta gives two possible values of total angular momentum, $j = 3/2$ and $j =$

---

[1]We remind that s stands for states with angular momentum $\ell = 0$ and p denotes $\ell = 1$.
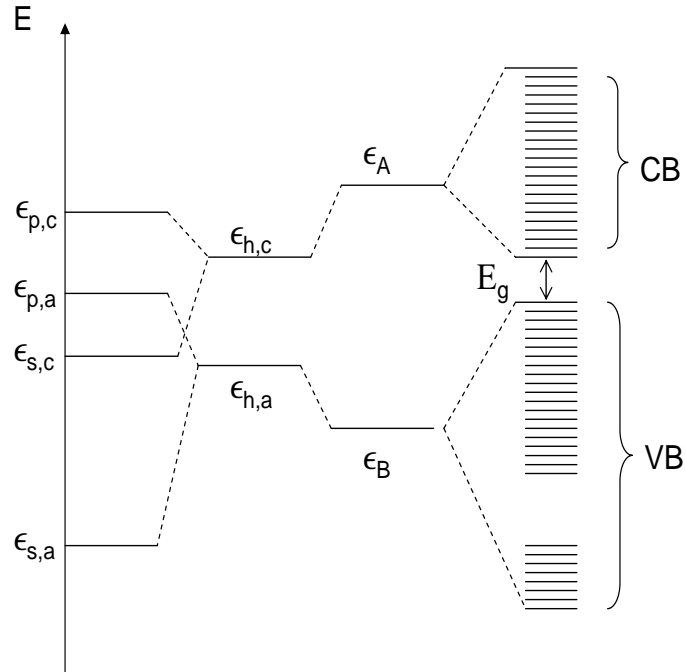
II.1   Schematic representation of band formation in a III-V semiconductor. Both the cation (c) and the anion (a) form sp^3 atomic hybrids (with energies $\epsilon_{h,c}$ and $\epsilon_{h,a}$, respectively) which combine to give rise to a bonding (ϵ_B) and antibonding (ϵ_A) molecular level. Those levels broaden into the valence (VB) and conduction (CB) bands respectively. The top of the valence band consists of predominantly p-character states (hence the three-fold degeneracy), while the bottom of the conduction band is of s character.

1/2, which are split by $\Delta_0 = 3\lambda/2$, the spin-orbit splitting. The two degenerate $j = 1/2$ states get shifted to lower energy and are also known as split-off holes. Δ_0 varies from 10 meV to almost 1eV as the atomic number increases. For the GaAs and InAs it is about 0.4eV, so that split-off holes may be safely ignored in the discussion of optical transitions.

B. k · p and Effective Mass Approximation

The $\mathbf{k} \cdot \mathbf{p}$ method is an approximate method for calculating band structure by inputting a small number of experimental parameters. We will mostly follow the treatment in [149] to review the method. Starting with the one-electron Schrödinger equation, and inserting the Bloch functions we obtained Eq. (II.2).

For $\mathbf{k}_0 = 0$, Eq. (II.2) reduces to

$$\left(\frac{p^2}{2m} + V \right) u_{n0} = E_{n0} u_{n0}. \tag{II.3}$$

Once (II.3) is solved, the omitted terms $\frac{\hbar \mathbf{k} \cdot \mathbf{p}}{m}$ and $\frac{\hbar^2 k^2}{2m}$ can be treated as perturbations. For example, let us assume that the band structure has a nondegenerate extremum at E_{n0}. Then, to second order in perturbation theory, we find for the functions $u_{n\mathbf{k}}$ and the energies $E_{n\mathbf{k}}$

$$u_{n\mathbf{k}} = u_{n0} + \frac{\hbar}{m} \sum_{n' \neq n} \frac{\langle u_{n0}|\mathbf{k} \cdot \mathbf{p}|u_{n'0}\rangle}{E_{n0} - E_{n'0}} u_{n'0} \tag{II.4}$$

$$E_{n\mathbf{k}} = E_{n0} + \frac{\hbar^2 k^2}{2m} + \frac{\hbar^2}{m^2} \sum_{n' \neq n} \frac{|\langle u_{n0}|\mathbf{k} \cdot \mathbf{p}|u_{n'0}\rangle|^2}{E_{n0} - E_{n'0}}. \tag{II.5}$$

Rewriting (II.5) as $E_{n\mathbf{k}} = E_{n0} + \frac{\hbar^2 k^2}{2m^*}$, we define the quantity m^* as the effective mass of the band. Its inverse is given by

$$\frac{1}{m^*} = \frac{1}{m} + \frac{2\hbar^2}{m^2 k^2} \sum_{n' \neq n} \frac{|\langle u_{n0}|\mathbf{k} \cdot \mathbf{p}|u_{n'0}\rangle|^2}{E_{n0} - E_{n'0}}. \tag{II.6}$$

Equation (II.6) shows that an electron in the solid has a different mass than the free electron mass, due to the coupling to other bands. The effective mass is dictated by the strength of the coupling to other bands and by the energy separation from those bands.

Thus far we considered a non degenerate band with an extremum in the energy and with spin-orbit interaction neglected; the effective mass turned out to be a scalar. This treatment is appropriate for a conduction-band electron. The valence band, as mentioned above, is degenerate and spin orbit interaction plays a significant role for heavy compounds, such as GaAs or InAs. One can repeat the above treatment for the valence band, treating exactly the six Γ_4 valence band states (spin degeneracy included), by first taking spin-orbit interaction into account by forming eigenstates of the total j. This gives rise to four states with $j = 3/2$ (The Γ_8 states from Section A.) and two $j = 1/2$ states (the two Γ_7 split-off states from from Section A.). The interaction with the eight lowest conduction band states can be treated by second order perturbation theory as an extra interaction, folded back into the 6×6 Hamiltonian.

We should also note that in principle the $\mathbf{k} \cdot \mathbf{p}$ term can give rise to a linear term in k. In diamond-type semiconductors these terms vanish exactly because of parity selection rule. However, in zinc-blend crystals there is a small but nonzero linear in k term originating from the inversion asymmetry of the crystal. The linear k terms do not come alone from the $\mathbf{k} \cdot \mathbf{p}$ term, but also from omitted spin-dependent terms, known as Dresselhaus terms [38].

C.   Luttinger Hamiltonian

An alternative approach to obtain valence-band dispersion in zinc-blend semiconductors was given by Luttinger [88]. It treats the Γ_8 valence bands by an effective $\mathbf{k} \cdot \mathbf{p}$ Hamiltonian derived from group theory arguments. The Luttinger Hamiltonian has the following form (choosing $\hbar = 1$)

$$H_L = \frac{1}{2m}\left[\left(\gamma_1 + \frac{5}{2}\gamma_2\right)k^2 - 2\gamma_2 k_i^2 J_i^2 - 2\gamma_3 \sum_{i \neq j} k_i k_j \{J_i, J_j\}\right],\qquad \text{(II.7)}$$

where the repeated indices are summed over and $\{a, b\} \equiv \frac{ab+ba}{2}$. The dimensionless parameters $\gamma_1, \gamma_2, \gamma_3$ are the Kohn-Luttinger parameters,[2] and $\mathbf{J}$ is the angular momentum operator, with $J = 3/2$.

To make the symmetry of (II.7) more apparent, it is useful to rearrange terms. Then we get

$$H_L = \frac{1}{2m}\left[\left(\gamma_1 + \frac{5}{2}\gamma_2\right)k^2 - 2\gamma_3(\mathbf{k}\cdot\mathbf{J})^2 + 2(\gamma_3 - \gamma_2)k_i^2 J_i^2\right].\qquad \text{(II.8)}$$

Clearly, the two first terms of (II.8) are spherically symmetric. The cubic symmetry is represented by the last terms, so that taking $\gamma_2 = \gamma_3$ amounts to the spherical approximation, i.e., the energy depends only on the absolute value of k, through parabolic dispersion, and not on its direction.

When k points along one of the three high symmetry directions, z for example, the Hamiltonian H_L reduces to

$$H_L^{HH} = \frac{k_z^2}{2m}(\gamma_1 - 2\gamma_2) \quad \text{for} \quad m_j = \pm 3/2 \qquad \text{(II.9)}$$

$$H_L^{LH} = \frac{k_z^2}{2m}(\gamma_1 + 2\gamma_2) \quad \text{for} \quad m_j = \pm 1/2, \qquad \text{(II.10)}$$

so that the effective masses are

$$m_{HH} = m(\gamma_1 - 2\gamma_2)^{-1} \quad \text{for} \quad m_j = \pm 3/2 \qquad \text{(II.11)}$$

$$m_{LH} = m(\gamma_1 + 2\gamma_2)^{-1} \quad \text{for} \quad m_j = \pm 1/2, \qquad \text{(II.12)}$$

and thus the terms heavy and light holes for the $m_j = \pm 3/2$ and $m_j = \pm 1/2$ respectively.

---

[2] for GaAs, $\gamma_1 = 6.85, \gamma_2 = 2.1, \gamma_3 = 2.9$

For the general case of **k** pointing along an arbitrary direction, we need to diagonalize the Hamiltonian in order to find the dispersion relation. We write the Luttinger Hamiltonian in matrix form, in the $\{|\frac{3}{2}\frac{3}{2}\rangle, |\frac{3}{2}\frac{\bar{1}}{2}\rangle, |\frac{3}{2}\frac{1}{2}\rangle, |\frac{3}{2}\frac{\bar{3}}{2}\rangle\}$ basis:

$$H_L = \begin{bmatrix} P+Q & R & -S & 0 \\ R^\dagger & P-Q & 0 & S \\ -S^\dagger & 0 & P-Q & R \\ 0 & S^\dagger & R^\dagger & P+Q \end{bmatrix}, \tag{II.13}$$

where

$$P = \frac{\gamma_1}{2m}(k_z^2 + k_x^2 + k_y^2) \tag{II.14}$$

$$Q = \frac{\gamma_2}{2m}(-2k_z^2 + k_x^2 + k_y^2) \tag{II.15}$$

$$R = -\frac{\sqrt{3}}{2m}\bar{\gamma}k_-^2 + \frac{\sqrt{3}}{2}\mu k_+^2 \tag{II.16}$$

$$S = \sqrt{3}\gamma_3 k_z k_-, \tag{II.17}$$

$$k_\pm = k_x \pm ik_y, \tag{II.18}$$

and

$$\bar{\gamma} = \frac{1}{2}(\gamma_2 + \gamma_3) \tag{II.19}$$

$$\mu = \frac{1}{2}(\gamma_3 - \gamma_2). \tag{II.20}$$
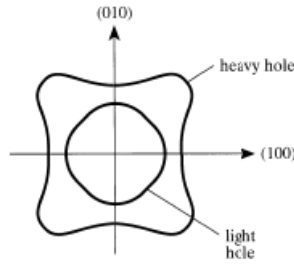
II.2   Constant energy surfaces of the Γ_8 valence bands.

Diagonalization of the above Hamiltonian gives the dispersion

$$E_\pm = \frac{1}{2m}\left(\gamma_1 k^2 \pm 2\left[\gamma_2^2 k^4 + 3(\gamma_3^2 - \gamma_2^2)(k_x^2 k_y^2 + \text{c.p.})\right]^{1/2}\right), \tag{II.21}$$

where the upper signs refer to the 'heavy hole' and the lower to the 'light hole'. The constant energy surfaces are no longer parabolic; they are "warped", as shown in Fig. II.2.

D.   Electronic States of a Quantum Dot

The Luttinger Hamiltonian is a powerful tool in that it allows for additional perturbations of known symmetry, so it is attractive for calculations in quantum dots and wells of given symmetry. The symmetry of the nanostructures is lowered compared to the bulk due to the confinement potential, so the assumption of an infinite crystal no longer holds. For quantum wells, there is no translational symmetry along the confinement direction, and in quantum dots the translational symmetry is broken along all three directions. Here we will study the quantum dot.

To account for the dot potential, which has a characteristic length large compared to the atomic scale, we will assume the so-called envelope function approximation, which amounts to taking the wavefunction of each (quasi)particle to be the product of the Bloch function, originating from the underlying semiconductor structure, and a slowly varying envelope function, which is the solution of the quantum-dot Hamiltonian. For the electron in the conduction band we have

$$\Psi(r) = \Phi_0(r) F_c(r) \chi(\sigma), \tag{II.22}$$

where Φ_0 is a Bloch function with $k = 0$, F_c is the envelope function and χ carries the spin information. To find F_c we have to solve the one-particle Schrödinger equation

$$H_c(x, y, z) F_c(x, y, z) = E F_c(x, y, z) \tag{II.23}$$

$$H_c = -\frac{\nabla^2}{2m_c} + V_1(x) + V_2(y) + V_3(z), \tag{II.24}$$

where the confining potential has been assumed separable in the three cartesian coordinates.

For the valence band, the relevant equation is

$$H_v(x, y, z)F_v(x, y, z) = EF_v(x, y, z) \qquad (\text{II.25})$$

$$H_v = H_L + V_1(x) + V_2(y) + V_3(z), \qquad (\text{II.26})$$

where the same dot potential has been assumed for the electrons and the holes, and H_L is the Luttinger Hamiltonian for the four Γ_8 valence band states. It can be written, again in the $\{|\frac{3}{2}\frac{3}{2}\rangle, |\frac{3}{2}\frac{\bar{1}}{2}\rangle, |\frac{3}{2}\frac{1}{2}\rangle, |\frac{3}{2}\frac{\bar{3}}{2}\rangle\}$ basis, as

$$H_L = \begin{bmatrix} P+Q & R & -S & 0 \\ R^\dagger & P-Q & 0 & S \\ -S^\dagger & 0 & P-Q & R \\ 0 & S^\dagger & R^\dagger & P+Q \end{bmatrix}, \qquad (\text{II.27})$$

with P, Q, R, S defined by (II.14)-(II.17), but the k's are now replaced by operators [20]:

$$k_x = -i\frac{\partial}{\partial x} \qquad (\text{II.28})$$

$$k_y = -i\frac{\partial}{\partial y} \qquad (\text{II.29})$$

$$k_z = -i\frac{\partial}{\partial z} \qquad (\text{II.30})$$

$$k_\pm = k_x \pm ik_y. \qquad (\text{II.31})$$

We will assume that the symmetry of the quantum dot to be such that the Luttinger Hamiltonian decouples to two, doubly degenerate bands. We will examine the consistency of this assumption using the solution we will obtain, and the mixing will be accounted for as a perturbation on those solutions. Under this approximation, the Hamiltonian for the valence band is the sum of three terms

$$H_z^\pm = -\frac{1}{2m}(\gamma_1 \mp 2\gamma_2)\frac{\partial^2}{\partial z^2} + V_3(z) \qquad (\text{II.32})$$

$$H_x^\pm = -\frac{1}{2m}(\gamma_1 \pm \gamma_2)\frac{\partial^2}{\partial x^2} + V_1(x) \qquad (\text{II.33})$$

$$H_y^\pm = -\frac{1}{2m}(\gamma_1 \pm \gamma_2)\frac{\partial^2}{\partial y^2} + V_2(y), \qquad (\text{II.34})$$

where the upper (lower) signs refer to the heavy (light) hole.

From the above, we can define the anisotropic effective masses

$$m_z^H = \frac{m}{(\gamma_1 - 2\gamma_2)} \tag{II.35}$$

$$m_{||}^H = \frac{m}{(\gamma_1 + \gamma_2)} \tag{II.36}$$

$$m_z^L = \frac{m}{(\gamma_1 + 2\gamma_2)} \tag{II.37}$$

$$m_{||}^L = \frac{m}{(\gamma_1 - \gamma_2)} \tag{II.38}$$

Note that the terms 'heavy' and 'light' hole are still used to denote the $m_j = \pm\frac{3}{2}$ and $m_j = \pm\frac{1}{2}$ respectively, even along the in-plane directions where there is mass reversal, i.e., the heavy hole has a smaller effective mass than the light hole.

To find an explicit expression for the functions $F_v(r)$, we will model the potential of the dot by a simple harmonic oscillator in each direction.

$$V_1(x) = \frac{1}{2}K_x x^2 \tag{II.39}$$

$$V_2(y) = \frac{1}{2}K_y y^2 \tag{II.40}$$

$$V_3(z) = \frac{1}{2}K_z z^2, \tag{II.41}$$

where K_i is the spring constant along direction i. We define the following frequencies

$$\omega_{c,z} = \sqrt{K_z/m_c} \tag{II.42}$$

$$\omega_{c,x} = \sqrt{K_x/m_c} \tag{II.43}$$

$$\omega_{c,y} = \sqrt{K_y/m_c} \tag{II.44}$$

$$\omega_{H,z} = \sqrt{K_z/m_z^H} \tag{II.45}$$

$$\omega_{H,x} = \sqrt{K_x/m_{||}^H} \tag{II.46}$$

$$\omega_{H,y} = \sqrt{K_y/m_{||}^H} \tag{II.47}$$

$$\omega_{L,z} = \sqrt{K_z/m_z^L} \tag{II.48}$$

$$\omega_{L,x} = \sqrt{K_x/m_{||}^L} \tag{II.49}$$

$$\omega_{L,y} = \sqrt{K_y/m_{||}^H} \tag{II.50}$$

The eigenfunctions are

$$F^j_{n_x n_y n_z} = \prod_i \phi^j_{n_i}(x_i) \tag{II.51}$$

$$\phi^j_{n_i}(x_i) = \left[\frac{m_j \omega_{j,i}}{2^{2n_i} \pi \hbar (n_i!)^2} \right]^{1/4} H_{n_i}\left(\sqrt{\frac{m_j \omega_{j,i}}{\hbar}} x_i \right) e^{-m_j \omega_{j,i} x_i^2 / 2\hbar}, \tag{II.52}$$

and the eigenenergies

$$E^j_{n_x n_y n_z} = \sum_i (n_i + \frac{1}{2}) \hbar \omega_{j,i}, \tag{II.53}$$

where the x_i's are the three cartesian coordinates and j denotes the band index, i.e., $j = c, H, L$.

Typically in quantum dots the lateral size is about an order of magnitude larger than the vertical size. Therefore, the confinement along the growth direction is a lot stronger, which translates to

$$\omega_{j,z} \gg \omega_{j,x}, \omega_{j,y}. \tag{II.54}$$

Thus, we assume that the electron remains in the lowest state of the confining potential along z, and ignore it in the rest of the discussion. Also, combining the fact that $m_z^H > m_z^L$, Eqs. (II.35) and (II.37), with Eq. (II.54), we can explain the experimental result that the lowest heavy-hole states are lower in energy than the lowest light-hole states. The experimental values for this splitting are in the order of tens of meV's.

We also assume cylindrical symmetry of the dot about the z axis, i.e., $K_x = K_y \equiv K$, so that we can simplify the problem to the 2D harmonic oscillator. We also define $\omega_{j,\parallel} = \omega_{j,x} = \omega_{j,y}$. We can add deviations from this as a perturbation.

Now, we should examine the neglected valence-band mixing terms from the Luttinger Hamiltonian. First, notice that whenever the potential has inversion symmetry, and hence the wavefunctions have definite parity, the expectation values of $\partial/\partial x$ and $\partial/\partial y$ are zero. Therefore, the mixing induced by the S term and part of the R vanish. The remaining mixing terms are proportional to the expectation

value of $\partial^2/\partial x^2 - \partial^2/\partial y^2$ of R. In the case of cylindrical symmetry these terms cancel exactly. We can account for deviations from cylindrical symmetry as a perturbation by taking, for example, $K_y = K_x + \Delta K$. It is clear that deviation from cylindrical symmetry will cause some mixing between heavy- and light-hole states. In the largest part of this dissertation we will ignore the valence band mixing, and return to it in Chapter VII in the design of optical spin rotations.

Since the problem now possesses cylindrical symmetry, it may be solved in cylindrical coordinates where the axial symmetry is manifested. This is useful for calculation of exciton states, where Coulomb interactions between electrons and holes are taken into account. The single-particle eigenstates are

$$\psi^j_{nm}(\rho, \phi) = \lambda_j^{(|m|+1)/2} \sqrt{\frac{n!}{\pi(n+|m|)!}} \rho^{|m|} e^{-\lambda_j \rho^2/2} L_n^{|m|}\left(\lambda_j \rho^2\right) e^{-im\phi}, \qquad (\text{II.55})$$

where

$$n = n_x + n_y \qquad (\text{II.56})$$

$$m = n_x - n_y \qquad (\text{II.57})$$

$$\lambda_j = m_j \omega_{j,\parallel}, \qquad (\text{II.58})$$

and $L_n^{|m|}$ are the generalized Laguerre polynomials, ρ, ϕ are the usual cylindrical coordinates and λ_j has units of $(\text{length})^{-2}$. The energy is

$$E_n^j = (n+1)\omega_{j,\parallel}. \qquad (\text{II.59})$$

The two new quantum numbers n, m correspond to the total energy and the angular momentum about z respectively (m should not be confused with the free electron mass). States II.55 are called Fock-Darwin states [48, 35]. In the absence of a magnetic field there is $n+1$ degeneracy for every n. Physically, we expect to have nonzero angular momentum whenever a state with $n_x \neq n_y$ is excited, so that only states with even n possess an $m = 0$ state.

Finally, we should also note that spin-orbit terms originating from inversion asymmetry of the dot [115] have been omitted in our discussion.

E. Optical excitations

The typical bandgaps of semiconductors are in the 1-2 eV range, i.e., in the optical range of the energy spectrum. Moreover, for semiconductors with direct bandgaps, like the III-V's, an electron can be optically excited from the top of the valence to the bottom of the conduction band, since photons carry very small momentum. Henceforth, as in the previous section, we will be thinking of a missing electron from the valence band as a hole, a quasiparticle with positive charge and opposite k and spin from the missing electron, i.e., it is its time reversal. The electron in the conduction band is attracted to the hole by Coulomb interaction. They can form a bound state, which is an excitation below the free-particle energies, i.e., in the band gap. Excitons in the bulk have been studied for many years. Below we briefly review the theory of bulk excitons.

1. Bulk excitons

The Hamiltonian of the system of electrons and holes in second quantization notation is

$$H = H_{free} + H_C \tag{II.60}$$

where

$$H_{free} = \sum_{k\sigma} \epsilon_{ck} a^\dagger_{ck\sigma} a_{ck\sigma} + \sum_{k\sigma} \epsilon_{vk} a^\dagger_{vk\sigma} a_{vk\sigma} \tag{II.61}$$

and

$$
\begin{aligned}
H_C = \frac{1}{2} & \sum_{ijkl;\sigma_1\sigma_2} a^\dagger_{ci\sigma_1} a^\dagger_{cj\sigma_2} a_{ck\sigma_2} a_{cl\sigma_2} \; G^{cccc}(ijkl) \\
+\frac{1}{2} & \sum_{ijkl;\sigma_1\sigma_2} a^\dagger_{vi\sigma_1} a^\dagger_{vj\sigma_2} a_{vk\sigma_2} a_{vl\sigma_2} \; G^{vvvv}(ijkl) \\
+ & \sum_{ijkl;\sigma_1\sigma_2} a^\dagger_{ci\sigma_1} a^\dagger_{vj\sigma_2} a_{vk\sigma_2} a_{cl\sigma_2} \; G^{cvvc}(ijkl) \\
+ & \sum_{ijkl;\sigma_1\sigma_2} a^\dagger_{ci\sigma_1} a^\dagger_{vj\sigma_2} a_{ck\sigma_2} a_{vl\sigma_2} \; G^{cvcv}(ijkl) \tag{II.62}
\end{aligned}
$$

The a's are annihilation operators and the $a^\dagger$'s creation operators. The operator $a^\dagger_{ck}$ ($a^\dagger_{vk}$) creates an electron in the conduction (valence) band with wavefuction $\psi_{ck}(\mathbf{r})$ ($\psi_{vk}(\mathbf{r})$). In Eq. (II.62), $G(ijkl)$ is the Coulomb integral. The Coulomb integral is given by

$$G(ijkl) = \int \int d\mathbf{r_1} d\mathbf{r_2} \psi_i^*(\mathbf{r_1})\psi_j^*(\mathbf{r_2}) \frac{e^2}{|\mathbf{r_1} - \mathbf{r_2}|} \psi_k(\mathbf{r_2})\psi_l(\mathbf{r_1}). \qquad (\text{II.63})$$

To solve for the exciton states, we use the single-particle electron and hole states and take into account the direct Coulomb interaction (II.62). This process is the usual two-body problem, where from electron and hole coordinates we move to relative and center-of-mass motion and $M = m_h + m_e$. The exciton is labelled by a wave-vector $\mathbf{q}$, which is the sum of the electron and hole wavevectors. Noticing that, when exchange interaction between electron and hole is neglected, the problem can be mapped to the Hydrogen atom problem with different masses we can readily write down the exciton energy, which is

$$E_n(q) = -\frac{Ry^*}{n^2} + \frac{\mathbf{q}^2}{2M}, \qquad (\text{II.64})$$

with Ry^* the effective Rydberg energy. We point out that the concept of the exciton goes beyond the independent electron approximation and can be defined in a fully interacting electronic system. Its effective mass M can be defined in the many body problem in the limit of small binding energy, small total momentum q, large spatial extent of the exciton, and slowly varying external potential [124].

2. Biexcitons

Excitons are not the only possible excitations in a semiconductor. If we view excitons like atoms, then we expect them to interact with each other and form molecular states. Indeed, excitons interact and form biexcitons.

Biexcitons are, in analogy to molecules, states of lower total energy than the two non-interacting excitons. The energy difference $2E_{exc} - E_{biexc}$ is the binding

energy of the biexciton. In the following sections we discuss the importance of biexcitons and of other composite bound states in optical quantum computation schemes in semiconductors. Typical values of biexiton binding energies are of the order of several meV's in quantum dots [83].

F. Excitons in the Quantum Dot

The treatment of excitons in the quantum dot is quite similar to that in the bulk semiconductor.

In the envelope function approximation, the optical selection rules are found by requiring

$$\langle \Psi_c(r)|\mathbf{r}|\Psi_v(r)\rangle \neq 0. \tag{II.65}$$

The envelope part of the wavefunction–as slowly varying–can be pulled out of the integral, so that the selection rules are the usual optical selection rules from the bulk, with the additional restriction on the envelope functions

$$\langle F_c(r)|F_v(r)\rangle \neq 0. \tag{II.66}$$

The above relation predominantly allows for transitions between envelope states with the same quantum numbers (n, m). For the cylindrically symmetric dot, we can readily see that $\Delta m = 0$ should strictly hold, since for $\Delta m \neq 0$ the integral vanishes due to the radial part $e^{i\Delta m\phi}$.

The direct Coulomb integrals are now given by

$$G_d(ijkl) = \int \int d\mathbf{r}_1 d\mathbf{r}_2 F_i^*(\mathbf{r}_1)F_j^*(\mathbf{r}_2)\frac{e^2}{|\mathbf{r}_1 - \mathbf{r}_2|}F_k(\mathbf{r}_2)F_l(\mathbf{r}_1), \tag{II.67}$$

and the creation and annihilation operators in Eq. (II.62) acquire an extra index, which carries the envelope function information. The replacements of the envelope function in the Coulomb integral is because the Coulomb interaction becomes

much stronger with confinement, due to stronger overlap of the electron and hole wavefunctions. This is also why the optical dipole matrix elements in quantum dots are much larger than those of atoms.

Using the Fock-Darwin states from Section D., analytical expressions for the Coulomb integrals can be found. We list them here. The derivation can be found in ref. [116] for electrons, and straightforwardly modified to include interactions between electrons and holes.

$$
\begin{aligned}
V^{eeee}_{n_1m_1,n_2m_2,n_3m_3,n_4m_4} = \quad & \frac{e^2}{4\pi\epsilon\epsilon_r}\sqrt{\lambda_e}\,\delta_{m_1+m_2,m_3+m_4}\left[\prod_{i=1}^{4}\frac{n_i!}{(n_i+|m_i|)!}\right]^{1/2}\\
& \times\sum_{(4)j=0}^{n}\frac{(-1)^{j_1+j_2+j_3+j_4}}{j_1!j_2!j_3!j_4!}\prod_{\ell=1}^{4}\binom{n_\ell+|m_\ell|}{n_\ell-j_\ell}\\
& \times 2^{-K/2-1/2}\sum_{(4)\ell=0}^{\kappa}\delta_{\ell_1+\ell_2,\ell_3+\ell_4}\prod_{t=1}^{4}\binom{\kappa_t}{\ell_t}(-1)^{\kappa_2+\kappa_3-\ell_2-\ell_3}\\
& \times\Gamma(\Lambda/2+1)\Gamma([K-\Lambda+1]/2)
\end{aligned}
$$

$$
\begin{aligned}
V^{hhhh}_{n_1m_1,n_2m_2,n_3m_3,n_4m_4} = \quad & \frac{e^2}{4\pi\epsilon\epsilon_r}\sqrt{\lambda_h}\,\delta_{m_1+m_2,m_3+m_4}\left[\prod_{i=1}^{4}\frac{n_i!}{(n_i+|m_i|)!}\right]^{1/2}\\
& \times\sum_{(4)j=0}^{n}\frac{(-1)^{j_1+j_2+j_3+j_4}}{j_1!j_2!j_3!j_4!}\prod_{\ell=1}^{4}\binom{n_\ell+|m_\ell|}{n_\ell-j_\ell} \qquad\text{(II.68)}\\
& \times 2^{-K/2-1/2}\sum_{(4)\ell=0}^{\kappa}\delta_{\ell_1+\ell_2,\ell_3+\ell_4}\prod_{t=1}^{4}\binom{\kappa_t}{\ell_t}(-1)^{\kappa_2+\kappa_3-\ell_2-\ell_3}\\
& \times\Gamma(\Lambda/2+1)\Gamma([K-\Lambda+1]/2)
\end{aligned}
$$

$$
\begin{aligned}
V^{ehhe}_{n_1m_1,n_2m_2,n_3m_3,n_4m_4} = \quad & \frac{e^2}{4\pi\epsilon\epsilon_r}\frac{\lambda_e^{(|m_1|+|m_4|+1)/2}\lambda_h^{(|m_2|+|m_3|+1)/2}}{\sqrt{\lambda_e+\lambda_h}}\\
& \left[\prod_{i=1}^{4}\frac{n_i!}{(n_i+|m_i|)!}\right]^{1/2}\sum_{(4)j=0}^{n}\frac{(-1)^{j_1+j_2+j_3+j_4}}{j_1!j_2!j_3!j_4!}\prod_{\ell=1}^{4}\binom{n_\ell+|m_\ell|}{n_\ell-j_\ell}\\
& \lambda_e^{(j_1+j_4)}\lambda_h^{(j_2+j_3)}\sum_{(4)\ell=0}^{\kappa}\delta_{\ell_1+\ell_2,\ell_3+\ell_4}(-1)^{\kappa_2+\kappa_3-\ell_2-\ell_3}\\
& \lambda_e^{(\kappa_3+\kappa_2-\ell_3-\ell_2)}\lambda_h^{(\kappa_1+\kappa_4-\ell_1-\ell_4)}(\lambda_e+\lambda_h)^{-K/2}(\lambda_e\lambda_h)^{(\Lambda-K)/2}\\
& \times\prod_{t=1}^{4}\binom{\kappa_t}{\ell_t}\Gamma(\Lambda/2+1)\Gamma([K-\Lambda+1]/2)
\end{aligned}
$$

$$V^{eheh}_{n_1m_1,n_2m_2,n_3m_3,n_4m_4} = \beta \frac{e^2}{4\pi\epsilon\epsilon_r} 2\lambda_e^{(|m_1|+|m_3|+2)/2}\lambda_h^{(|m_2|+|m_4|+2)/2}\left(\lambda_e + \lambda_h\right)^{-3/2}$$

$$\left[\prod_{i=1}^{4}\frac{n_i!}{(n_i+|m_i|)!}\right]^{1/2}\sum_{(4)j=0}^{n}\frac{(-1)^{j_1+j_2+j_3+j_4}}{j_1!j_2!j_3!j_4!}\prod_{\ell=1}^{4}\binom{n_\ell+|m_\ell|}{n_\ell-j_\ell}$$

$$\lambda_e^{(j_1+j_3)}\lambda_h^{(j_2+j_4)}(\lambda_e+\lambda_h)^{-K/2}\sum_{(4)\ell=0}^{\kappa}\delta_{\ell_1+\ell_2,\ell_3+\ell_4}(-1)^{\kappa_2+\kappa_3-\ell_2-\ell_3}$$

$$\times\prod_{t=1}^{4}\binom{\kappa_t}{\ell_t}\Gamma(\Lambda/2+1)\Gamma([K-\Lambda+1]/2), \qquad \text{(II.69)}$$

where

$$\kappa_1 = j_1 + j_4 + (|m_1|+m_1)/2 + (|m_4|-m_4)/2, \qquad \text{(II.70)}$$

$$\kappa_2 = j_2 + j_3 + (|m_2|+m_2)/2 + (|m_3|-m_3)/2, \qquad \text{(II.71)}$$

$$\kappa_3 = j_2 + j_3 + (|m_2|-m_2)/2 + (|m_3|+m_3)/2, \qquad \text{(II.72)}$$

$$\kappa_4 = j_1 + j_4 + (|m_1|-m_1)/2 + (|m_4|+m_4)/2, \qquad \text{(II.73)}$$

and $\Lambda = \ell_1 + \ell_2 + \ell_3 + \ell_4$, $K = \kappa_1 + \kappa_2 + \kappa_3 + \kappa_4$, and β comes from the Bloch function overlap.

Taking only heavy holes into account, there are four possible excitonic states, corresponding to the four combinations of the spin up and spin down electron with the two $m_j = \pm 3/2$ holes. The four excitons differ in their total angular momentum and its projection. The four possible states are degenerate in the absence of a magnetic field and when electron-hole exchange interaction is neglected. They are listed below, in the $|JM_J\rangle$ basis:

- $|22\rangle$

- $|2\bar{2}\rangle$

- $|11\rangle$

- $|1\bar{1}\rangle$

From these, only the two last ones can be excited optically. This is due to selection rules; the photon carries angular momentum $\ell = 1$, whereas the vacuum of the quantum dot is not polarized. Therefore, the final state should have $\ell = 1$ and a projection of ± 1, depending on the polarization of the exciting laser.

Fine structure of excitons has been observed in experiments [7, 130], and it is due to exchange interaction between electron and hole.

1. The Exciton Qubit

Excitons in quantum dots have been studied as possible implementations of qubits for quantum computing [12, 131, 24]. The two qubit states are the absence ($\equiv |0\rangle$) and the presence ($\equiv |1\rangle$) of an exciton in the dot. By use of energy selectivity and Pauli's exclusion principle, a laser tuned at the first excitonic transition will create a single exciton. Rabi oscillations of excitons, which constitute the single-qubit rotations, have been demonstrated [129]. Another attractive aspect is that initialization of this qubit is trivial, since one of the states is the semiconductor vacuum (no excitons present), which is robust up to high temperatures. Two-qubit controlled operations have also been demonstrated experimentally, by clever use of the biexciton states [83]. We briefly review the idea.

As already mentioned, the presence of an exciton in the dot changes the resonant energy of a second exciton by the biexciton binding energy. Therefore, after creating–by use of a Π_x linearly polarized laser–the superposition state $|0\rangle + |1\rangle$ (unnormalized), a second, Π_y linearly polarized π-pulse, tuned at the biexciton transition and with bandwidth small enough compared to the biexciton binding energy, will create the entangled state $|00\rangle + |11\rangle$, from the initial factorizable $|00\rangle + |10\rangle$ state. The truth table of this gate has been shown to be a C-ROT with fidelity almost 80%. Clearly, the gate is limited by the short recombination times of the excitons. Moreover, this is not a scalable scheme for a quantum computer. Thus, the spin of an excess electron in a quantum dot is now pursued in semiconductor quantum computing research, in order to take advantage of the long dephasing

times of the spin. In the following section we introduce the charged exciton–also called a trion–which is the key auxiliary state for optically controlled spins in quantum dots for quantum computation and quantum information processing.

G.   Trions

Excitons and biexcitons are not the only composite particle aggregates in semiconductor nanostructures. A whole hierarchy of composite particles was already predicted in the late '50's [76]. Among those, a positively or negatively charged exciton was also predicted, but only demonstrated experimentally in the 90's in semiconductor quantum wells [66]. The charged exciton, also known as a trion, is a bound state of two electrons and a hole (X^-) or two holes and one electron (X^+). The lowest energy trion in a dot is realized when two electrons occupy the same dot (orbital) state, and thus form a singlet spin state, in the presence of a hole in the lowest (heavy) hole dot state. Higher excited trion states have also been observed in self-assembled dots [140]. For concreteness we will focus on the lowest X^- trion. The two electrons occupy the same dot state and are thus in a spin singlet state. Therefore their exchange interaction with the hole cancels, and unlike the exciton there is no fine structure for the trion [130].

1.   Trion spectra

Within the simple harmonic oscillator model assumed for the single-particle Hamiltonian, the Coulomb integrals can be calculated analytically. Due to the definite parity of the Coulomb interaction, most matrix elements cancel by symmetry considerations, so that the problem amounts to diagonalizing at most 4×4 matrices.

H.   Quantum Computing with Spin Qubits Manipulated via Intermediate Trion States

Spins in semiconductor quantum dots offer the possibility of an attractive qubit. They can be trapped in the dot, which is grown on a semiconductor substrate, and are thus integrable with existing semiconductor technology. They have a long spin lifetime T_1, of the order of 1 ms at low temperatures, and an anticipated long coherence time T_2, which has a lower bound of 10 ns, as measured from ensemble experiments [41].
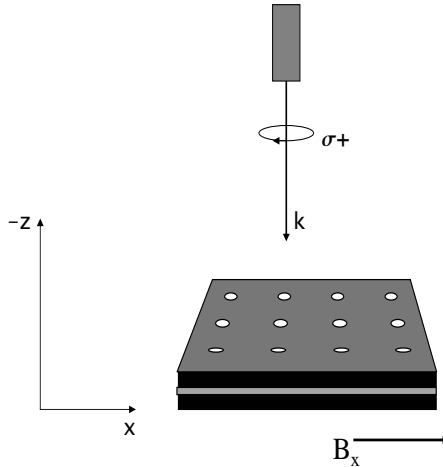
II.3   Cartoon picture of the quantum dots and laser.

However, the single-qubit rotations are a challenging issue. To avoid direct control between the two spin states via a pulsed magnetic field, which would be slow and more importantly hard to focus on a single spin, optical control of the spins was suggested [61] through intermediate trion states. The three relevant states in this scheme are the two spin states of the extra electron, split by a static in-plane magnetic field and the trion state. The optical axis of the laser coincides with the growth direction, z, as shown in Fig. II.3. When circularly polarized laser is used and focused on the heavy hole trion only one of the two heavy-hole trion states is excited, depending on the sense of the polarization. The relevant system

can be thought of as a three-level Λ system, in the language of atomic physics. Of course, contrary to the atom, the excited state in the dot is a multi-particle state. Note that we use the convention of using z to denote the growth axis, and x is the single-electron spin quantization axis.

A peculiarity of the semiconductor Λ system is that the trion state, although polarized along the z direction, i.e., perpendicularly to the magnetic field, it does not precess about it for fields up to about 5 T [130]. This is due to the energy separation of the light-hole from the heavy-hole states, as explained above: for the $m_j = 3/2$ to flip to the $m_j = -3/2$ it has to pass through the $m_j = \pm 1/2$ light-hole states. If we fold those states back into the heavy-hole Hamiltonian, the term coupling the two heavy-hole states is proportional to $B^3/\Delta_{H,L}^2$, where $\Delta_{H,L}$ is the heavy-hole light-hole splitting due to the confinement. Therefore, the precession is suppressed for low fields.

In Fig. II.4 we show the energy levels, in the single-particle picture (left panel) and in the energy level configuration, II.5, on the right. In the remaining chapters we will focus on this three-level system, and study both the optical decay, in Chapter V, and the optical single-qubit rotations, in Chapter VII, where we also review other schemes for single optical spin rotations.
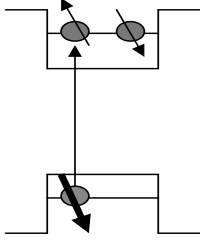
II.4 Valence and conduction band in a single-particle depiction of the optical excitation. The laser excites an electron-hole pair. The composite three-particle state is the trion.
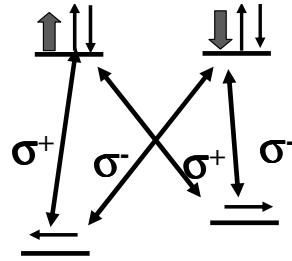
II.5 Two independent three-level Λ systems, depending on the sense of circular polarization of the exciting laser. The lower levels are the electron spin states along x and the excited states are the two heavy-hole trions.

III.

Elements of Semiclassical and Quantum Optics

As artificial atoms, quantum dots feature many of the phenomena of quantum optics of atoms. Examples of such effects that have been observed in dots are photon anti-bunching [94], Rabi oscillations [129], and AC Stark shift [133]. In this Chapter we provide an introduction to concepts of semiclassical and quantum optics that are also relevant in quantum dots. The term semiclassical optics implies that the system (atom, quantum dot, molecule) is treated quantum mechanically, but the light is treated classically. For example, in the excitation process, the incoming laser beam contains a large number of photons that it allows for a semiclassical treatment. On the other hand, to derive spontaneous emission, quantum mechanical treatment of radiation is needed, as the vacuum fluctuations play an important role.

A.   Light-Matter Interaction Basics

The coupling Hamiltonian between an atom and a laser is given by $\hat{\mathbf{d}} \cdot \mathbf{E}$, where $\hat{\mathbf{d}}$ is the dipole operator and $\mathbf{E}$ is the electric field. In a full quantum

mechanical formulation, the electric field is also an operator, given by

$$\mathbf{E}(\mathbf{r}, t) = i \sum_j \sqrt{\frac{\hbar \omega_j}{2 V \epsilon_0}} \left[\hat{\varepsilon}_j a_j e^{i \mathbf{k}_j \cdot \mathbf{r} - i \omega_j t} - \hat{\varepsilon}_j^* a_j^\dagger e^{-i \mathbf{k}_j \cdot \mathbf{r} + i \omega_j t} \right], \quad \text{(III.1)}$$

where ω_j is the frequency, ε_j is the polarization and $a_j^\dagger$ (a_j) is the creation (anni-hilation) operator of a photon in mode j. The exponent multiplying the creation and annihilation operator may be expanded in a Taylor series $e^{i \mathbf{k} \cdot \mathbf{r}} = 1 + i \mathbf{k} \cdot \mathbf{r} + \dots$. Given that the wave vector of light is at least two orders of magnitude larger than a typical size of an atom, usually linear and higher terms in $\mathbf{k} \cdot \mathbf{r}$ are neglected. This is the so-called dipole approximation.

The coupling between the field and the system can also be written

$$(\mathbf{d} \sigma^\dagger + \mathbf{d}^* \sigma) i \sum_j \sqrt{\frac{\hbar \omega_j}{2 V \epsilon_0}} \left[\hat{\varepsilon}_j a_j e^{i \mathbf{k}_j \cdot \mathbf{r} - i \omega_j t} - \hat{\varepsilon}_j^* a_j^\dagger e^{-i \mathbf{k}_j \cdot \mathbf{r} + i \omega_j t} \right], \quad \text{(III.2)}$$

where $\sigma^\dagger$ (σ) is the raising (lowering) operator and $\mathbf{d}$ is the dipole matrix element for a given transition in the atom. In Eq. (III.2) there are four terms. Two of these are energy conserving and physically correspond to the excitation (de-excitation) of an atom –or other quantum system– by the absorption (emission) of a photon.

The other two terms are not energy conserving, and they express the ex-citation (de-excitation) of the system by emission (absorption) of a photon. These terms are usually dropped. This is the so-called rotating-wave approximation (RWA). However, as with any approximation, care should be exercised in some cases (see ref. [70] for an example where RWA is not valid).

A photon is characterized by its frequency, by its propagation direction, and by its polarization. It has spin-1 and hence is a vector field. Not all photons can be absorbed by a given transition. It is well known that the resonance condition is required, i.e., the energy of the single absorbed photon should match a transition frequency of the atom (or molecule, or dot). There are more such *selection rules* related to the polarization degree of freedom. A photon can excite (or de-excite) a $|\Delta L| = 1$ transition only, due to its vector character. A list of dipole selection rules follows.

- $\Delta n = \pm 1$

- $\Delta L = \pm 1$

- $\Delta S = 0$

- $\Delta J = 0, \pm 1$, except $0 \longleftrightarrow 0$

- $\Delta M_J = 0, \pm 1,$

where n, L, S, J, M_J are the principal (energy) quantum number, the orbital angular momentum, the spin, the total angular momentum and the projection of the latter along the quantization axis. When hyperfine coupling is included (i.e., coupling between the electron and nuclear spin) there is the extra selection rule $\Delta F = 0, \pm 1$, and M_J is replaced by M_F.

B. Two-Level Systems

Two-level systems have been studied widely in quantum mechanics, as they constitute the simplest non-trivial quantum systems. The electron spin is a natural two-level system. As we show in this Section, any two-level system can be mapped onto a spin-1/2 [49], and is sometimes called a pseudospin. Recently, two-level systems have attracted a lot of attention due to their fundamental importance in Quantum Computing and Quantum Information Processing. The term qubit (unit of quantum information, physically implemented by two-level quantum systems) is sometimes used in the quantum information community to refer to a generic two-level system.

1. Rabi Oscillations

A well-known example of interaction of matter with radiation is the Rabi problem. It comprises an example of reversible transitions of a two-level system due to its coupling with radiation. We follow in large ref. [126]. Consider a two-level system (spin in a static magnetic field, atom, etc) of energy splitting ω_o

interacting with a time-dependent field (r.f. magnetic field, laser, etc) of frequency ω. We define the following quantities

$$\Delta = \omega_o - \omega \tag{III.3}$$

$$\Omega_R = 2\mathbf{d} \cdot \mathbf{E}. \tag{III.4}$$

The latter is called the Rabi frequency, and it constitutes a measure of the strength of the driving field. The Hamiltonian in the dipole and RWA is

$$H = \frac{1}{2} \begin{bmatrix} -\omega_o & \Omega_R e^{i\omega t} \\ \Omega_R e^{-i\omega t} & \omega_o \end{bmatrix}. \tag{III.5}$$

In a rotating frame, defined by the transformation $\mathcal{W} = diag(e^{i\omega t/2}, e^{-i\omega t/2})$, the Schrödinger's equation becomes

$$i\frac{d}{dt} \begin{bmatrix} c_1 \\ c_2 \end{bmatrix} = \frac{1}{2} \begin{bmatrix} -\Delta & \Omega_R \\ \Omega_R & \Delta \end{bmatrix} \begin{bmatrix} c_1 \\ c_2 \end{bmatrix}. \tag{III.6}$$

The resulting equation III.6 has the form of the time-independent Schrödinger equation with a constant potential. Defining

$$\Omega = \sqrt{\Omega_R^2 + \Delta^2}, \tag{III.7}$$

which is sometimes called the grand or effective Rabi frequency, and also

$$\cos\theta = \Delta/\Omega, \tag{III.8}$$

the eigenstates are

$$\psi_+ = \begin{bmatrix} \sin\frac{\theta}{2} \\ \cos\frac{\theta}{2} \end{bmatrix} \tag{III.9}$$

$$\psi_- = \begin{bmatrix} \cos\frac{\theta}{2} \\ -\sin\frac{\theta}{2} \end{bmatrix}, \tag{III.10}$$

with corresponding eigenvalues $\pm\Omega/2$. Taking the initial condition to be that the system is in the lower state, we find for the time evolved state *in the interaction*

picture

$$\Psi(t) = \begin{bmatrix} -i \sin\theta \ \sin(\Omega t/2) \ e^{-i\Delta t/2} \\ \cos(\Omega t/2) - i\cos\theta \ \sin(\Omega t/2) \ e^{i\Delta t/2} \end{bmatrix}. \qquad \text{(III.11)}$$

After the application of the time-dependent field, the probability of finding the system in the excited state at time t is given by

$$P(t) = \frac{1}{2}\sin^2\theta \left[1 - \cos(\Omega t)\right]. \qquad \text{(III.12)}$$

There are two important facts to remember from equation III.12; one is that it oscillates with the effective Rabi frequency, and the other is that the maximum is 1 only in the case of resonance ($\Delta=0$). In general, for random t the system is in a superposition of the two states.

In the above treatment, we have assumed that Ω_R is time independent. Actually, we may generalize the above results for a time-dependent, slowly varying envelope. In that case, the area of the pulse is defined as

$$\mathcal{A} = 2\int dt\, \Omega_R(t), \qquad \text{(III.13)}$$

and for a resonant pulse it expresses the angle by which the Bloch vector, defined in the next subsection, has been rotated by the pulse. For an atom initially in the ground state, a resonant π-pulse transfers all the population to the excited state.

2. Bloch Vector

The spin $1/2$ is a well-known representation of SU(2). It has some unusual characteristics compared to the familiar three-vectors; after a 2π rotation it does not return to the initial state, but acquires a minus sign. An arbitrary pure spin state is characterized by two real numbers, since the state is normalized and an overall phase is immaterial. Thus, as was first shown by Bloch, it can be mapped onto a vector on a unit sphere (called the 'Bloch sphere'), expressed in terms of the two angles, the polar ϑ and the azimuthal φ. It is called Bloch vector or spin vector (SV). For a general state, which can be partially or fully mixed, the spin

vector has length smaller than one. A completely mixed state corresponds to a SV of length zero (no spin polarization). Given a density matrix ρ, the SV is

$$\overrightarrow{S} = \text{Tr}(\widehat{S}\rho), \qquad\qquad (\text{III.14})$$

where $\widehat{S} = \sum_i \hat{i}\sigma_i$, the σ_i's are the Pauli matrices, the $\hat{i}$'s are the cartesian unit vectors.

C.   Decay and Decoherence

It is well known that *closed* quantum systems obey the Schrödinger equation and are thus governed by unitary evolution. On the other hand, *open* quantum systems are usually characterized by non-unitary evolution. A familiar example is an atom in an excited state, which spontaneously decays via the emission of a photon. To take into account non-unitary dynamics, a density matrix replaces the usual wavefunction formalism. Then using a master equation approach, rate equations can be found for the density matrix. In place of the Schrödinger equation, a Liouville-von Neumann (L-VN) equation expresses the time evolution of the density matrix, and the non-unitary dynamics are described by the so-called Lindblad operators L_j, which form a semigroup (meaning that there are no inverse elements in the group). The L-VN equation is governed by unitary dynamics. Including dissipative terms, the general form of the evolution (Lindblad equation) is

$$\dot{\rho} = i[\rho, H] - \frac{1}{2}\sum_j \left(\{L_j^\dagger L_j, \rho\} - 2L_j\rho L_j^\dagger\right). \qquad\qquad (\text{III.15})$$

To find the operators L_j a master equation is solved. The general process is that the density matrix of the whole system (atom + reservoir) is considered, and the L-VN equation is iterated, so that the coupling between system and reservoir is taken up to second order in perturbation theory. A partial trace of the reservoir is taken, leading to the relevant rate equations for the system, which express decay and decoherence. By decay we refer to the leak of population out of a state or set of states and by decoherence the loss of phase coherence, but the term decoherence

is sometimes used to refer to both population and coherence loss. A detailed derivation of spontaneous emission equations via a master equation is given in Chapter V.

D.   Unitary Versus Non-Unitary Dynamics

The dominant view of spontaneous emission and in general non-unitary dynamics is that they cause decoherence and/or decay. However, this view does not always hold. In general the following is true for unitary (U) and non-unitary (Λ) evolution:

- pure state $\xrightarrow{U}$ pure state

- mixed state $\xrightarrow{U}$ mixed state

- pure state $\xrightarrow{\Lambda}$ mixed/pure state

- mixed state $\xrightarrow{\Lambda}$ pure/mixed state

The first two are easily seen by using the definition of the purity of a state, $\mathcal{P} = \mathrm{Tr}(\rho^2)$. Then for the time-evolved density matrix we have

$$\mathcal{P}' = \mathrm{Tr}(\rho'^2) = \mathrm{Tr}\left(\left[U^\dagger \rho U\right]^2\right) = \mathrm{Tr}\left(U^\dagger \rho U U^\dagger \rho U\right) = \mathrm{Tr}\left(U^\dagger \rho^2 U\right) = \mathrm{Tr}(\rho^2) = \mathcal{P}.$$

In the last but one step we have used the cyclic property of the trace. We have hence shown that a unitary operation cannot change the purity of a density matrix. For the remaining two cases in the list we shall use examples. A pure state becoming mixed when subjected to non-unitary evolution is a common situation. A pure state remaining pure under non-unitary evolution will be investigated in great detail in Chapters V and VI. A familiar example is a two-level system, initially in the excited state. After a long time compared to the decay time, the final state is the ground state, i.e., a pure state. An example of a mixed state becoming pure under non-unitary evolution is again a two-level system initially in a complete mixture of the two states. Again, after long enough time so that the decay will have taken place, the final state is the ground state, a pure state.

1. Optical Pumping

It is clear from the above discussion that in order to initialize a system (that is, steer it from a mixed into a pure state), unitary evolution is not sufficient. Non-unitary dynamics are necessary, in order for entropy to be removed from the system. A common way of initializing a system in atomic physics is through so-called optical pumping. The basic idea is to use a laser, which populates an excited, unstable state. This state will decay, thus increasing the purity of the system. For example, consider a three-level system with two lower levels and a single excited state. Initially, the system is in a mixture of the two lower levels. If a π pulse, focused only at the one transition, is used then all the population from that level will be transferred to the excited state. Assuming equal decay to the two lower levels, the population of the one state, after the decay, will have increased by 0.25, while the other's will have decreased by the same amount. Repeating this process several times can asymptotically transfer all the population to the one of the two lower levels and thus initialize the system. We will also discuss optical pumping in the context of a quantum dot in Chapters V and especially VII.

E. Strong field effects

When the laser is strong, sometimes a more intuitive understanding of the physics is achieved by considering the eigenstates of the total atomic Hamiltonian, including the dipole coupling. The states of the atom are then called dressed states, since they can be viewed as the bare atomic states 'dressed' by the radiation.

Strong field effects known from atomic physics that have been recently studied in semiconductors include coherent population trapping [50] in bound donors in the bulk and electromagnetically induced transparency (EIT) [59, 106] in quantum wells. EIT in its simplest version requires a three-level system and two strong optical fields. The basic idea is that when the one transition is strongly driven by the one field, then the system becomes transparent to a field of given

strength resonant with the other transition. This means that the absorption is cancelled, owing to destructive quantum interference of two pathways, and the speed of the light in the medium becomes very small or zero. This has significant implications in quantum technologies in general, as it allows for slow or stopped light, which would form a basis of a quantum memory. EIT has also been proposed as a mechanism to generate a Kerr effect, i.e., effective (nonlinear) coupling of photons [120].

F.   Interaction of Laser with Ensembles

An ensemble of systems, for example an ensemble of atoms or quantum dots is quite different than a single such system. In atomic physics, there are effects such as collisions between atoms, which have to be taken into account in the study of the dynamics. In quantum dots, there is the issue that all the dots are not identical, and therefore when an ensemble quantity is calculated, an average has to be taken of this quantity over the ensemble. Moreover, in the quantum dots, the trapped electron interacts with a large number of nuclear spins, about $10^5 - 10^6$, via hyperfine coupling. Each spin is subject to a different local magnetic field created by the nuclear spins. This is an extra inhomogeneous contribution, and typically gives rise to dephasing mechanisms, not related to population decay, called pure dephasing. The dephasing time of an ensemble is called T_2^*, taken from NMR literature, and includes both dephasing originating from population relaxation and pure dephasing.

In some cases, the radiation propagates inside the ensemble, i.e., the emitted radiation from one part of an ensemble is reabsorbed by another. Then in the theoretical treatment, the spatial degree of freedom is kept, and the Schrödinger-Maxwell equations are solved. An example of an ensemble effect of matter-radiation coupling is the so-called Self Induced Transparency (SIT) of McCall and Hahn [91]. In this phenomenon, resonant 2π sech pulses are used, which have the special prop-

erty that they do not lose their shape or get attenuated as they propagate in the medium (solitons). SIT has also been theoretically investigated in an ensemble of quantum dots [104].

G. Types of Pulses

Light coming out of a laser may be pulsed or continuous. In the former case, the pulse shape is an important feature of the laser and may play an important role on the coupling with matter. A comparative study of various commonly used pulse shapes is given in [11]. On the other hand, when the laser is not pulsed but comes out continuously[1] it is called continuous wave (CW).

Pulsed lasers are amplitude modulated by definition. A laser can also have phase modulation, which means that the central frequency is not a constant, but varies with time. Frequency modulation is also called 'chirping'.

A laser is not completely monochromatic. From the time-frequency uncertainty relation, it is clear that a monochromatic laser field would correspond to infinitely long pulses. Pulsed lasers are characterized by their bandwidth, which expresses the size of the frequency range about the central frequency of the laser. When a pulse has the minimum time length allowed by its spectrum it is called transform limited, or Fourier-transform limited.

H. Three-Level Systems

Three-level systems involve two dipole transitions. There are three types of three-level systems, all taking their names from Greek and Latin letters: Λ systems, which have two lower levels coupled to an excited one, Ξ (or cascade) systems, which have an excited state coupled to a lower state, coupled to a ground state, and V systems, which have one ground state coupled to two excited states, as

---

[1]clearly, there is a rising and falling time, and the pulse itself has a finite duration, but it is still long enough to be thought of as continuous.
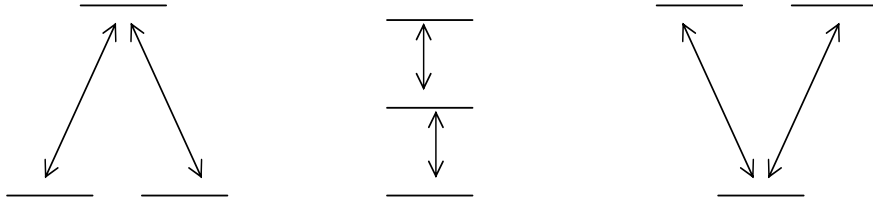
III.1   Three-level systems in the Λ, Ξ and V configurations respectively.

shown in Fig. III.1. Λ systems appear in quantum computing schemes [61, 32, 19], as it is sometimes preferable to couple the two qubit states via a Raman transition to an auxiliary excited state. They are also important in coherent population trapping, lasing without inversion and EIT. In this dissertation Λ systems will be extensively studied. V systems also appear in quantum computing schemes with excitons [12, 131, 24].

I.   Quantum Optics

In the previous Sections of this Chapter we focused on semiclassical optics. In the context of quantum dots, quantum optics appear in master equations for the derivation of spontaneous emission, which we present in Chapter V.

Quantum optics also appear in schemes involving cavities, where a single mode or a finite number of electromagnetic modes are allowed. Cavities are relevant in many quantum information processing schemes besides quantum computing, such as quantum networks [98, 147] and quantum memory architectures [89]. The original proposed scheme of quantum information processing with optically controlled spins in quantum dots made use of a cavity in order to achieve two-qubit operations [61]. In atomic physics, cavities are usually implemented by mirrors and they are called optical cavities. In semiconductors, they are are called microcavities, due to their size which is in the micron range. They can be micropillar structures, microdiscs, or defects in photonic crystals. An advantage of

the quantum-dot–microcavity system as compared to the atom in an optical cavity is that the quantum dot, unlike the atom, does not require to be trapped inside the microcavity since its position is fixed by its growth and thus, unlike the atom, does not exhibit motional thermal fluctuations.

1.   Quantum Optics with Quantum Dots

In the recent years there has been considerable interest in quantum optics with quantum dots. In particular, quantum dots are being researched for their potential use as single-photon sources on demand [119, 95, 153, 150] from the lowest excitonic transition. Single-photon sources are of importance in quantum information tasks, such as quantum cryptography (for a review, see [54]) and linear optics quantum computing [80]. Compared to other quantum single-photon sources, such as single atoms, ions, molecules, and defects (e.g. nitrogen vacancies in diamond) the advantages of the QDs are their radiative efficiency, their tailored emission properties, their compatibility with semiconductor technology and their integrability in cavities, so that spontaneous emission may be controlled. The main challenges are the required low temperatures and the problem of photon extraction out of the solid.

Another application of quantum optics in quantum dots is entangled photon generation [47, 2]. The states used in this case are the biexciton cascade (Ξ) transition. The two emitted photons have opposite linear polarizations as we have discussed in Chapter II, so for some emission directions they are polarization-entangled. However, they are distinguishable in frequency, and therefore spectral filtering has been used to erase the which-path information and produce an entangled state [2]. Alternatively, a quantum eraser could be employed to the same end. Again, the advantage of using quantum dots for entangled photon generation is the fast spontaneous emission rate in the dots and the integrability with semiconductor technology.

IV.

Mathematical Description of the Optical Processes in Coherent Nonlinear Pump-Probe Experiments

Nonlinear pump-probe experiments have been used to measure the spin state of an electron in a dot [41], and the excitonic state in a dot [129], and can be used both for a single dot measurement and for an ensemble measurement. In the single dot case, near-field techniques are used, such as coated fiber tips and masks with apertures. The latter method involves an aluminum mask with submicron apertures, opened with electron beam lithography. The small size of the apertures results in the scattering of the passing beams, and thus a lens is used to collect the scattered light.

The pump is used to create spin polarization and the probe to measure it. In the experiments, what is measured is differential transmission of the probe, which is the transmission of the probe beam in the presence of the pump minus the transmission of the probe in the absence of the pump (hence differential), as a function of the time delay between pump and probe. In the following section we

will provide some further details on how this is achieved experimentally.

A. Homodyne-detected Nonlinear Response and Differential Transmission Signal

To understand how this works, first we will expand the density matrix ρ of the system in the presence of the electric field of the laser beam in a sum

$$\rho = \sum_{n=0}^{\infty} \rho^{(n)},$$

where $\rho^{(n)}$ expresses the contribution to n^{th} order in the applied electric field, then clearly the odd terms are optical coherences (or polarizations) and the even terms are populations, and the sum of the terms of a given order in the sum is not necessarily a density matrix itself. The optical polarization is

$$\mathbf{P}^{(n)} = \mathrm{Tr}(\rho^{(n)}\mathbf{d}),$$

where $\mathbf{d}$ is the optical dipole operator. For weak fields, the lowest nonlinear polarization is of third order. It can be expressed as

$$P^{(3)}(\omega) = \chi^{(3)}(\omega = \omega_\ell - \omega_m + \omega_n)\widetilde{E}_\ell \widetilde{E}_m^* \widetilde{E}_n,$$

where $\chi^{(3)}$ is the third order nonlinear susceptibility. In the case of two fields, the pump and the probe, the two first fields come from the pump and the third from the probe. To experimentally isolate the third order response from the much stronger transmitted field and from the linear response, the intensities of the the two fields are amplitude modulated at different frequencies, by use of acousto-optical modulators. The two signals are homodyne-detected at the difference of the two frequencies. Using the index α for the pump and β for the probe, we will sketch why this is the case. For more details, see ref. [28]. The total photocurrent is proportional to the intensity

$$\left| \sum_{k=\alpha,\beta} (\mathbf{E}_k + \mathbf{E}_k^{(1)}) + \mathbf{E}^{(3)} \right|^2 = \left| \sum_{k=\alpha,\beta} (\mathbf{E}_k + \mathbf{E}_k^{(1)}) \right|^2 + \left| \mathbf{E}^{(3)} \right|^2$$

$$+2 \sum_{k=\alpha,\beta} \Re(\mathbf{E}^{(3)} \cdot (\mathbf{E}_k^{(1)})^*) + 2 \sum_{k=\alpha,\beta} \Re(\mathbf{E}^{(3)} \cdot \mathbf{E}_k^*). \qquad \text{(IV.1)}$$

Let us examine now the various terms of Eq. (IV.1). The first term is clearly not modulated at the difference frequency, since it is the intensity that gets modulated and not the electric field. The second term has the right modulation frequency, but it will be negligible in the weak field regime. The third term is also weak and will be dropped. Therefore, the strongest term that oscillates at the right frequency and is therefore detected is the last term of Eq. (IV.1).

Now we shall show why this term is equivalent to the differential transmission signal (DTS). In the absence of the pump, the signal is

$$T_{off} = \left| \mathbf{E}_\beta + \mathbf{E}_\beta^{(1)} + \mathbf{E}_\beta^{(3)} \right|^2, \qquad \text{(IV.2)}$$

where $\mathbf{E}_\beta^{(3)}$ is the nonlinear signal originating from the probe only. In the presence of the pump, the signal instead is

$$T_{on} = \left| \mathbf{E}_\beta + \mathbf{E}_\beta^{(1)} + \mathbf{E}_\beta^{(3)} + \mathbf{E}_\alpha + \mathbf{E}_\alpha^{(1)} + \mathbf{E}_\alpha^{(3)} + \mathbf{E}_{\alpha\beta}^{(3)} \right|^2. \qquad \text{(IV.3)}$$

We assume that the pump and probe propagate along different directions. Taking the difference between Eqs. (IV.3) and (IV.2), again neglecting higher order terms, and retaining only terms that propagate along the probe field direction we find

$$T_{on} - T_{off} \propto 2\Re(\mathbf{E}_\alpha^* \cdot \mathbf{E}_{\alpha\beta\beta}^{(3)}). \qquad \text{(IV.4)}$$

B. Density Matrix Control and Measurement

Now we shall focus on the three-level system, consisting of the two spin states of the excess electron in the dot and the trion state. The magnetic field is in the so-called Voigt geometry, which means that the external static magnetic field is in the plane. The following analysis will include, besides the pump and probe pulses, a control pulse as well. This is necessary if we want to talk about optical control of the spin. The pump pulse is used to initialize the spin, the control

pulse ideally rotates it or more generally controls it, and the probe measures it. To ensure that the spin vector measured is the one initialized by the pump and controlled by the control pulse, the pump and probe should be acousto-optically modulated as explained above, and the control will remain unmodulated, so its effect is measured to all orders. In what follows, we will not include the probe explicitly, but we will keep in mind the above analysis and keep only the relevant terms that the probe will detect.

We take the initial state of the system to be a mixture of the two spin states. The density matrix is

$$\rho^{(0)} = \begin{bmatrix} 1/2 & 0 & 0 \\ 0 & 1/2 & 0 \\ 0 & 0 & 0 \end{bmatrix}, \tag{IV.5}$$

where the superscripts denote the order in the applied electric field. No superscript indicates that all orders are kept.

Assume that the pump, acting at $t = 0$, is circularly polarized $\sigma-$ pulse of area $\Delta\theta \equiv 2\int E(t)dt$. For simplicity, we also take the pulses to be instantaneous. The bandwidth of the pulses is thus large enough to cover both transitions. Then, right after the action of the pulse, the system in the $\{|z\rangle, |\bar{z}\rangle, |\bar{\mathcal{T}}\rangle\}$ basis is described by

$$\rho = \begin{bmatrix} 1/2 & 0 & 0 \\ 0 & 1/2 - P_\alpha & 0 \\ 0 & 0 & P_\alpha \end{bmatrix}, \tag{IV.6}$$

where P_α is the population transferred to the trion. We also ignore spontaneously generated coherence (explained in the following Chapter), which means that the trion equally decays to the two spin basis states and this decay can be taken to be instantaneous. Then the density matrix is

$$\rho = \begin{bmatrix} 1/2 + P_\alpha/2 & 0 & 0 \\ 0 & 1/2 - P_\alpha/2 & 0 \\ 0 & 0 & 0 \end{bmatrix}, \tag{IV.7}$$

In the experiment, acousto-optical modulation of the pump and probe, as explained above, ensures that only the part P_α is measured. We can separate ρ in the following way

$$\sum_{n=1}^{\infty} \rho^{(n)} = \rho - \rho^{(0)} = \begin{bmatrix} 1/2 + P_\alpha/2 & 0 & 0 \\ 0 & 1/2 - P_\alpha/2 & 0 \\ 0 & 0 & 0 \end{bmatrix} - \begin{bmatrix} 1/2 & 0 & 0 \\ 0 & 1/2 & 0 \\ 0 & 0 & 0 \end{bmatrix}$$

$$= \begin{bmatrix} P_\alpha/2 & 0 & 0 \\ 0 & -P_\alpha/2 & 0 \\ 0 & 0 & 0 \end{bmatrix} \equiv \tilde{\rho}_\alpha. \tag{IV.8}$$

The latter is the part of the density matrix that is measured; note that it is not a density matrix itself. We will proceed the analysis keeping only this part of the density matrix, $\tilde{\rho}_\alpha$, the tilde reminding us that we are not looking at a density matrix, but at a part of one. The effect of the control pulse on the mixed part of the density matrix will be similar to the pump pulse to create some polarization. This will not be modulated at the pump frequency, and so it will not be detected. For completeness we write it here:

$$\rho - \tilde{\rho}_{\alpha\beta} = \begin{bmatrix} 1/2 + P_\beta/2 & 0 & 0 \\ 0 & 1/2 - P_\beta/2 & 0 \\ 0 & 0 & 0 \end{bmatrix}. \tag{IV.9}$$

It is common in experiments to use a probe of the same circular polarization (SCP) as the pump, and then repeat the experiment with a probe of opposite circular polarization (OCP) and subtract the signals. This way irrelevant terms are subtracted off, reducing the noise and amplifying the measurement of the spin vector.

$$\text{DTS} \sim \text{DTS}(\sigma-) - \text{DTS}(\sigma+) = \rho_{\bar{T}\bar{T}} + (\rho_{zz} - \rho_{\bar{z}\bar{z}}) = \rho_{\bar{T}\bar{T}} - <S_z>. \tag{IV.10}$$

From Eq. (IV.10) it is clear that when both probe polarizations are used and the signals are subtracted after the decay of the trion what it is measured is the z component of the spin vector.

C. Derivation of expression for the spin vector

The Hamiltonian in the z basis is

$$H^o = \begin{bmatrix} 0 & \omega_B & 0 \\ \omega_B & 0 & 0 \\ 0 & 0 & \epsilon_{\mathcal{T}} \end{bmatrix}, \tag{IV.11}$$

and the unitary operation representing the precession about the B-field is given by

$$U_{pr}(t) = \begin{bmatrix} \cos(\omega_B t) & -i\sin(\omega_B t) & 0 \\ -i\sin(\omega_B t) & \cos(\omega_B t) & 0 \\ 0 & 0 & e^{-i\epsilon_{\mathcal{T}} t} \end{bmatrix}. \tag{IV.12}$$

Then at time t the $\sum_{n=1}^{\infty} \rho^{(n)}$ part of the density matrix is given by

$$\tilde{\rho}_\alpha(t) = U_{pr}(t)\tilde{\rho}_\alpha U_{pr}^\dagger(t) = \frac{P_\alpha}{2} \begin{bmatrix} \cos(2\omega_B t) & i\sin(2\omega_B t) & 0 \\ -i\sin(2\omega_B t) & -\cos(2\omega_B t) & 0 \\ 0 & 0 & 0 \end{bmatrix} \tag{IV.13}$$

Now, let us consider a control pulse, acting at time $t = t_c$, i.e., when

$$\tilde{\rho}_\alpha(t_c) = \frac{P_\alpha}{2} \begin{bmatrix} \cos(2\omega_B t_c) & i\sin(2\omega_B t_c) & 0 \\ -i\sin(2\omega_B t_c) & -\cos(2\omega_B t_c) & 0 \\ 0 & 0 & 0 \end{bmatrix}, \tag{IV.14}$$

which is described by the Hamiltonian

$$H_c(t) = \begin{bmatrix} 0 & 0 & 0 \\ 0 & 0 & \Omega(t - t_c) \\ 0 & \Omega^*(t - t_c) & 0 \end{bmatrix}, \tag{IV.15}$$

The control is also taken to be instantaneous (no spin precession during its action) and of area $\Delta\theta$. Then the unitary transformation induced by the control is

$$U_c = \begin{bmatrix} 1 & 0 & 0 \\ 0 & \cos(\frac{\Delta\theta}{2}) & -i\sin(\frac{\Delta\theta}{2}) \\ 0 & -i\sin(\frac{\Delta\theta}{2}) & \cos(\frac{\Delta\theta}{2}) \end{bmatrix}. \tag{IV.16}$$

And right after the action of the control we have

$$\tilde{\rho}_{\alpha\beta} = U_c\tilde{\rho}_\alpha(t_c)U_c^\dagger$$

$$= \frac{P_\alpha}{2} \begin{bmatrix} \cos(2\omega_B t_c) & i\sin(2\omega_B t_c)\cos(\frac{\Delta\theta}{2}) & -\sin(2\omega_B t_c)\sin(\frac{\Delta\theta}{2}) \\ -i\sin(2\omega_B t_c)\cos(\frac{\Delta\theta}{2}) & -\cos(2\omega_B t_c)\cos^2\frac{\Delta\theta}{2} & -\frac{i}{2}\cos(2\omega_B t_c)\sin(\Delta\theta) \\ -\sin(2\omega_B t_c)\sin(\frac{\Delta\theta}{2}) & \frac{i}{2}\cos(2\omega_B t_c)\sin(\Delta\theta) & -\cos(2\omega_B t_c)\sin^2\frac{\Delta\theta}{2} \end{bmatrix}. \tag{IV.17}$$

Then, *right after* the control pulse, the DTS is given by

$$\mathrm{DTS}(\Delta\theta, t_c) = -\frac{P_\alpha}{2}\cos(2\omega_B t_c)\sin^2\left(\frac{\Delta\theta}{2}\right) + \frac{P_\alpha}{2}\cos(2\omega_B t_c)\left(1 + \cos^2\left(\frac{\Delta\theta}{2}\right)\right), \tag{IV.18}$$

and the difference $\mathrm{DTS}(\Delta\theta, t_c)$-$\mathrm{DTS}(\Delta\theta = 0, t_c)$, which might be easier to compare with experiment, equals

$$\mathrm{DTS}(\Delta\theta, t_c) - \mathrm{DTS}(\Delta\theta = 0, t_c) =$$
$$-\frac{P_\alpha}{2}\cos(2\omega_B t_c)\sin^2\left(\frac{\Delta\theta}{2}\right) + \frac{P_\alpha}{2}\cos(2\omega_B t_c)\left(1 + \cos^2\left(\frac{\Delta\theta}{2}\right)\right) - P_\alpha\cos(2\omega_B t_c), \tag{IV.19}$$

which becomes

$$\mathrm{DTS}(\Delta\theta, t_c) - \mathrm{DTS}(\Delta\theta = 0, t_c) = -\frac{P_\alpha}{2}(1 - \cos(\Delta\theta))\cos(2\omega_B t_c). \tag{IV.20}$$

After the trion decay, we have:

$$\tilde{\rho}'_{\alpha\beta} = \frac{P_\alpha}{2}\times$$

$$\begin{bmatrix} \cos(2\omega_B t_c) - \frac{1}{2}\cos(2\omega_B t_c)\sin^2\frac{\Delta\theta}{2} & i\sin(2\omega_B t_c)\cos(\frac{\Delta\theta}{2}) & 0 \\ -i\sin(2\omega_B t_c)\cos(\frac{\Delta\theta}{2}) & -\cos(2\omega_B t_c)\cos^2\frac{\Delta\theta}{2} - \frac{1}{2}\cos(2\omega_B t_c)\sin^2\frac{\Delta\theta}{2} & 0 \\ 0 & 0 & 0 \end{bmatrix}.$$

And at a later time, after precession, it is given by

$$\tilde{\rho}_{\alpha\beta}(t) = U_{pr}(t - t_c)\tilde{\rho}'_{\alpha\beta}U^{\dagger}_{pr}(t - t_c) \tag{IV.21}$$

The matrix elements of $\tilde{\rho}_{\alpha\beta}(t) \equiv R$ are

$$\begin{aligned}
R_{11} &= \frac{P_\alpha}{8}\Big[(3 + \cos\Delta\theta)\cos\left(2\omega_B(t - t_c)\right)\cos(2\omega_B t_c) \\
&\quad - 4\cos\frac{\Delta\theta}{2}\sin\left(2\omega_B(t - t_c)\right)\sin(2\omega_B t_c)\Big] \tag{IV.22} \\
R_{12} &= \frac{iP_\alpha}{4}\Big[\frac{1}{2}(3 + \cos\Delta\theta)\sin\left(2\omega_B(t - t_c)\right)\cos(2\omega_B t_c) \\
&\quad + 2\cos\frac{\Delta\theta}{2}\cos\left(2\omega_B(t - t_c)\right)\sin(2\omega_B t_c)\Big] \tag{IV.23} \\
R_{22} &= -\frac{P_\alpha}{8}\Big[(3 + \cos\Delta\theta)\cos\left(2\omega_B(t - t_c)\right)\cos(2\omega_B t_c) \\
&\quad - 4\cos\frac{\Delta\theta}{2}\sin\left(2\omega_B(t - t_c)\right)\sin(2\omega_B t_c)\Big] = -R_{11} \tag{IV.24} \\
R_{21} &= R_{12}^*. \tag{IV.25}
\end{aligned}$$

The z projection of the associated spin vector is given by

$$\begin{aligned}
< S_z^{\alpha\beta}(t) > &= R_{11} - R_{22} \\
&= \frac{P_\alpha}{4}\Big[(3 + \cos\Delta\theta)\cos\left(2\omega_B(t - t_c)\right)\cos(2\omega_B t_c) \\
&\quad - 4\cos\frac{\Delta\theta}{2}\sin\left(2\omega_B(t - t_c)\right)\sin(2\omega_B t_c)\Big] \tag{IV.26}
\end{aligned}$$

To summarize, the measured spin vector (SV) affected by the action of a resonant $\sigma-$ control pulse of area $\Delta\theta$ at time t_c is given by

$$\begin{aligned}
< S_z^\alpha > &= P_\alpha\cos\left(2\omega_B t\right) \quad \text{for } t < t_c, \quad \text{and} \tag{IV.27} \\
< S_z^{\alpha\beta}(t) > &= \frac{P_\alpha}{4}\Big[(3 + \cos\Delta\theta)\cos\left(2\omega_B(t - t_c)\right)\cos(2\omega_B t_c) \\
&\quad - 4\cos\frac{\Delta\theta}{2}\sin\left(2\omega_B(t - t_c)\right)\sin(2\omega_B t_c)\Big] \text{ for } t > t_c. \tag{IV.28}
\end{aligned}$$

From Eq. (IV.28) we see that for any pulse area other that $\Delta\theta = 2\pi$ there will be population transfer to the trion, *with subsequent reduction of the size of the spin vector through the trion decay.*

Let us take a look at the case $\Delta\theta = \pi$. Then the SV for $t > t_c$ is given by:

$$< S_z^{\alpha\beta}(t; \Delta\theta = \pi) >= \frac{P_\alpha}{4} \left[\cos(2\omega_B t) + \cos\left(2\omega_B(t - 2t_c)\right) \right]. \qquad \text{(IV.29)}$$

From Eq. (IV.29), we can see what happens to the SV depending on the incidence time of the control pulse, t_c. For $tc = n\pi/2\omega_B$, with n integer, which is when the SV is pointing along $\pm z$, the SV after the control pulse keeps precessing with the same phase but with the amplitude reduced to half. On the other hand, when $tc = \frac{(2n+1)}{4}\pi/\omega_B$, i.e., SV pointing along y, the SV vanishes after the control pulse. These conclusions are in agreement with the numerical simulations, shown in Figs. IV.1 and IV.2.
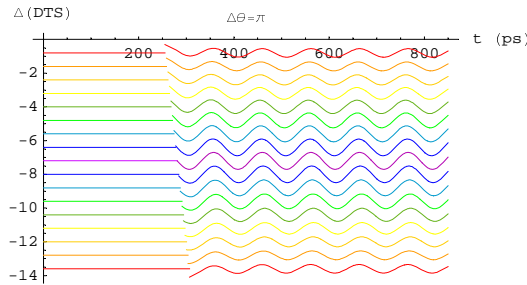
IV.1   Difference in DTS signals between a control pulse with area π and no control for varying t_c, based on the simple analytical model.
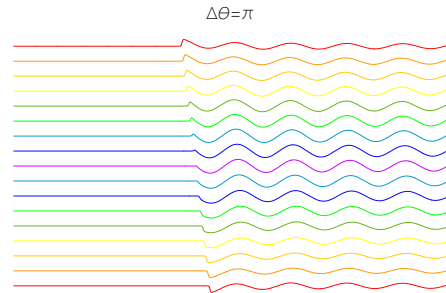
IV.2   Numerical simulation of the difference in DTS signals between a control pulse with area π and no control for varying t_c.

D.   Spin Rotation

When $\Delta\theta = 2\pi$ and the control pulse is resonant, we have a π rotation of the spin about the growth direction. This is rather obvious if we realize that

the $|\bar{z}\rangle$ state and the trion $|\bar{\mathcal{T}}\rangle$ form an SU(2). A 2π rotation of the pseudospin results in a sign change, which is relative to the $|z\rangle$ state, and hence a π rotation of the spin. Other angles of rotation can be achieved, and expressed analytically as functions of the pulse parameters. The analysis is given in Chapter VII.

For pulses of area other than 2π, clearly population is transferred to the trion and therefore there is leakage out of the computational spin subspace of the total Hilbert space. Hence, care has to be exercised in experiments where the objective is optical spin rotation. An unambiguous demonstration of spin rotation requires proof that there is no leakage out of the relevant Hilbert subspace.

V.

Spontaneously Generated Coherence in Quantum Dots

In this Chapter we introduce the concept of Spontaneously Generated Coherence (SGC), which –as the name suggests– is coherence generated by spontaneous emission. Starting from a master equation, we give a microscopic derivation of the spontaneously generated coherence term.

We review SGC in the context of atomic physics, where it was initially predicted [64] and we discuss the obstacles of experimental confirmation of SGC in an atomic system. SGC is introduced for a semiconductor quantum dot and an intuitive picture of SGC in terms of the spin vector is given. Finally, we present results from the experiment we interpret as the effects that demonstrated SGC in an ensemble of quantum dots. This was the first demonstration ever of the SGC phenomenon. We explained why it occurred in a solid state system despite numerous suggestions of experiments for SGC in atoms.

A.   Spontaneously Generated Coherence

The common view of spontaneous emission is that it destroys coherence. This is usually the case, and it is therefore not possible in general to describe an open system with the wavefunction formalism. Therefore, in order to account
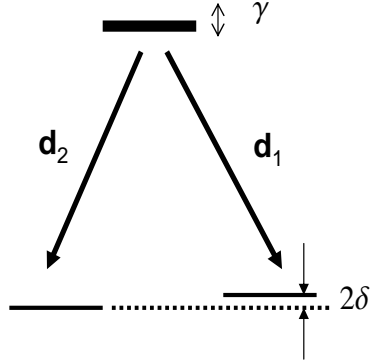
V.1   A three-level system in the Λ configuration. The relevant quantity for SGC is the excited state linewidth γ compared to the lower-level separation 2δ.

for spontaneous emission, a density function formalism is needed. However, cases where spontaneous emission may actually lead to coherence have been investigated both in textbooks [33] and in research papers [22]. An example is a Λ system which meets the following conditions [64]

- the dipole matrix elements of the two transitions are non-orthogonal, i.e., $\mathbf{d}_1 \cdot \mathbf{d}_2 \neq 0$

- the splitting between the lower levels is smaller than or comparable to the excited state linewidth, i.e., $2\delta \leq \gamma$

B.   Derivation of SGC from a Master Equation

In quantum mechanics, decay and decoherence arise when part of a composite system is ignored. Then, the dynamics of the remaining part, which we usually call 'system' are non-unitary. To describe the effect of the 'ignored' part, usually termed the bath or the reservoir, master equations are employed [33]. The basic assumption is that the coupling is weak, so that the interaction between the system and the reservoir may be treated by perturbation theory. Then, the idea is to start from the total density matrix of the composite system and iterate the

formal solution once. Then the square of the coupling appears in the equations. By taking partial trace with respect to the reservoir, rate equations are derived for the density matrix of the system, and in general they are non-unitary. This treatment amounts to a second order perturbation theory in the coupling.

We start with the master equation for the total system, which is the three-level system (S) plus the vacuum of the electromagnetic field, which acts as a reservoir (R). We will assume that the dipole matrix elements of the two transitions from the trion state are equal, $\mathbf{d}_1 = \mathbf{d}_2$, but no assumptions are made on the size of the splitting 2δ yet. The two lower levels will be denoted by $|1\rangle$ and $|2\rangle$. The temperature is taken to be zero. In the calculation, the following symbols are used:

- P is the density matrix for the whole system S+R in the interaction picture

- ρ is the density matrix for the three level system in the interaction picture

- V is the interaction between R and S in the interaction picture

- V_s is the interaction in the Schrödinger picture,

and $\hbar$ is set to unity.

The Liouville-Von Neumann equation for the whole system is

$$\dot{P} = i[P, V]. \tag{V.1}$$

Formally integrating and iterating, we have

$$\dot{P}(t) = -\int_{-\infty}^{t} dt' [[P(t'), V(t')], V(t)] \tag{V.2}$$

We will solve this equation using the adiabatic 'switching on', rather than coarse graining.

$$\dot{P}(t) = \lim_{\eta \to 0^+} \int_{-\infty}^{t} dt' [[P(t'), V(t')], V(t)] e^{\eta t'} \tag{V.3}$$

In the Rotating Wave Approximation, the interaction has the form

$$V_s = \sum_{j=0}^{\infty} {\sum_{k}}' (g_{jk} b_{jk} \sigma^+ + g_{jk}^* b_{jk}^\dagger \sigma) \tag{V.4}$$

where g_{jk} is the frequency dependent coupling strength, b_{jk} $(b_{jk}^\dagger)$ is the annihilation (creation) operator for a photon of frequency Ω_j, the index $k \equiv (\hat{\mathbf{k}}, \varepsilon)$ carries the propagation direction and polarization information. Note that the sum on k is restricted to the allowed propagation directions and polarizations, as dictated by selection rules. We have already made use of the assumption that the two transitions have parallel dipoles, by restricting the geometrical features of the emitted photon *in the same way* for the two transitions.

σ^+ (σ) is the raising (lowering) operator for the three-level system, given by:

$$\sigma^+ = |\mathcal{T}\rangle\langle 1| + |\mathcal{T}\rangle\langle 2|, \tag{V.5}$$

where $|\mathcal{T}\rangle$ is the excited state (later on, in the quantum dot case, to be the trion state).

$$V_s = \sum_{j=0}^{\infty}\sum_{k}{}'(g_{jk}b_{jk}|\mathcal{T}\rangle\langle 1| + g_{jk}b_{jk}|\mathcal{T}\rangle\langle 2| + h.c.), \tag{V.6}$$

which in interaction picture is given by

$$V(t) \equiv e^{iH_o t}V_s e^{-iH_o t}, \tag{V.7}$$

where

$$H_o = H_S + H_R, \tag{V.8}$$

$$H_S = \sum_{\lambda=1,2,\mathcal{T}} E_\lambda |\lambda\rangle\langle\lambda|, \tag{V.9}$$

$$H_R = \sum_{j=0}^{\infty}\sum_{k} \Omega_j b_{jk}^\dagger b_{jk}. \tag{V.10}$$

Also, we define

$$\omega_\lambda \equiv (E_\mathcal{T} - E_\lambda), \ \lambda = 1, 2. \tag{V.11}$$

Then

$$V(t) = \sum_{\lambda=1,2} \sum_{j=0}^{\infty} \sideset{}{'}\sum_{k} (g_{jk} b_{jk} |\mathcal{T}\rangle\langle\lambda| e^{i\omega_\lambda t} e^{-i\Omega_j t} + h.c.). \tag{V.12}$$

Substituting, and also taking into account $\langle b_{jk}^\dagger b_{j'k'}\rangle = 0$, $\langle b_{jk} b_{j'k'}^\dagger\rangle = \delta_{jj'}\delta_{kk'}$, and tracing out the reservoir, the equation for ρ becomes

$$\begin{aligned}
\dot{\rho}(t) = \ & -\sideset{}{'}\sum_{k} \sum_{j=0}^{\infty} \lim_{\eta\to 0^+} \int_{-\infty}^{0} d\tau |g_{jk}|^2 e^{\eta\tau} (|\mathcal{T}\rangle\langle\mathcal{T}|\rho(t')e^{i\Omega_j\tau}e^{-i\omega_\lambda\tau} + \rho(t')|\mathcal{T}\rangle\langle\mathcal{T}|e^{-i\Omega_j\tau}e^{i\omega_\lambda\tau} \\
& - \sum_{\lambda=1,2}(|\lambda\rangle\rho_{\mathcal{T}\mathcal{T}}(t')\langle\lambda|e^{-i\Omega_j\tau}e^{i\omega_\lambda\tau} - |\lambda\rangle\rho_{\mathcal{T}\mathcal{T}}(t')\langle\lambda|e^{i\Omega_j\tau}e^{-i\omega_\lambda\tau}) \\
& - |1\rangle\rho_{\mathcal{T}\mathcal{T}}(t')\langle 2|e^{-i\Omega_j\tau}e^{i(\omega_2 t'-\omega_1 t)} - |2\rangle\rho_{\mathcal{T}\mathcal{T}}(t')\langle 1|e^{-i\Omega_j\tau}e^{i(\omega_1 t'-\omega_2 t)} \\
& - |2\rangle\rho_{\mathcal{T}\mathcal{T}}(t')\langle 1|e^{i\Omega_j\tau}e^{-i(\omega_2 t'-\omega_1 t)} - |1\rangle\rho_{\mathcal{T}\mathcal{T}}(t')\langle 2|e^{i\Omega_j\tau}e^{-i(\omega_1 t'-\omega_2 t)}), \tag{V.13}
\end{aligned}$$

where $\tau \equiv t' - t$. Notice that the four last terms in the sum have survived, due to the fact that the sum on k was the same for the two transitions, and therefore tracing out the photon operators gave an identical contribution for the last four terms.

At this point we perform the markovian approximation, which amounts to setting $\rho(t') = \rho(t)$ and hence pulling it out of the integral. Then, by replacing the sum on the photon modes by an integral and the photon density of states, i.e.,

$$\sum_j \longrightarrow \int_0^\infty d\Omega\, \mathcal{D}(\Omega), \tag{V.14}$$

where $\mathcal{D}(\omega) = \frac{V}{2\pi^2 c^3}\omega^2$, the expression multiplying the projection operator $|\mathcal{T}\rangle\langle\mathcal{T}|$ in the first term of V.13,

$$\lim_{\eta\to 0^+} \sum_{j=0}^{\infty} \int_{-\infty}^{0} d\tau |g_j|^2 e^{i\Omega_j\tau}e^{-i\omega_\lambda\tau}e^{\eta\tau}, \tag{V.15}$$

becomes

$$\lim_{\eta\to 0^+} \int_0^\infty d\Omega\, \mathcal{D}(\Omega) \int_{-\infty}^{0} d\tau |g(\Omega)|^2 e^{i\Omega\tau}e^{-i\omega_\lambda\tau}e^{\eta\tau}. \tag{V.16}$$

Performing the integral on τ, Eq.(V.16) becomes

$$\lim_{\eta \to 0^+} \int_0^\infty d\Omega \, \mathcal{D}(\Omega) \frac{|g(\Omega)|^2}{-i(\omega_\lambda - \Omega) + \eta} \tag{V.17}$$

$$= \lim_{\eta \to 0^+} \eta \int_0^\infty d\Omega \, \mathcal{D}(\Omega) \frac{|g(\Omega)|^2}{(\Omega - \omega_\lambda)^2 + \eta^2} - i \lim_{\eta \to 0^+} \int_0^\infty d\Omega \, \mathcal{D}(\Omega) \frac{|g(\Omega)|^2 \, (\omega_\lambda - \Omega)}{(\Omega - \omega_\lambda)^2 + \eta^2}. \tag{V.18}$$

Also, to account for the restricted sum on the direction of k, we use the spatial distribution of the emitted radiation, and have

$$\sum_k{}' \longrightarrow 2 \int d\Omega \, \mathcal{G}_+(\theta), \tag{V.19}$$

where $\mathcal{G}_+$ is the distribution on the propagation direction of the emitted radiation for a $\Delta m = 1$ transition. The factor of 2 is to include the two polarization states. The explicit form is $\mathcal{G}_+(\theta) = 1 + \cos^2 \theta$ [34, 90], and for completeness we also include the distribution for a linearly polarized transition, $\Delta m = 0$, $\mathcal{G}_0(\theta) = \sin \theta$. Clearly, a photon spontaneously emitted from a $\Delta m = 1$ transition may propagate along any direction, whereas a photon spontaneously emitted from a $\Delta m = 0$ transition cannot propagate along z. Also, as expected from the azimuthal symmetry of the problem, neither distribution depends on the angle ϕ.

Similarly we obtain the remaining integrals of (V.13). In the above expression, Eq. (V.18), the first term is related to the broadening (linewidth) of the excited state, and the second term is a small shift in the energy of the excited state, analogous to the well-known Lamb shift. In order to keep it regulated we would have to introduce a frequency cutoff for the photons, but we will ignore it or assume it has been absorbed into the transition frequencies. We use the relation

$$\lim_{\eta \to 0} \frac{\eta}{(x - x_o)^2 + \eta^2} = \pi \delta(x - x_o), \tag{V.20}$$

and find

$$\gamma_\lambda = \frac{32\pi^2}{3} \mathcal{D}(\omega_\lambda) \, |g(\omega_\lambda)|^2. \tag{V.21}$$

From Eq. (V.21) we see that there is a linear in ω contribution from the coupling squared (see Chapter III) and an ω^2 from the DOS, hence the well-known cubic dependence of the spontaneous emission rate on the frequency. The equations for ρ become

$$
\begin{aligned}
\dot{\rho}(t) = \quad & -\frac{\gamma_1 + \gamma_2}{2}|\mathcal{T}\rangle\langle\mathcal{T}|\rho(t) - \frac{\gamma_1 + \gamma_2}{2}\rho(t)|\mathcal{T}\rangle\langle\mathcal{T}| + \gamma_1|1\rangle\rho_{\mathcal{T}\mathcal{T}}(t)\langle 1| + \gamma_2|2\rangle\rho_{\mathcal{T}\mathcal{T}}(t)\langle 2| \\
+ \quad & e^{-2i\delta t}\frac{\gamma_1 + \gamma_2}{2}|2\rangle\rho_{\mathcal{T}\mathcal{T}}(t)\langle 1| + e^{2i\delta t}\frac{\gamma_1 + \gamma_2}{2}|1\rangle\rho_{\mathcal{T}\mathcal{T}}(t)\langle 2|,
\end{aligned} \tag{V.22}
$$

where $2\delta \equiv \omega_2 - \omega_1 = E_1 - E_2$ is the splitting between the lower levels. The functions appearing in (V.21) are slowly varying, so we are setting $\gamma_1 = \gamma_2 = \gamma$, and the equations of motion become:

$$
\dot{\rho}_{\mathcal{T}\mathcal{T}} = -2\gamma\rho_{\mathcal{T}\mathcal{T}} \tag{V.23}
$$

$$
\dot{\rho}_{11} = \gamma\rho_{\mathcal{T}\mathcal{T}} \tag{V.24}
$$

$$
\dot{\rho}_{22} = \gamma\rho_{\mathcal{T}\mathcal{T}} \tag{V.25}
$$

$$
\dot{\rho}_{1\mathcal{T}} = -\gamma\rho_{1\mathcal{T}} \tag{V.26}
$$

$$
\dot{\rho}_{2\mathcal{T}} = -\gamma\rho_{2\mathcal{T}} \tag{V.27}
$$

$$
\dot{\rho}_{12} = \gamma e^{2i\delta t}\rho_{\mathcal{T}\mathcal{T}} \tag{V.28}
$$

In converting to the Schrödinger picture, the only equation to change from the above is Eq. (V.28). This is easily seen by inspection, since the terms ρ_{jj} are the same in the two pictures. On the other hand, for Eqs. (V.26) and (V.27), the same exponentials appear on the right and left handside and cancel. Eq. (V.28) becomes in the Schrödinger picture

$$
(\dot{\rho^s}_{12})_{sp} = \gamma\rho_{\mathcal{T}\mathcal{T}} \tag{V.29}
$$

This term shows that the coherence ρ_{12} is affected by the population of the excited state. In the usual decay equations of the Λ-system, the coherence ρ_{12} does not

have a contribution from spontaneous emission. Hence, Eq. (V.29) is known as a spontaneously generated coherence term. It expresses the fact that the excited state does not incoherently decay to the two lower ones, but rather decays to a certain superposition of the two states. To understand this result first notice that in the absence of SGC terms the decay equations from the excited state to the two lower states, (V.24) and (V.25), can be written in any basis, i.e., we may rotate in any linear superposition of $|1\rangle$ and $|2\rangle$ and get equations of the same form. In the presence of the SGC term though, there is *a single* preferred state where the excited state decays, namely the superposition $\frac{|1\rangle+|2\rangle}{2}$. Taking this into account, we may notice that the raising operator from Eq. (V.5) may be rewritten in this new basis, and will only possess one nonzero matrix element. Then the derivation would lead to the familiar decay equations for a two-level system, which is a much simpler way to derive our result.

Note also that if we had chosen $\mathbf{d}_1$ and $\mathbf{d}_2$ to be antiparallel, then Eq. (V.29) would have a minus sign on the RHS. This would still be an SGC term, only that the final state would be $\frac{|1\rangle-|2\rangle}{2}$. The fact that there is a single final state also implies the existence of an orthogonal dark state, i.e., a state which is not connected to the excited via dipole coupling. In the case of the quantum dot when the trion state polarized along $+z$ (the quantum dot growth direction) is the excited state, the final state is of course $|z\rangle$, and the dark state is $|\bar{z}\rangle$, which is a $\Delta m_j = 2$ transition from $|\mathcal{T}\rangle$.

The above derivation shows the necessity of the condition that the two polarizations be non-orthogonal, but it does not restrict the splitting. Indeed, whenever the two transitions have parallel (or antiparallel) polarization, the SGC term is formally there. However, it will have a negligible effect as their energy separation increases. The way to understand physically why the energy requirement enters is by realizing that the superposition state $\frac{|1\rangle+|2\rangle}{2}$ has a finite linewidth, associated to the fact that it is not an energy eigenstate. Therefore, for the spontaneously emitted photon to cover this linewidth it has to itself have a comparable

energy spread. Clearly, the spread in the energy of the spontaneously emitted photon originates from the linewidth of the excited state. This point will be further studied and put in mathematical terms partly in this, but mainly in the following Chapter.

C.   SGC in Atoms

The prediction of spontaneously generated coherence for atomic systems [64] generated considerable interest, mostly because of the implications it would have in various experiments [92, 145]; however, atomic or molecular systems where it would occur and be detectable experimentally have not been found.

The difficulty with meeting the stringent conditions of SGC in atoms lies in the fact that it is not easy to find a Λ-system such that the two lower levels are closely spaced, so that the linewidth of the excited state can cover both transitions. For example, the fine structure splitting is of the order of 1 meV, and the atomic state linewidths in atoms are a lot smaller, in the order of 1 μeV.

The hyperfine splittings are smaller than the spin-orbit split states. They are still larger than the linewidths, but clearly comparable, so there is a chance of SGC being detectable in hyperfine levels. Even then, there would be a problem of isolating a three-level system: in general there will be more states with orthogonal polarizations, degenerate to the ones of interest. For example, there would be SGC between states $|F, M_F = 1\rangle$ and $|F + 1, M_F = 1\rangle$. But relaxation to states with $M_F \neq 1$ would be incoherent with respect to the two previous states.

Another issue with atoms is that they are free to move and therefore, unlike the quantum dots, they do not share a common quantization axis. Using the spin states and splitting them by an external magnetic field, similarly to the quantum dot, would also not provide the SGC conditions: the excited state–unlike the trion–would also mix, and the level configuration would no longer be Λ-type; at least an extra level would enter in the dynamics. Actually, this would lead to

the Hanle effect, [33, 121], in which an ensemble of atoms in a magnetic field is illuminated with an x-polarized pulse and the reradiated light may be polarized along y. This effect is another example where coherence plays an important role; it has recently been observed in doped GaAs quantum wells, in the heavy-hole trion system with confinement in one dimension [40].

To our knowledge, despite the ongoing research, SGC has not yet been demonstrated for atomic or molecular systems. In the next Chapter, we revisit the possibility of SGC detection in atomic systems and demonstrate that SGC can be detected *probabilistically* in single trapped ions.

D.   SGC in a Quantum Dot

In the quantum dot the polarization selection rules are satisfied, since the two ground states, $|\pm x\rangle$, are coupled to the trion by parallel dipole matrix elements, and the Zeeman splitting is tunable by means of the external magnetic field, so it can be made arbitrarily small, and thus be in the SGC regime. Another important feature of the quantum dot is that application of an in-plane magnetic field does not cause the trion, which is polarized along z, to precess about the field. This is valid for fields up to about 5T [130]. Physically, it is a consequence of the combined underlying semiconductor and the quantum dot confining potential. Due to the semiconductor symmetry, heavy holes ($m_j = \pm 3/2$) and light holes ($m_j = \pm 1/2$) have different effective masses. Since the energy levels of a particle in a potential depend on its mass, the light hole and heavy hole states will be shifted by different amounts. The splitting between them is of the order of tens of meV's. Now, for a $j = 3/2$ particle to flip from the highest $m_j = 3/2$ value to the lowest $m_j = -3/2$, it has to pass through the intermediate $m_j = \pm 1/2$ states. Since these are higher in energy, it takes a third order process in the magnetic field, and it will thus be suppressed for low fields.

The most straightforward experiment to demonstrate SGC would be to

transfer all the population in the excited state, and make a measurement in the $|\pm z\rangle$ basis when a spontaneously generated photon is emitted. SGC is present if the final state is *always* $|z\rangle$. This might be a relatively simple experiment in atoms, for example it can be carried out in single trapped ion in the setting of ref. [13], which we will examine in the next Chapter. In the case of the quantum dot it is quite hard to deterministically initialize the dot in the trion state, and the spontaneously emitted photon may be reabsorbed by other degrees of freedom in the solid.

Instead, a pump-probe nonlinear experiment is sufficient for SGC detection in an ensemble of quantum dots, even when the initial state is completely mixed (unpolarized spin ensemble). As we shall show in the next section, the SGC term induces a magnetic-field dependent nonlinear response of the dots. The amplitude and the phase of the spin beats become magnetic-field dependent, whereas in the absence of SGC the beats are magnetic-field independent. In the following we will derive the expression for the differential transmission signal (DTS), which is the quantity measured in a pump-probe homodyned experiment. We will solve the Liouville-von Neumann equations order by order. The DTS signal measures the third order nonlinear response for low excitation powers. For higher powers, higher orders are measured as well.

E.   Derivation of DTS in the presence of SGC

The optical field of the pump and probe pulses can be written as

$$\mathbf{E}(t) = (\mathbf{e}_+ E_{1+} + \mathbf{e}_- E_{1-})\,\mathcal{E}_1(t)e^{-i\omega_1 t} + (\mathbf{e}_+ E_{2+} + \mathbf{e}_- E_{2-})\,\mathcal{E}_2(t - t_\mathrm{d})e^{-i\omega_2(t-t_\mathrm{d})},$$

where the subscripts 1 and 2 denote the pump and probe pulses, respectively, and $\mathbf{e}_\pm = \hat{x} \pm i\hat{y}$ are the unit vectors of the $\sigma\pm$-polarizations, and t_d is the time interval between the center of the pump and probe pulses. In the experiment, t_d is varied and the nonlinear signal is measured as a function of t_d. The dipole operator is

$$\hat{\mathbf{d}} = d\big(\mathbf{e}_+|\bar{\mathcal{T}}\rangle\langle\mp| \pm \mathbf{e}_-|\mathcal{T}\rangle\langle\pm|\big) + \text{h.c.},$$

where $|\pm\rangle$ are the electron spin states along x, $|\pm x\rangle$.

Thus, in the rotating wave approximation, the Hamiltonian in the basis $\{|-\rangle, |+\rangle, |\mathcal{T}\rangle, |\bar{\mathcal{T}}\rangle\}$ can be written in matrix form as

$$
H = \begin{bmatrix}
-\omega_{\mathrm{L}} & 0 & +d^*E_+^*(t) & -d^*E_-^*(t) \\
0 & \omega_{\mathrm{L}} & -d^*E_+^*(t) & -d^*E_-^*(t) \\
+dE_+(t) & -dE_+(t) & \epsilon_{\mathcal{T}} & 0 \\
-dE_-(t) & -dE_-(t) & 0 & \epsilon_{\mathcal{T}}
\end{bmatrix}, \tag{V.30}
$$

where $\epsilon_{\mathcal{T}}$ is the energy of the trion states. In what follows γ_2, 2Γ denote the spin depolarizing rate and the trion decay rate, respectively. The explicit equations for each element of the density matrix are

$$
\dot{\rho}_{\mathcal{T},+} = i[\rho, H]_{\mathcal{T},+} - \Gamma \rho_{\mathcal{T},+}, \tag{V.31}
$$

$$
\dot{\rho}_{\mathcal{T},-} = i[\rho, H]_{\mathcal{T},-} - \Gamma \rho_{\mathcal{T},-}, \tag{V.32}
$$

$$
\dot{\rho}_{+,+} = i[\rho, H]_{+,+} + \Gamma \left(\rho_{\mathcal{T}\mathcal{T}} + \rho_{\bar{\mathcal{T}},\bar{\mathcal{T}}} \right), \tag{V.33}
$$

$$
\dot{\rho}_{-,-} = i[\rho, H]_{-,-} + \Gamma \left(\rho_{\mathcal{T}\mathcal{T}} + \rho_{\bar{\mathcal{T}}\bar{\mathcal{T}}} \right), \tag{V.34}
$$

$$
\dot{\rho}_{+,-} = i[\rho, H]_{+,-} - \gamma_2 \rho_{+,-} - \Gamma_{\mathrm{c}} \left(\rho_{\mathcal{T}\mathcal{T}} - \rho_{\bar{\mathcal{T}},\bar{\mathcal{T}}} \right), \tag{V.35}
$$

$$
\dot{\rho}_{\mathcal{T}\mathcal{T}} = i[\rho, H]_{\mathcal{T}\mathcal{T}} - 2\Gamma \rho_{\mathcal{T}\mathcal{T}}, \tag{V.36}
$$

$$
\dot{\rho}_{\bar{\mathcal{T}},\mathcal{T}} = i[\rho, H]_{\bar{\mathcal{T}},t} - 2\Gamma \rho_{\bar{\mathcal{T}},t}, \tag{V.37}
$$

$$
\dot{\rho}_{\bar{\mathcal{T}}\bar{\mathcal{T}}} = i[\rho, H]_{\bar{\mathcal{T}}\bar{\mathcal{T}}} - 2\Gamma \rho_{\bar{\mathcal{T}}\bar{\mathcal{T}}}. \tag{V.38}
$$

The above equations have been derived from a master equation, similarly to the derivation in Section B.. As before, the Markov-Born approximation for the system-photon has been employed. The term representing the spontaneously generated spin coherence due to the trion recombination is indicated by the suffix c; Γ_{c} in Eq. (V.35) should be equal to Γ. However, we singled out the SGC term so that Γ_{c} can be artificially set to zero for a theoretical comparison between the results with and without the SGC effect.

The density matrix can be calculated straightforwardly order by order with respect to the pulse. We take a general initial state of the system to be

$\rho^{(0)} = \rho_+^{(0)}|+\rangle\langle+|+\rho_-^{(0)}|-\rangle\langle-|$, so that $\rho_+^{(0)} = \rho_-^{(0)} = 1/2$ corresponds to a completely mixed state. The density matrix may be written as

$$\rho = \sum_{n=0}^{\infty} \rho^{(n)}, \tag{V.39}$$

where n denotes the order to the electric field. Note that $\rho^{(n)}$ is not necessarily a density matrix itself, so it does not have to satisfy the conditions of unit trace and positive semi-definiteness. It should however be hermitian, to guarantee hermiticity of ρ.

The order-by-order calculation may be carried in Fourier space. Here we only show explicitly the calculation of $\rho_{T,+}$.

$$\dot{\rho}_{T,+} = i[\rho, H]_{T,+} - \Gamma\rho_{T,+} \tag{V.40}$$

$$\dot{\rho}_{T,+}^{(1)} = -i\omega_{T,+}\rho_{T,+}^{(1)} - iH_{T,+}\rho_{+,+}^{(0)} - \Gamma\rho_{T,+}^{(1)} \tag{V.41}$$

$$-i\omega\tilde{\rho}_{T,+}^{(1)}(\omega) = -i\omega_{T,+}\tilde{\rho}_{T,+}^{(1)}(\omega) - i\rho_{++}^{(0)}d\tilde{\mathcal{E}}_1(\omega) - \Gamma\tilde{\rho}_{T,+}^{(1)}(\omega), \tag{V.42}$$

where $\tilde{\rho}_{ij}(\omega)$ is the Fourier transform of $\rho_{ij}(t)$.

By transforming back to time domain, we find

$$\rho_{T,+}^{(1)}(t) = \rho_{++}^{(0)} d \int \frac{d\omega}{2\pi} \frac{\tilde{\mathcal{E}}_1(\omega)e^{-i\omega t}}{\omega - \omega_{T,+} + i\Gamma}. \tag{V.43}$$

In the pump-probe experiment, the DTS corresponds to the third-order in the electric field optical response, for low pump and probe powers. The absorption of the probe pulse is proportional to the work W done by the probe pulse, and the DTS is [15]

$$\begin{aligned}
\Delta T(t_d) &\propto -W^{(3)} = -2\Re \int \dot{\mathbf{P}}^{(3)}(t) \cdot \mathbf{E}_2^*(t - t_d) \\
&\approx -2\omega_2 \Im \int \tilde{\mathbf{P}}^{(3)}(\omega + \omega_2) \cdot \tilde{\mathbf{E}}_2^*(\omega + \omega_2)\frac{d\omega}{2\pi}.
\end{aligned} \tag{V.44}$$

The third-order optical polarization of the system can be calculated directly by expanding the density matrix according to the order of the optical perturbation

$$\mathbf{P}^{(3)} = \mathbf{e}_+ d \left[\rho_{\mathcal{T},-}^{(3)} + \rho_{\mathcal{T},+}^{(3)} \right] + \mathbf{e}_- d \left[\rho_{\mathcal{T},-}^{(3)} - \rho_{\mathcal{T},+}^{(3)} \right], \tag{V.45}$$

Thus, given the σ+-polarized pump pulse, the third-order optical polarization in the case of the pump and the probe having the same circular polarization (SCP) and opposite circular polarizations (OCP) can be respectively calculated as [15]

$$\mathbf{P}_{\mathrm{SCP}}^{(3)}(t) = \mathbf{e}_+ d \left[\rho_{\mathcal{T},-}^{(3)}(t) + \rho_{\mathcal{T},+}^{(3)}(t) \right], \tag{V.46}$$

$$\mathbf{P}_{\mathrm{OCP}}^{(3)}(t) = \mathbf{e}_- d \left[\rho_{\mathcal{T},-}^{(3)}(t) - \rho_{\mathcal{T},+}^{(3)}(t) \right]. \tag{V.47}$$

We have carried out the calculation for the more general case where the pump and probe have a random polarization. Carrying out the calculation in Fourier space, as explained above, the result for the second-order spin coherence due to the pump pulse $\mathbf{E}_1(t)$ is:

$$
\begin{aligned}
\tilde{\rho}_{+-}^{(2)}(\omega) = &+ X_1 \frac{\rho_-^{(0)}}{\omega - 2\omega_{\mathrm{L}} + i\gamma_2} \int_{-\infty}^{+\infty} \frac{\mathcal{E}_1^*(\omega' - \omega)\mathcal{E}_1(\omega')}{\omega' - \Delta_1 - \omega_{\mathrm{L}} + i\Gamma} \frac{d\omega'}{2\pi} \\
&- X_1 \frac{\rho_+^{(0)}}{\omega - 2\omega_{\mathrm{L}} + i\gamma_2} \int_{-\infty}^{+\infty} \frac{\mathcal{E}_1(\omega' + \omega)\mathcal{E}_1^*(\omega')}{\omega' - \Delta_1 + \omega_{\mathrm{L}} - i\Gamma} \frac{d\omega'}{2\pi} \\
&+ X_1 \frac{i\Gamma_{\mathrm{c}}\rho_\pm^{(0)}}{(\omega - 2\omega_{\mathrm{L}} + i\gamma_2)(\omega + i2\Gamma)} \int_{-\infty}^{+\infty} \frac{\mathcal{E}_1(\omega' + \omega)\mathcal{E}_1^*(\omega')}{\omega' - \Delta_1 \pm \omega_{\mathrm{L}} - i\Gamma} \frac{d\omega'}{2\pi} \\
&- X_1 \frac{i\Gamma_{\mathrm{c}}\rho_\pm^{(0)}}{(\omega - 2\omega_{\mathrm{L}} + i\gamma_2)(\omega + i2\Gamma)} \int_{-\infty}^{+\infty} \frac{\mathcal{E}_1^*(\omega' - \omega)\mathcal{E}_1(\omega')}{\omega' - \Delta_1 \pm \omega_{\mathrm{L}} + i\Gamma} \frac{d\omega'}{2\pi},
\end{aligned}
\tag{V.48}
$$

where $\Delta_1 \equiv \epsilon_{\mathcal{T}} - \omega_1$ is the detuning of the pump, and $X_1 \equiv |dE_{1+}|^2 - |dE_{1-}|^2$ is the circular degree of the pulse polarization. In the equation above, the first two terms correspond to the Raman coherence generated by the pump excitation [77], and the last two terms represent the spontaneously generated coherence. The two phenomena are of course very closely related: the role of the laser in Raman coherence is played by the radiation in SGC. Obviously, for a linearly polarized pump, $X_1 = 0$, no spin coherence is generated either by excitation or by recombination, so there will be no spin beats in DTS.

In the short-pulse limit, the spin coherence after the pump and recombination can be approximately expressed as

$$\rho_{+,-}^{(2)}(t) \approx X_1 |\mathcal{E}_1(\Delta_1)|^2 \left(\frac{\Gamma_c}{2\Gamma - \gamma_2 - 2i\omega_L} - \frac{1}{2} \right) e^{-i(2\omega_L - i\gamma_2)(t-t_1)}. \quad (V.49)$$

The physical meaning of the two terms in Eq. (V.49) is transparent: the first term is SGC, whose amplitude and phase shift depend on the ratio of the recombination rate to the Zeeman splitting, and the second term is just the optically pumped Raman coherence which in the short pulse limit is independent of the Zeeman splitting.

Having obtained the second-order results, we can readily derive the third-order density matrix and, in turn, the DTS can be calculated by use of Eq. (V.44). In general, the DTS can be expressed as

$$\Delta T \propto A \cos(2\omega_L t_d - \phi) e^{-\gamma_2 t_d} + B e^{-2\Gamma t_d}, \quad (V.50)$$

and the spin coherence amplitude A and phase shift ϕ, the Pauli blocking amplitude B can all be numerically calculated and, in the short-pulse limit, can also be analytically derived as

$$A \approx |\mathcal{E}_1(\Delta_1)|^2 |\mathcal{E}_2(\Delta_2)|^2 X_1 X_2 \sqrt{\frac{\gamma_2{}^2 + 4\omega_L^2}{(2\Gamma_c - \gamma_2)^2 + 4\omega_L^2}}, \quad (V.51)$$

$$\phi \approx -\arctan\left(\frac{2\Gamma_c - \gamma_2}{2\omega_L} \right) - \arctan\left(\frac{\gamma_2}{2\omega_L} \right), \quad (V.52)$$

$$B \approx |\mathcal{E}_1(\Delta_1)|^2 |\mathcal{E}_2(\Delta_2)|^2 \left[I_1 I_2 + 2I_{1+}I_{2+} \right.$$
$$\left. +2I_{1-}I_{2-} + X_1 X_2 \frac{2\Gamma_c(2\Gamma - \gamma_2)}{(2\Gamma - \gamma_2)^2 + 4\omega_L^2} \right], \quad (V.53)$$

where $\Delta_2 \equiv \epsilon_T - \omega_2$ is the detuning of the probe, $I_{j\pm} \equiv |dE_{j\pm}|^2$, $I_j \equiv I_{j+} + I_{j-}$, and $X_j \equiv I_{j+} - I_{j-}$ ($j = 1$ or 2).

Several conclusions can be immediately drawn from the short-pulse approximation: (1) the SCP and OCP signals reveal beats with the same amplitude and opposite signs; (2) no spin beat can be observed when either of the pulses is linearly polarized ($X_1 = 0$ or $X_2 = 0$); (3) due to the SGC effect, the beat amplitude increases with increasing Zeeman splitting until it saturates at the value it
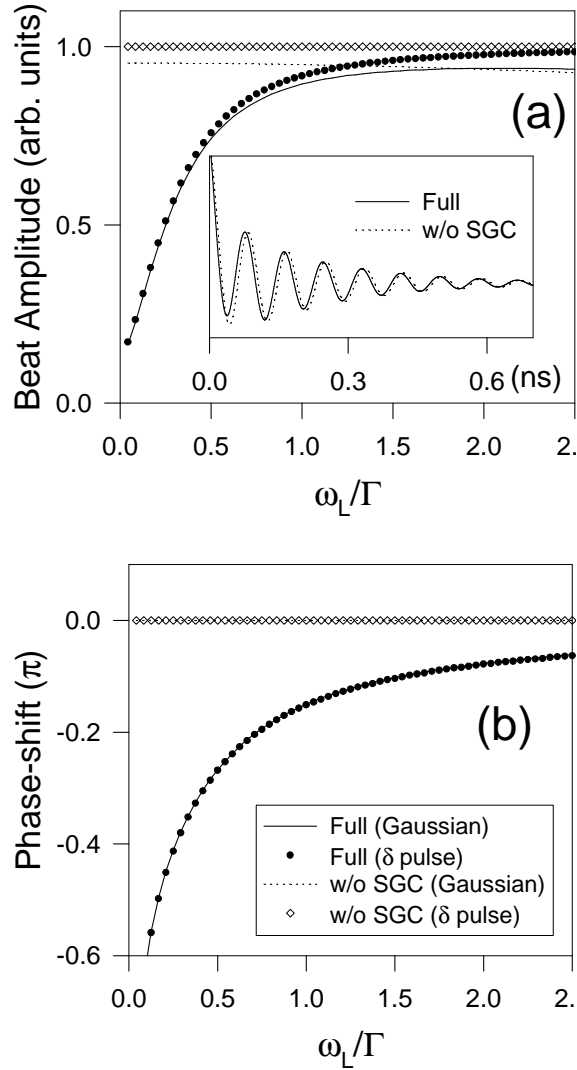
V.2 (a) The amplitude and (b) the phase shift of the spin beat (shown in the insert) as functions of the Zeeman splitting in units of the trion state width, Γ. The fulled-circle and solid lines include the SGC effect, calculated with and without the short-pulse approximation, respectively. The diamond and dotted lines are the results without the SGC effect, calculated with and without the short-pulse approximation, respectively.

would have in the absence of the SGC effect; the phase shift increases from $-\pi/2$, saturating at 0. The SGC effect is negligible when the Zeeman splitting is large compared to the trion decay rate Γ because the rapid oscillation averages the effect to zero.

F.   Intuitive Picture of SGC Experiment

An intuitive picture of the pump-probe experiment in a mixed ensemble of quantum dots can be drawn. Here we attempt to explain our results of section E. based on a simple picture of the spin-vector representation of the spin.

Initially, all the dots are in thermal equilibrium and hence there is no spin polarization, or equivalently the spin vector is zero. When a (fast) circularly polarized $\sigma+$ pulse is shone on the dots, population from the $|z\rangle$ state is transferred to the trion state $|\mathcal{T}\rangle$, leaving behind net spin polarization (nonzero spin vector) pointing along $-z$. This will precess under the perpendicular magnetic field. In the absence of SGC, which means incoherent decay of the trion to both states, spontaneous emission does not affect this spin-vector. However, SGC means, as explained above, that the excited state (the trion in this case) decays to a single state, in this case the $|z\rangle$ state. Thus, after some precession of the spin vector, a contribution along $+z$ will add to it coherently, causing the spin vector to shrink by a small amount and change phase. The new spin vector will continue to precess when a second contribution along $+z$ will add to it, with the same effect. After all the population has decayed from the trion, the final spin vector will clearly have a smaller length and a phase difference compared to the no-SGC case. These are the amplitude and phase derived above, which were shown to be functions of the magnetic field due to the presence of SGC. In our intuitive picture, one can see that for large Zeeman splittings, i.e. fast precession, the spin vector would be pointing at random directions in the yz plane when each SGC contribution added to it, so that altogether they would average out. This is how one intuitively understands

that dependence on the magnetic field of the amplitude and phase of the beats is expected.
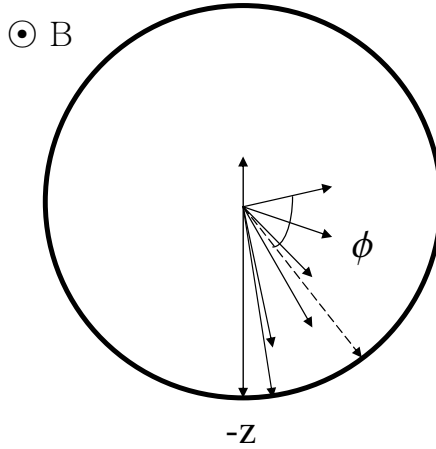
V.3   Initially the spin vector points along $-z$. In the absence of SGC the final spin vector after the decay of the trion would be the dashed line. In the presence of SGC, which opposes to initialization by optical pumping, the final spin vector is of smaller amplitude and has a phase ϕ compared to the dashed vector.

It is clear that in the case of initialization by optical pumping, which is what we are discussing here, the spontaneous contribution to the coherence will be opposite to the stimulated one. This is expected, since optical pumping is based on spontaneous emission in its usual incoherent sense. Therefore, the coherent nature of SGC will oppose to generation of coherence through optical pumping.

On the other hand, for single-qubit operations, SGC is either a neutral or positive contribution, since there the unitarity is desirable. This point will be re-examined in Chapter VI, where we will focus on optical single-spin rotations.

G.   SGC Experiment

The experiment which measured SGC in quantum dots–and to our knowledge constitutes the first detection of SGC–also demonstrated optical generation

of spin coherence via optical pumping, as discussed above [41]. In this section, we briefly review the experiment from a more technical point of view, and we show the experimental results and compare to the theory.

The sample consisted of interface fluctuation GaAs QDs, formed by growth interrupts at the interface of a narrow (4.2 nm) GaAs quantum well, which were remotely doped with electrons. Magneto-photoluminescence measurements on single charged QDs showed a small electron g factor and a maximum splitting of 80 μeV at the highest fields reached in the experiment. The etched sample was mounted in a superconducting magnetic cryostat held at 4.8 K. The pump and probe pulses were obtained from a mode-locked Ti:Sapphire laser, with a shaped pulse bandwidth (FWHM 0.84 meV), about an order of magnitude larger than the Zeeman splitting between the electron spin states, so that the two states were coherently excited (Raman coherence).

The pump-probe experiment was performed on an ensemble of QDs, with a gaussian distribution of g-factors of about $\Delta g/g \sim 8\%$. Due to the ensemble nature of the experiment, T_2^*, the inhomogeneously broadened spin dephasing time was measured, i.e., an average of the spin dephasing, both spatial and temporal. The measured T_2^* was about 10 ns, which provides a lower bound to the spin coherence time T_2. The trion recombination time $(2\Gamma)^{-1}$ was measured to be about 80 ps.

The text of this Chapter is in part a reprint of the material as it appears in Sophia E. Economou, Ren-Bao Liu, L. J. Sham, and D. G. Steel, "Unified theory of consequences of spontaneous emission in a Lambda system," Phys. Rev. B 71, 195327 (2005). "Copyright (2005) by the American Physical Society." The dissertation author was the primary researcher and author and the co-authors listed in this publication directed and supervised the research which forms the basis for this chapter. The text of this Chapter is also in part a reprint of the material as it appears in M. V. Gurudev Dutt, Jun Cheng, Bo Li, Xiaodong Xu, Xiaoqin Li, P. R. Berman, D. G. Steel, A. S. Bracker, D. Gammon, Sophia E. Economou,
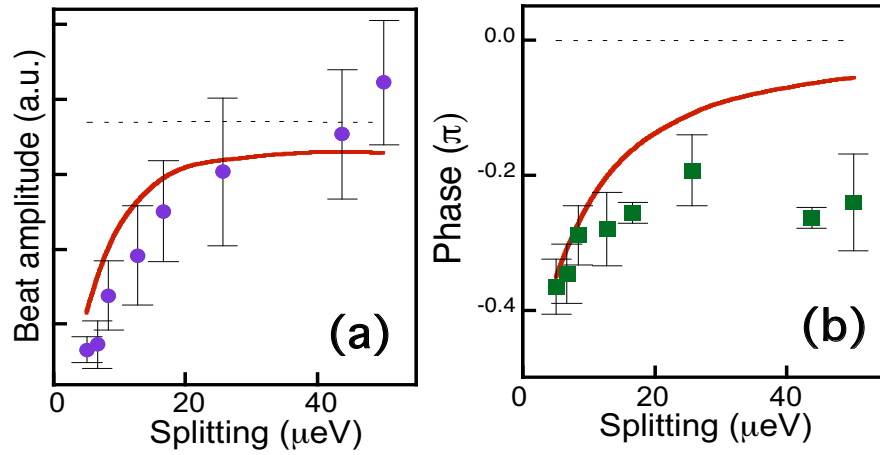
V.4   (a)Amplitude and (b) phase of the quantum beats as functions of the magnetic field. Solid (dashed) lines denote theoretical predictions for these parameters with (without) the effects of SGC, and are plotted along with the experimental points. The agreement between theory and experiment is excellent in the case of the amplitude. Both amplitude and phase strongly deviate from the constant, which demonstrates the presence of SGC. This constitutes the first experimental demonstration of SGC based on the theory developed in Section E.

Ren-Bao Liu, and L. J. Sham, "Stimulated and Spontaneous Optical Generation of Electron Spin Coherence in Charged GaAs Quantum Dots," Phys. Rev. Lett. 94, 227403 (2005). "Copyright (2005) by the American Physical Society." The dissertation author was a coauthor listed in this publication.

VI.

Unified Theory of Consequences of Spontaneous Emission in a Λ system

The electromagnetic vacuum is commonly treated as a reservoir which causes decoherence and decay of a quantum mechanical system coupled to it. An alternative view holds that the two subparts ('quantum system' and 'bath') are constituents of a single closed quantum mechanical whole, which is governed by unitary evolution until a projection (measurement) is performed. Different projections may give rise to a variety of phenomena which on the surface appear unrelated. In this Chapter, we treat spontaneous emission as unitary evolution, in order to study these effects from a unifying perspective.

A.   Spontaneous Emission as Unitary Evolution

Consider a single Λ system in a photon bath with modes $|k\rangle$, where $k = (\mathbf{k}, \sigma)$, $\mathbf{k}$ being the wave vector and σ the state with the polarization vector ε_σ. In the dipole and rotating-wave approximation, the Hamiltonian for the whole system

is given by

$$
\begin{aligned}
H &= \sum_k \omega_k b_k^\dagger b_k + \sum_{i=1}^3 \epsilon_i |i\rangle\langle i| + \sum_{k; i=1,2} g_{ik} b_k^\dagger |i\rangle\langle 3| \\
&\quad + \sum_{k; i=1,2} g_{ik}^* b_k |3\rangle\langle i|,
\end{aligned}
\tag{VI.1}
$$

where b_k destroys a photon of energy or frequency ω_k ($\hbar = 1$) and $|i\rangle$ is the electronic state with energy or frequency ϵ_i. The coupling between the photon and the electron is $g_{ik} \propto \varepsilon_\sigma \cdot \mathbf{d}_i$, where $\mathbf{d}_i$ is the dipole matrix element for the transition $3 \leftrightarrow i$. The Λ system is taken to be at $t = 0$ in the excited level $|3\rangle$ (which can be prepared by a short pulse), and the photon bath is in the vacuum state, i.e., the whole system is in a product state. For $t > 0$, the composite wavepacket can be written as

$$
|\psi(t)\rangle \equiv c_3(t)|3\rangle|\text{vac}\rangle + \sum_k c_{1k}(t)|1\rangle|k\rangle + \sum_k c_{2k}(t)|2\rangle|k\rangle,
\tag{VI.2}
$$

where $|\text{vac}\rangle$ is the photon vacuum state. Evolution of this state is governed by the Schrödinger equation.

By the Weisskopf-Wigner theory [141] of spontaneous emission [121], the coefficient c_3 is obtained by one iteration of the other coefficients:

$$
\begin{aligned}
\partial_t c_3 &= -i\epsilon_3 c_3 - \sum_k |g_{1k}|^2 \int_0^t e^{-i(\epsilon_1 + \omega_k)(t-t')} c_3(t')dt' \\
&\quad - \sum_k |g_{2k}|^2 \int_0^t e^{-i(\epsilon_2 + \omega_k)(t-t')} c_3(t')dt'.
\end{aligned}
\tag{VI.3}
$$

Since the electron–photon coupling is much weaker than the transition energy in the Λ system, the integrals in the equation above can be evaluated in the Markovian approximation, resulting in:

$$
\partial_t c_3 \approx -i\epsilon_3 c_3 - \frac{\Gamma_{31}}{2} c_3 - \frac{\Gamma_{32}}{2} c_3,
\tag{VI.4}
$$

where

$$
\Gamma_{3i} = 2 \sum_k |g_{2k}|^2 \int_0^t e^{-i(\epsilon_i + \omega_k)(t-t')} dt'.
\tag{VI.5}
$$

Thus, the solution is

$$c_3 \approx e^{-(i\epsilon_3 + \Gamma/2)t}, \tag{VI.6}$$

where $\Gamma \equiv \Gamma_{31} + \Gamma_{32}$ is the radiative linewidth of the excited state. Furthermore, c_{1k} and c_{2k} are given by

$$c_{1k} \approx -\frac{g_{1k}}{\epsilon_3 - \epsilon_1 - \omega_k - i\frac{\Gamma}{2}} \left[e^{-i(\epsilon_1 + \omega_k)t} - e^{-i\epsilon_3 t - \frac{\Gamma}{2}t} \right],$$

$$c_{2k} \approx -\frac{g_{2k}}{\epsilon_3 - \epsilon_2 - \omega_k - i\frac{\Gamma}{2}} \left[e^{-i(\epsilon_2 + \omega_k)t} - e^{-i\epsilon_3 t - \frac{\Gamma}{2}t} \right].$$

In order to study the system in the 2×2 subspace of the lower states, we take the limit $t \gg \Gamma^{-1}$. After the spontaneous emission process, the final state is a electron–photon wavepacket $\sum_{k;i=1,2} c_{ik}|i\rangle|k\rangle$, with the coefficients

$$c_{1k} \approx -\frac{g_{1k}}{\epsilon_3 - \epsilon_1 - \omega_k - i\frac{\Gamma}{2}} e^{-i(\epsilon_1 + \omega_k)t}, \tag{VI.7}$$

$$c_{2k} \approx -\frac{g_{2k}}{\epsilon_3 - \epsilon_2 - \omega_k - i\frac{\Gamma}{2}} e^{-i(\epsilon_2 + \omega_k)t}. \tag{VI.8}$$

The state of a photon is specified by its propagation direction $\mathbf{n}$, polarization σ ($\varepsilon_\sigma \perp \mathbf{n}$), and frequency ω. So we can formulate the total wavepacket as

$$\sum_{\mathbf{n},\sigma} \left[g_{1\sigma} e^{-i\epsilon_1 t} |1\rangle |\mathbf{n}, \sigma, f_1(t)\rangle + g_{2\sigma} e^{-i\epsilon_2 t} |2\rangle |\mathbf{n}, \sigma, f_2(t)\rangle \right], \tag{VI.9}$$

where we have taken the coupling constants to be frequency-independent. In Eq. (VI.9) $f_j(t)$ is the pulse shape of the photon. From Eq. (VI.7) and (VI.8), we see that the photon wavepacket has a finite bandwidth; this point, which was first studied by Weisskopf and Wigner in their classic treatment of spontaneous emission [141], is reflected in the structure of $f_j(t)$. These functions have a central frequency equal to $\epsilon_3 - \epsilon_j$ and a bandwidth equal to Γ. As a consequence of the finite bandwidth, for a given propagation direction and polarization, the basis states $\{|\mathbf{n}, \sigma, f_j\rangle\}$ are not orthogonal, the overlap between them being

$$\langle \mathbf{n}, \sigma, f_l | \mathbf{n}, \sigma, f_j \rangle = \frac{i\Gamma}{i\Gamma + \epsilon_{lj}}, \tag{VI.10}$$

where $\epsilon_{lj} = \epsilon_l - \epsilon_j$.

We should emphasize that the wavepacket formed in Eq. (VI.9) does not rely on the Markovian approximation. In a full quantum kinetic description of the photon emission process, the wavepacket of the whole system would still have the same form, the central frequency and bandwidth of the pulses would be close to those found using the Markovian approximation, but the specific profile of $f_j(t)$ would be different from those given by Eq. (VI.7) and (VI.8).

The various phenomena (electron and photon polarization entanglement, SGC, and two-pathway decay) can all be derived from the wavepacket of Eq. (VI.9).

If the spontaneously emitted photon is not detected at all, we have to average over the ensemble of photons of all possible propagation directions to obtain the electronic state. This is the usual textbook treatment of spontaneous emission. However, if detection of an emitted photon leads to a knowledge that its direction of propagation is $\mathbf{n}_0$, then the (unnormalized) electron-photon wavepacket should be projected along that direction:

$$\sum_\sigma \left[g_{1\sigma} e^{-i\epsilon_1 t} |1\rangle |\mathbf{n}_0, \sigma, f_1(t)\rangle + g_{2\sigma} e^{-i\epsilon_2 t} |2\rangle |\mathbf{n}_0, \sigma, f_2(t)\rangle \right]. \qquad \text{(VI.11)}$$

When the two transitions are very close in frequency, i.e., $\eta \equiv |\epsilon_1 - \epsilon_2|/\Gamma \ll 1$, the overlap of the two photon wavepackets deviates from unity by $\mathcal{O}(\eta)$. After tracing out the envelopes of the photon by use of any complete basis (e.g. monochromatic states), the state of the electron and photon polarization is, with the propagation direction $\mathbf{n}_0$ understood,

$$|\Upsilon\rangle = \sqrt{N} \sum_\sigma \left[g_{1\sigma} |1\rangle |\sigma\rangle + g_{2\sigma} |2\rangle |\sigma\rangle \right] + \mathcal{O}(\eta), \qquad \text{(VI.12)}$$

where N is a normalization constant, given by

$$N^{-1} = \sum_{j=1,2} \sum_{\sigma=\alpha,\beta} |g_{j\sigma}|^2. \qquad \text{(VI.13)}$$

The order η error recorded here, in Eq. (VI.12), is meant to indicate the magnitude of the *mixed-state* error which, if neglected, results in a pure state. From this pure state, we can find explicitly the necessary conditions for entanglement or SGC. However, the approximation of neglecting η is unnecessary for computing a measure of entanglement of the resultant mixed state [8].

1. Entanglement

A measure of entanglement of the bipartite state $|\Upsilon\rangle$ in Eq. (VI.12) is given by the von Neumann entropy of the reduced density matrix of the state [143] for either the subsystem E of the two low-lying electronic states or the subsystem P of the photon polarization states. Taking the partial trace of the polarization states of the density matrix $|\Upsilon\rangle\langle\Upsilon|$ of the pure state leads to the 2×2 reduced density matrix for the electronic states,

$$\rho_E = N \sum_{ij} |i\rangle \left[\sum_{\sigma} g_{i\sigma} g_{j\sigma}^* \right] \langle j|. \tag{VI.14}$$

Diagonalization of this partial density matrix leads to two eigenvalues,

$$p_\pm = \frac{1}{2} \pm \sqrt{\frac{1}{4} - D^2}, \tag{VI.15}$$

where D^2 is the determinant of the reduce density matrix ρ_E, or

$$D = N|g_{1\alpha}g_{2\beta} - g_{1\beta}g_{2\alpha}|, \tag{VI.16}$$

for the two electronic state and two polarizations, α, β, normal to the propagation direction $\mathbf{n}_0$. The entropy of entanglement is given by

$$S = -p_+ \log_2 p_+ - p_- \log_2 p_- \tag{VI.17}$$

As D ranges from 0 to $1/2$, the entropy ranges from 0 to 1 giving a continuous measure of entanglement as the state $|\Upsilon\rangle$ goes from no entanglement to maximum entanglement. To find the axis $\mathbf{n}_0$ along which the entanglement is maximum, we have to maximize D as a function of the orientation. For a particular system, this axis can be found in terms of the dipole matrix elements of the two transitions. However, not all systems can have maximally entangled states. We will apply this to specific examples in the following section.

2. SGC

From the reduced density matrix, we can also find the conditions for SGC. Maximum SGC occurs when the reduced density matrix is a pure state.

In terms of the electron-photon coupling constants the condition is the vanishing of the discriminant D in Eq. (VI.16). This means that when the SGC effect is maximized, there exists a particular transformation which takes the basis of the electronic states $\{|1\rangle, |2\rangle\}$ to a basis $\{|\mathcal{B}\rangle, |\mathcal{D}\rangle\}$ which has the property that $|\mathcal{B}\rangle$ is always the final state of the Λ-system immediately after the spontaneous emission process, and $|\mathcal{D}\rangle$ is a state disconnected from the excited state by dipolar coupling, i.e. a dark state. This point will be further explored in section B.. The extreme values of $D = 0$ and $1/2$ make it clear that maximum SGC means no entanglement and conversely that maximal entanglement leads to no SGC. However, partial entanglement can coexist with the potentiality of some SGC for values of D between the two extremes.

Our theory can be easily extended to systems with more than two ground states. For example, in a system whose ground states are the four states from two electron spins, the SGC may lead to the coherence and entanglement between the two spins, which is the mechanism of a series of proposals of using vacuum fluctuation to establish entanglement between qubits [109].

3. Two-pathway decay

So far we have investigated the consequences when the two transitions are close in frequency ($\eta \ll 1$). When this is not the case, tracing-out the wavepacket of the photon will generally produce a mixed state in electron spins and photon polarizations. In the limit of large η, i.e., $|\epsilon_2 - \epsilon_1| \gg \Gamma$, the overlap between the two photon wave functions, $\langle f_1(t)|f_2(t)\rangle \simeq 0$, and the reduced density matrix for the spin and photon polarization would be mixed. In this case there is neither spin-polarization entanglement nor SGC, but instead the time development can be described as a two-pathway decay process: the excited state can relax to two different states by the emission of photons with distinct frequencies. However, for η between these two limits, the state in Eq. (VI.11) is still frequency-entangled: there is entanglement between the pulse shapes of the photon and the two lower

electronic levels. Furthermore, from the entangled state in Eq. (VI.11), SGC or polarization entanglement may still be recovered (provided of course that the necessary conditions on the g's are satisfied) if the quantum information carried by the frequency of the photon is erased [69]. This can be done by chopping part of the photon pulse, and thus subjecting its frequency to (more) uncertainty. In a time-selective measurement, only photons emitted at a specific time period, say from t_o to $t_o + dt$, are selected. So the projection operator associated with this measurement is $P_o = |\delta(t - t_o)\rangle\langle\delta(t - t_o)|$, which represents a δ photon pulse passing the detector at $t = t_o$. The projected state after this measurement

$$\sum_\sigma \left[g_{1\sigma} e^{-i\epsilon_1 t_o} f_1(t_o) |1\rangle + g_{2\sigma} e^{-i\epsilon_2 t_o} f_2(t_o) |2\rangle \right] |\mathbf{n}_0 \sigma\rangle \tag{VI.18}$$

is a pure state of the electron and photon-polarization, so that entanglement or SGC is restored. By writing the projector in the frequency domain

$$\tilde{P}_o = \int d\omega \int d\omega' \, e^{i(\omega - \omega')t_o} |\omega'\rangle\langle\omega|, \tag{VI.19}$$

we see that it can be understood as a broadband detector with definite phase for each frequency channel; thus it can erase the frequency (which-path) information while retaining the phase correlation. We note that a usual broadband detector without phase correlation is not sufficient to restore the pureness of the state. It is also interesting that SGC and entanglement can be controlled by choosing a different detection time t_o, as seen from Eq. (VI.18).

B. Symmetry Considerations for SGC

In this section we investigate the symmetry relations between the different parts of the Hamiltonian necessary for SGC terms to appear. Our treatment is not restricted to Λ systems, but can be extended to a system with more than two lower levels.

Consider a quantum mechanical system with one higher energy level $|e\rangle$ and a set of lower-lying states, described by a Hamiltonian H^o. Taking into account

only dipole-type interactions, denote by $\mathcal{J}_z$ the polarization operator used in the selection rules. The z axis is defined by the excited state via

$$\mathcal{J}_z|e\rangle = M_e|e\rangle$$

Note that $\mathcal{J}_z$ can be either J_z, where $\mathbf{J} = \mathbf{L} + \mathbf{S}$ is the total angular momentum operator and $\mathbf{S}$ is the spin, or L_z, as determined by the condition

$$[\mathcal{J}_z, H^o] = 0.$$

That is to say there is an axial symmetry in the system associated with $\mathcal{J}_z$. Among the lower lying states, the ones of interest are the ones appearing in the final entangled state $|\Upsilon\rangle$ of the whole system. We will refer to these states as 'bright', because they are orthogonal to the familiar dark states from quantum optics. There are at most three such states, $\{\mathcal{B}_j\}$, within a given degenerate manifold, corresponding to the three different possible projections of the dipole matrix elements along the z axis, so $j = 1, 0, \bar{1}$. In general, not all systems will have all three bright states. This concept that the final state involves only a small number of states (three in our case), gives a physical understanding of the electron-photon entangled state [25].

In order to have SGC, i.e., one or more terms of the type $\dot{\rho}_{jk} = \Gamma\rho_{ee}$, with $j \neq k$ and $j, k \neq e$, there has to be a perturbation H^B that breaks the symmetry associated with $\mathcal{J}_z$; in particular, the following conditions have to be satisfied:

(i) $[H^B, \mathcal{J}_z] \neq 0$;

(ii) $H^B|e\rangle \propto |e\rangle$;

(iii) $|\epsilon_{12}| < \Gamma$.

In general, we expect SGC between two eigenstates of the Hamiltonian $H = H^o + H^B$ which have nonzero overlap with the same bright state. The role of the first condition is to make SGC non-trivial; without this condition, it would always be possible to rotate to a different basis and formally acquire an SGC-like term in the

equations (e.g. by rotating to the x basis in the zero magnetic field case in the heavy-hole trion system). The second condition ensures that the excited state will not mix under the action of H^B; relaxing this condition gives rise to the Hanle effect, in which, as explained in the previous Chapter, an ensemble of atoms in a magnetic field is illuminated with an x-polarized pulse and the reradiated light may be polarized along y.

The third condition provides the valid regime for the occurrence of SGC. As shown before, when the radiative line-width of the excited state is smaller than the energy differences of the lower states the SGC effect will be averaged out.

The perturbation H^B can be realized by a static electric or magnetic field, by the spin-orbit coupling, by hyperfine coupling, etc. Note the different origins of H^B in different systems and that it may or may not be possible to control H^B. Examples of various systems follow, exhibiting the above conditions and demonstrating the different origins of H^B.

C. SGC in atoms

Consider an atom with Hamiltonian H^o; excluding relativistic corrections, it can be diagonalized in the $|N, L, S, M_L, M_S\rangle$ basis. Consider as the system of interest the subspace of H^o formed by $|N, 1, 1, 1, 1\rangle = |e\rangle$ and the lower-energy states $|N-1, L, S, M_L, M_S\rangle$. The various quantum numbers are of course restricted by selection rules, and $\mathcal{J}_z = L_z$. Here we will list only the three bright states:

$$|\mathcal{B}_1\rangle = |N - 1, 2, 1, 2, 1\rangle$$

$$|\mathcal{B}_0\rangle = |N - 1, 2, 1, 1, 1\rangle$$

$$|\mathcal{B}_{\bar{1}}\rangle = a|N - 1, 2, 1, 0, 1\rangle + b|N - 1, 0, 1, 0, 1\rangle$$

where the coefficients a and b can be determined in the following way: in the original $|NJM_JLS\rangle$ basis, the matrix elements for the transitions $|N - 1, 2, 1, 0, 1\rangle \leftrightarrow |N, 1, 1, 1, 1\rangle$ and $|N - 1, 0, 1, 0, 1\rangle \leftrightarrow |N, 1, 1, 1, 1\rangle$ are given by the Wigner-Eckart

theorem. By rotating to the $\{|\mathcal{B}\rangle, |\mathcal{D}\rangle\}$ basis, and requiring the transition $|\mathcal{D}\rangle \leftrightarrow |N, 1, 1, 1, 1\rangle$ to be forbidden, we find a and b. Inclusion of the spin-orbit inter-action, which plays the role of H^B, i.e. $H^B = \alpha \mathbf{L} \cdot \mathbf{S}$, condition (i) is obviously satisfied. The state $|e\rangle \equiv |N, L = 1, S = 1, M_L = 1, M_S = 1\rangle = |N, J = 2, M_J = 2, L = 1, S = 1\rangle$ is an eigenstate of $\mathbf{L} \cdot \mathbf{S} = (\mathbf{J}^2 - \mathbf{L}^2 - \mathbf{S}^2)/2$; hence, condition (ii) is also satisfied (a state of maximum M_L and M_S, does not mix under the spin-orbit coupling). In the new basis, SGC is expected to occur between states with the same value of M_J, which can also be verified by direct calculation. In this example the line-width of $|e\rangle$ is much smaller than the spin-orbit coupling strength α. Typical values in atoms are $\Gamma_e \sim 1\mu$ eV and $\alpha \sim 1$ meV, which means that SGC will not be observed in such a system.

Repeating the above line of thought, but with the role of the unperturbed states being $|NJM_JLS\rangle$, and the role of H^B played by the hyperfine coupling, the condition on the size of the splitting relatively to the linewidths is met, so there should be SGC between states $|NJFM_F\rangle$ and $|NJF'M_F\rangle$. There will be, however, incoherent decay to other states with the same F and F', but $M_F' \neq M_F$, so the purity of the final state will be very small.

1. Entanglement and SGC of atomic hyperfine states

In this example, the Λ system is formed by the hyperfine states of a single trapped Cd ion in the presence of a magnetic field along the z axis. In the $|FM_F\rangle$ basis, the excited state is $|21\rangle$ and the two lower levels are $|11\rangle$ and $|10\rangle$. The two lower levels have the same principal quantum number N. The entanglement between the polarization of the photon and the atom has been demonstrated ex-perimentally [13]. To illustrate the methods developed in Section A., we will make use of the fact that the two lower levels are states of definite angular momentum and its projection to the z axis. Then, by the Wigner-Eckart theorem we know that the dipole moment of the transition $|21\rangle \rightarrow |10\rangle$ has a nonzero component only along $\mathbf{e}_+ = \mathbf{x} + i\mathbf{y}$ whereas that of $|21\rangle \rightarrow |11\rangle$ has only a component along

z. The wavepacket of the system is then given by

$$|\Upsilon\rangle = \frac{-\sqrt{2}\sin\vartheta|\vartheta\rangle|11\rangle + e^{-i\varphi}\cos\vartheta|\vartheta\rangle|10\rangle - ie^{-i\varphi}|\varphi\rangle|10\rangle}{\sqrt{2+\sin^2\vartheta}} \qquad \text{(VI.20)}$$

where ϑ and φ are the spherical coordinates measured from z and x axis, respectively, and $|\vartheta\rangle$ and $|\varphi\rangle$ are the polarization basis states, which are linearly polarized parallel and normal to the plane formed by the z axis and the propagation direction, respectively. Then from Eq. (VI.20), we read off the g's:

$$g_{1\vartheta} \propto -\sqrt{2}\sin\vartheta \qquad \text{(VI.21)}$$

$$g_{1\varphi} = 0 \qquad \text{(VI.22)}$$

$$g_{2\vartheta} \propto e^{-i\varphi}\cos\vartheta \qquad \text{(VI.23)}$$

$$g_{2\varphi} \propto ie^{-i\varphi}, \qquad \text{(VI.24)}$$

where $|11\rangle \equiv |1\rangle$ and $|10\rangle \equiv |2\rangle$. The measure of entanglement by D is

$$D = \frac{\sqrt{2}\sin\vartheta}{2+\sin^2\vartheta}. \qquad \text{(VI.25)}$$

The maximum possible entanglement occurs at $\vartheta = \pi/2$, i.e., whenever the photon propagates perpendicularly to z. The maximum value of 0.47 is close to being maximally entangled. D does not depend on φ, as expected since there is azimuthal symmetry about z.

In terms of SGC and symmetry, it is interesting to notice that the role of the (external or internal) perturbation, H^B, introduced in section B. can be played by the different projections (measurements) because the state before the measurement is an eigenstate of the operator J_z (total angular momentum along z) but not after the measurement in general. The magnetic field along the z-axis is included in the Hamiltonian H^o. If the spontaneously emitted photons are measured along the quantization axis, only the ones emitted from the transition $|21\rangle \to |10\rangle$ will be detected, since only their polarization allows propagation along z. On the other hand, a photon detector placed at a finite angle from z can play the role of H^B. Suppose a photon is spontaneously emitted along an axis $n = (\vartheta, \varphi)$.

The density matrix of the state given by Eq. (VI.20) is $|\Upsilon\rangle\langle\Upsilon|$. If we are only interested in the dynamics of the ion, and the polarization of the photon is not measured, then the photon polarization has to be traced out. Then the reduced density matrix of the system, in the atomic states is

$$\rho_E = \frac{1}{2 + \sin^2 \vartheta} \begin{bmatrix} \cos^2 \vartheta + 1 & \sqrt{2}e^{-i\varphi} \cos \vartheta \sin \vartheta \\ \sqrt{2}e^{+i\varphi} \cos \vartheta \sin \vartheta & 2\sin^2 \vartheta \end{bmatrix}. \tag{VI.26}$$

The off-diagonal elements express coherence between the hyperfine states with dependence on the photon propagation direction. We can check that for $\vartheta = 0$ the probability of the atom being in the $|11\rangle$ state is zero and there are no off-diagonal elements, and for $\vartheta = \pi/2$ the off-diagonal elements are also zero, which means there is no SGC, but the state has the maximum possible entanglement. For all the intermediate values of ϑ the hyperfine states and the photon polarization are entangled, and there is also some SGC when the photon is traced out. Maximum SGC occurs when D is minimized; from Eq. (VI.25) we see that it is zero for $\vartheta = 0$. This is expected anytime the one of the two transitions involves a linearly polarized photon, since the latter cannot propagate along the quantization axis. So, for this orientation the final state can only be $|10\rangle$. For intermediate angles, for instance $\vartheta = \pi/4$, there is both entanglement and SGC involving both lower states, when the photon is traced out. Since SGC only does not always occur for most photon propagation directions we could view it as 'probabilistic' SGC.

D.   SGC in Quantum Dots Revisited

To demonstrate the theory of Section B. in the system where we have shown SGC to occur, i.e., the QD we will examine how the conditions of Section B. are satisfied. We take H^o to be the Hamiltonian of the Q.D., with $|e\rangle = |\mathcal{T}\rangle$, the trion state described above, excited by $\sigma+$ light; $\mathcal{J}_z = J_z$, since the spin-orbit interaction is included in H^o. The magnetic field is taken now to point at a random direction forming an angle ψ with the growth axis z, and any component

of the B field along z can also be included in H^o. H^B is the contribution to the Hamiltonian due to the magnetic field along x. Condition (i) is fulfilled since $g_x \simeq 0$, and condition (ii) is obviously satisfied. The only bright state is the electron spin s_z eigenstate, $|z\rangle \equiv |\uparrow\rangle$. For later use, we also define $|\bar{z}\rangle \equiv |\downarrow\rangle$ and

$$|\psi_+\rangle = \cos\frac{\psi}{2}|\uparrow\rangle + \sin\frac{\psi}{2}|\downarrow\rangle \tag{VI.27}$$

$$|\psi_-\rangle = \sin\frac{\psi}{2}|\uparrow\rangle - \cos\frac{\psi}{2}|\downarrow\rangle. \tag{VI.28}$$

Therefore we expect SGC between states $|\psi_+\rangle$ and $|\psi_-\rangle$ for any angle $\psi \neq 0$, and since the linewidth of the trion is large enough compared to the Zeeman splitting, SGC should moreover have a detectable effect.

The current discussion is focused on single Λ systems, but the experiment was carried out for an ensemble [41]. In general, for an ensemble of equivalent non-interacting atoms, an average over the different z axes would have to be performed. However, in this quantum-dot solid state system, there is a common z axis for all the dots, since they are grown on the same plane (xy), and they have a relatively large in-plane cross-section as compared to their height. This is a clear advantage of the quantum dot ensemble over an ensemble of atoms.

We can also analyze this system using the methods in Section A.. To find the g's, we need the dipole matrix elements between $|\psi_+\rangle, |\psi_-\rangle$ and the trion. Again, we will make use of the fact that $|\uparrow\rangle$ and $|\mathcal{T}\rangle$ are angular momentum eigenstates along the z axis, with the familiar selection rules. Only state $|\uparrow\rangle$ has nonzero dipole matrix element with $|\mathcal{T}\rangle$, $d_+\mathbf{e}_+$, so that the transitions $|\psi_+\rangle \to |\mathcal{T}\rangle$ and $|\psi_-\rangle \to |\mathcal{T}\rangle$ have dipole matrix elements equal to $d_+ \cos\frac{\psi}{2}\mathbf{e}_+$ and $d_+ \sin\frac{\psi}{2}\mathbf{e}_+$ respectively. Then, for a photon emitted along $\mathbf{n}_0 = (\vartheta, \varphi)$, we find the couplings:

$$g_{1\vartheta} = d_+ e^{i\varphi} \cos\vartheta \cos\frac{\psi}{2} \tag{VI.29}$$

$$g_{1\varphi} = d_+ i e^{i\varphi} \cos\frac{\psi}{2} \tag{VI.30}$$

$$g_{2\vartheta} = d_+ e^{i\varphi} \cos\vartheta \sin\frac{\psi}{2} \tag{VI.31}$$

$$g_{2\varphi} = d_+ i e^{i\varphi} \sin\frac{\psi}{2}, \tag{VI.32}$$

so that the determinant is always zero, independently of $\mathbf{n}_0$. This means that the system in this configuration will never be entangled with the polarization of the photon, which, as we have seen, implies maximum SGC. The final state of the Λ system is always $|\uparrow\rangle$, unentangled.

E. Proposed Experiment for Quantum Dot Spin-Photon Polarization Entanglement

The spin-photon entanglement can be also realized in a quantum dot system by employing the light-hole trion state. The heavy and light hole excitons are split by the breaking of the tetrahedral symmetry of the bulk III-V compound. It might also be possible to make the light hole states in quantum dots lower in energy than the heavy holes. The magnetic field is pointing along the x direction, so that the lower levels are the two S_x eigenstates, $|+\rangle$ and $|-\rangle$. The optical pulses used are such that the light hole trion polarized along the $+x$ direction is excited. The excited state is a trion of a singlet pair of electrons and a light hole which is in the $m_j = \pm 1/2$ component of the $j = 3/2$ state. The trion can thus be characterized by the state $|JM_J\rangle = |\frac{3}{2}, \pm\frac{1}{2}\rangle$. We choose the $M_J = \frac{1}{2}$ state as the excited state of the Λ system and denote it by $|\mathcal{T}_\ell\rangle$.

The transitions $|\mathcal{T}_\ell\rangle \rightarrow |+\rangle$ and $|\mathcal{T}_\ell\rangle \rightarrow |-\rangle$ involve a photon linearly polarized along x ($|X\rangle \equiv |\pi_x\rangle$) and one with elliptical polarization ($-i|Y\rangle + 2|Z\rangle \equiv |E_{yz}\rangle$), respectively. In particular, after $|\mathcal{T}_\ell\rangle$ has decayed, the state of the system is from Eq. (VI.12),

$$|\Upsilon\rangle = -\frac{1}{\sqrt{6}}[|X\rangle|-\rangle + (2|Z\rangle - i|Y\rangle)|+\rangle], \tag{VI.33}$$

We assume a measurement which determines the propagation direction of the photon $\mathbf{n}_0 = (\vartheta, \varphi)$. Then the state becomes:

$$|\Upsilon\rangle = \frac{-1}{\sqrt{2 + 3\sin^2\vartheta}}[\cos\vartheta\cos\varphi|\vartheta\rangle|-\rangle$$

$$-(2\sin\vartheta + i\sin\varphi\cos\vartheta)|\vartheta\rangle|+\rangle$$

$$-\sin\varphi|\varphi\rangle|-\rangle - i\cos\varphi|\varphi\rangle|+\rangle]. \qquad (VI.34)$$

Following the same procedure as in the trapped ion example, we find that the condition for maximum entanglement is $\vartheta = 0$; the value of D is then 0.5, maximal entnaglement. SGC will only occur when D in Eq. (VI.16) is less than 0.5 and it will be maximum for propagation along x, which means that the electron will be in the state $|+\rangle$. For all other values of ϑ there will be both entanglement and SGC between the two energy eigenstates when the photon is traced out. The phenomena following the spontaneous radiative decay of this system are indeed very similar to the trapped ion case. In the solid state system there is no need to isolate a single dot in order to observe SGC since all dots are oriented in the same direction.

For quantum information processing, entanglement between photon polarization and spin has to be established in a quantum dot. So isolating and addressing a single dot is required. Experimentally, this requirement is arguably feasible [17]. The system should be initialized at state $|+\rangle$ (or $|-\rangle$) and subsequently excited by y-(or x-) polarized light, so that only state $|\mathcal{T}_\ell\rangle$ gets excited. Other trion states, involving electrons in the triplet state and/or heavy holes, have an energy separation from $|\mathcal{T}_\ell\rangle$ large enough compared to the pulse bandwidth and so they can be safely ignored. Above we found that the state will be maximally entangled when the spontaneously emitted photon propagates along z. When the optical axis is along z, the spontaneously emitted photon may be distinguished from the laser photons by optical gating. As an alternative to the optical gating, to minimize scattered light the detector may be placed along y, i.e., at $(\vartheta, \varphi) = (\pi/2, \pi/2)$. The value of D is then 0.2, so that the entanglement will be significantly less than that along the optical axis, but should be measurable. The observation of the emitted photon and the measurement of its polarization can be made as in Ref. [13]. By use of the pump-probe technique, the state of the spin will also be measured to show the correlation with the polarization of the photon.
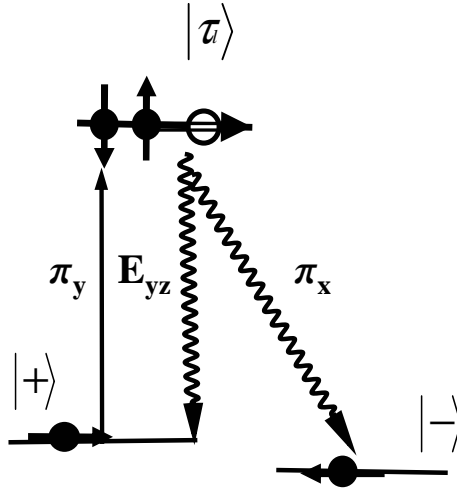
VI.1   The energy levels of the Λ system consisting of the two electron spin states (lower levels) and the light hole trion polarized along the $+x$ direction. The solid line represents the laser pulse, which propagates along z and is linearly polarized in the y direction. The wavy lines denote the spontaneously emitted photons from the transitions $|\mathcal{T}_\ell\rangle \to |+\rangle$ and $|\mathcal{T}_\ell\rangle \to |-\rangle$, which are elliptically polarized in the yz plane and linearly polarized along x, respectively.

To overcome the probabilistic nature of the entanglement (as projection is needed) and to improve the quantum efficiency degraded by the scattering problem, cavities and waveguides may be employed to enhance and select desired photon emission processes [78].

The text of this Chapter is in part a reprint of the material as it appears in Sophia E. Economou, Ren-Bao Liu, L. J. Sham, and D. G. Steel, "Unified theory of consequences of spontaneous emission in a Lambda system," Phys. Rev. B 71, 195327 (2005). "Copyright (2005) by the American Physical Society." The dissertation author was the primary researcher and author and the co-authors listed in this publication, directed and supervised the research which forms the basis for this chapter.

VII.

Optical spin rotation

In this Chapter, we present a proposal to optically implement rotations of the electron spin in a quantum dot about the growth axis. In particular, we make use of the analytic properties of hyperbolic secant (sech) pulses in two-level systems to realize spin rotations about the growth direction by an arbitrary angle, for which we give an analytical expression.

We propose to use this scheme for experimental demonstration of the spin rotation. Using realistic system and pulse parameters we find the fidelity of the rotation to be more than 96% for pulses in the picosecond regime, and robust against small errors in pulse parameters. We design an adaptive feedback loop to correct for errors originating from unintended dynamics. The rotation is still evident –albeit with a large fidelity loss– in the ensemble case, providing thus the possibility of demonstration of the optical spin rotation in an ensemble of quantum dots.

A.   Review of Existing Proposals

A proposal for arbitrary optical spin rotations in a quantum dot which does not explicitly require selectivity between the two transitions is available [23], but as will now be explained it implicitly requires long pulses when the Zeeman splitting is small. Specifically, in ref. [23] two pulses with a definite phase relation

are used. Both pulses act on both transitions. To remove fast oscillating terms, the condition

$$\omega_B >> \Omega_j(t) \tag{VII.1}$$

is imposed, where $2\omega_B$ is the Zeeman splitting and Ω_j is the Rabi frequency of pulse j. The axis of rotation depends on the ratio of the two Rabi frequencies and the phase between the two pulses. The angle of rotation is given by the time integral of

$$\lambda_2 = \frac{\Delta}{2} - \sqrt{\Omega_\uparrow^2 + \Omega_\downarrow^2 + \left(\frac{\Delta}{2}\right)^2}, \tag{VII.2}$$

where Δ, the detuning, is the difference between the central frequency of the laser and the trion energy. From the last relation, it is evident that in order to achieve large rotation angles, long pulses are needed, since the Rabi frequency is bounded from Eq. (VII.1).

Another proposal [100] suggested to use a π-pulse to populate the trion state for some time, during which the precession of the spin is used so that the $|\bar{z}\rangle$ state acquires a phase and subsequently a second π-pulse recovers the $|z\rangle$ state population by stimulated emission. This method of rotating requires populating the trion state for a significant amount of time, so that trion decay will significantly affect the fidelity. The operation will moreover be slowed down when the Zeeman splitting is small.

B. Proposal of rotations about the growth axis

In the current proposal, contrary to the use of any kind of selectivity between the two transitions, we choose a pulse with sufficient bandwidth to act on both transitions. The Hamiltonian in the $\{|\bar{z}\rangle, |z\rangle, |\mathcal{T}\rangle\}$ basis has the form

$$H = \begin{bmatrix} 0 & \omega_B & 0 \\ \omega_B & 0 & \Omega(t)\,e^{i\omega_o t} \\ 0 & \Omega(t)\,e^{-i\omega_o t} & \epsilon_T \end{bmatrix}. \tag{VII.3}$$

It is evident from the above form of the Hamiltonian, that the pulse only couples the $|z\rangle$ state to the excited trion state. The $|\bar{z}\rangle$ state is indirectly coupled through the B field. Therefore, for small Zeeman splitting and for a pulse much shorter than the spin precessing period we can view in our qualitative discussion the three-level system as two systems of dimensions 2 and 1, consisting of $\{|z\rangle, |\mathcal{T}\rangle\}$ and $\{|\bar{z}\rangle\}$ respectively.

It is well known that for a two-level system the sech pulse shape of Rosen and Zener (RZ) [117] yields an exactly solvable evolution, for arbitrary detuning. As was more recently shown, the RZ pulse belongs to a class of exactly solvable pulse shapes [5]. Here, we will make use of the properties of the RZ pulses to obtain an analytical expression for the angle of rotation.

C.   Review of the Rosen-Zener solution

Consider a two-state system, initially in the ground state, $|g\rangle$, with the two levels coupled by a time dependent Hamiltonian with a sech envelope and central frequency ω_o:

$$\Omega \ \mathrm{sech}(\sigma \ t) \ e^{i\omega_o t} \equiv f(t) \ e^{i\omega_o t}, \qquad (VII.4)$$

where Ω is the Rabi frequency, σ is the bandwidth of the pulse. Moving to the interaction picture, the problem reduces to solving two coupled first order equations or, equivalently, one second order equation of the form:

$$\ddot{c}_e + (i\Delta - \dot{f}/f)\dot{c}_e + f^2 c_e = 0, \qquad (VII.5)$$

where c_g (c_e) is the coefficient of the ground (excited) state, and Δ, the detuning, is the difference between the laser frequency ω_o and the energy splitting of the two levels; the initial condition is $c_e(-\infty) = 0$. By the change of variable

$$\zeta = \frac{1}{2} \left(\tanh(\sigma t) + 1 \right), \qquad (VII.6)$$

RZ bring the equation into the form of the Hypergeometric Equation, where

$$a = \frac{\Omega}{\sigma}, \tag{VII.7}$$

$$c = \frac{1}{2}\left(1 + i\frac{\Delta}{\sigma}\right). \tag{VII.8}$$

After imposing the initial conditions, the coefficients of the ground ($|g\rangle$) and excited ($|e\rangle$) states are:

$$c_g = F(a, -a, c^*, \zeta) \tag{VII.9}$$

$$c_e = -i\frac{a}{c^*}\,\zeta^{1-c}\,F(a+1-c, 1-a-c, 2-c, \zeta). \tag{VII.10}$$

We see from Eq. (VII.10) and by use of the properties of the Hypergeometric function that when

$$\sigma = \Omega \tag{VII.11}$$

there is no population transfer to the excited state for $t \to \infty$, i.e., $c_e(\infty) = 0$, and instead the pseudospin vector undergoes a full cycle from $|g\rangle$ to $|e\rangle$ and back to $|g\rangle$ with a ground state having acquired a phase factor

$$c_g(\infty) = -\frac{\sigma + i\Delta}{\sigma - i\Delta} \equiv e^{-i\phi}, \tag{VII.12}$$

$$\tan\phi = \frac{2\sigma\Delta}{\Delta^2 - \sigma^2}. \tag{VII.13}$$

For σ fixed, the path will be determined from the detuning, as shown in Fig. VII.1

.

D.   Use of RZ pulses for Raman qubit rotation

For an arbitrary sech pulse, the evolution operator of the whole three-level system, under the approximation of slow precession, is found by combining the solution of the Rosen-Zener problem for arbitrary initial conditions and including the decoupled (to a first approximation) $|\bar{z}\rangle$ level. In the $\{|\bar{z}\rangle, |z\rangle, |\mathcal{T}\rangle\}$ basis we obtain
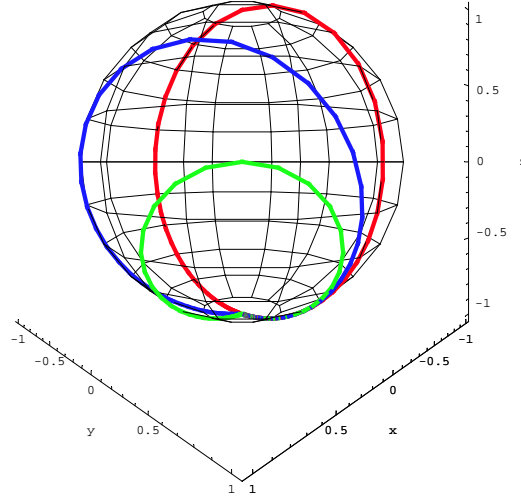
VII.1   Bloch vector representation of the pseudospin; The pulse bandwidth is fixed $\sigma = 1$ and the detuning varies: $\Delta = 0$ (red curve), $\Delta = 1$ (blue curve) and $\Delta = 0.5$ (green curve). The plot is in the rotating frame of the laser, not that of the unperturbed system.

$$U \simeq \begin{bmatrix} 1 & 0 & 0 \\ 0 & F(a, -a, c^*, \zeta) & -\frac{ia}{c}\zeta^c \, F(a+c, -a+c, 1+c, \zeta) \\ 0 & -\frac{ia}{c^*}\zeta^{c^*} F(a+c^*, -a+c^*, 1+c^*, \zeta) & F(a, -a, c, \zeta) \end{bmatrix}.$$

$$(VII.14)$$

To have a unitary operation, it is necessary that Eq. (VII.11) is satisfied, i.e., the trion state gets only virtually excited. We will refer to such pulses as 'transitionless'. Mathematically, this translates to $a = 1$. We are also interested only in the form of U after the passage of the pulse, when $\zeta = 1$. Then U becomes

$$U \simeq \begin{bmatrix} 1 & 0 & 0 \\ 0 & 1 - 1/c^* & 0 \\ 0 & 0 & 1 - 1/c \end{bmatrix} \equiv \begin{bmatrix} 1 & 0 & 0 \\ 0 & e^{-i\phi} & 0 \\ 0 & 0 & e^{i\phi} \end{bmatrix}. \qquad (VII.15)$$

The truncated evolution operator, in the 2×2 spin space is described by

the unitary matrix:

$$U_{spin} \simeq \begin{bmatrix} 1 & 0 \\ 0 & e^{-i\phi} \end{bmatrix} = e^{-i\phi/2} \begin{bmatrix} e^{i\phi/2} & 0 \\ 0 & e^{-i\phi/2} \end{bmatrix}. \qquad \text{(VII.16)}$$

A phase between the $|\pm z\rangle$ states translates to a rotation about the z axis by an angle ϕ. So, while for a true two-level system the induced phase of a transitionless pulse is trivial when all the population is initially in the $|z\rangle$ state, for the three-level system it yields a non-trivial rotation about the z axis, since the phase now is relative to the $|\bar{z}\rangle$ state. The expression for the angle of rotation may be simplified:

$$\tan\frac{\phi}{2} = \frac{\sin\phi}{1+\cos\phi} = \frac{\sigma}{\Delta}.$$

$$\phi = 2\arctan\frac{\sigma}{\Delta}. \qquad \text{(VII.17)}$$

E. Numerical simulation and Experimental proposal

Equations (VII.16) and (VII.17) are our main theoretical results. To check to what extent this theory can be implemented in an actual three level system with its inherent decoherence and unintended dynamics included, we studied by analytical work and detailed simulations the spin beats of an optical experiment in the dots.

The proposed experimental process involves three pulses.

1. An initializing pulse, which we call pump, for which $\Omega = \sigma/2$.

2. A rotating pulse, which we call control pulse, for which $\Omega = \sigma$.

3. A weak probe pulse.

The optical experiments on quantum dots are usually performed at 4K, which is well above the Zeeman splitting for GaAs [41]. We are thus starting with a completely mixed state of the qubit and initialize it with optical pumping [41]. We propose to use an RZ pulse which will probabilistically initialize the spin with $-1/2$

polarization as follows. A $\sigma+$ polarized pulse acts only on $|z\rangle$, exciting it to the trion state and leaving net population to the $|\bar{z}\rangle$ state, thus creating a spin vector (SV) initially pointing along $-z$ and precessing about the static B field. From the solution of the Rosen-Zener problem, we see that by setting $\Omega = \sigma/2$ and $\Delta = 0$ all the population of the $|z\rangle$ state is transferred to the trion, which subsequently decays incoherently to the two lower states, provided that the trion state linewidth is small compared to the Zeeman splitting, so that the Spontaneously Generated Coherence (SGC) [42, 41] may be ignored. In Section F. we will investigate the effect of SGC along with the other deteriorating mechanisms. However, we stress that SGC has been taken into account in all our numerical simulations.

Since the designed operation is a rotation about the z axis, the SV should not be affected when the incident control pulse finds it at a dip or peak, i.e. at $|\bar{z}\rangle$ or $|+z\rangle$ respectively. On the other hand, the most prominent effect should be when the SV intersects the time axis, i.e., when it is pointing along the y direction, which is the case in our simulations.

To experimentally achieve a transitionless pulse, the Rabi frequency of the initializing pulse could be doubled or preferably a separate pump-probe experiment with the control pulse in place of the pump may be performed. The transitionless pulse induces a large initial spike and then the spin beats essentially vanish, as shown in Fig. VII.2. The physics is simple: the transitionless pulse only virtually excites the trion, ideally transferring no population, so that it may not be used for initialization via optical pumping. Once the pulse duration and Rabi frequency of the control pulse are fixed, the detuning will be varied from $\Delta = 0$ which renders a π rotation, to $\Delta = \sigma/\tan(\pi/8)$, which yields a $\pi/4$ rotation.

In our simulations, the pulse duration is about 6 ps for GaAs, close to the ones used in ref.[41], which translates to about $\sigma = 0.4$ meV. We take the Zeeman splitting to be 40 μeV, which corresponds to a B field of about 6.5 T [41]. For InAs dots, we take $\sigma = 0.8$ meV and the Zeeman splitting to be 0.1 meV, which corresponds to B$\sim$ 2.3 T [72]. The trion decay rate for GaAs is also taken from
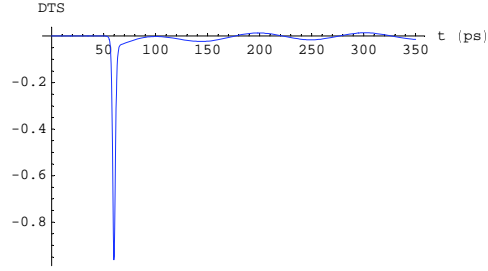
VII.2   Effect of transitionless pulse on mixed state, as calculated in the DTS versus t relation. Virtually no beats are generated when $\Omega = \sigma$. Here, $\sigma = 0.4$meV and $\Delta = 0$.

ref. [41], equal to 0.01 meV. For InAs dots it is about 0.6 μeV [140].

To demonstrate the unitarity of the control pulse, a second pulse is used to rotate the SV back to the yz plane and thus recover the initial beat amplitude, as shown in Fig. VII.3 GaAs and in Fig. VII.6 for InAs. We note that the beats are not recovered completely, due to errors originating from the trion decay and the (small but finite) precession of the spin during the operation. For π rotations, Figs. VII.4 and VII.5, the unitarity is evident, since the SV remains entirely in the yz plane. We will ignore spin dephasing in the following discussion on fidelity.

The spin will be measured via a weak probe. Given that a $\sigma+$ polarized probe measures the z component of the SV, the actual angle of rotation in the experiment will be given by

$$\phi_{exp} = \arccos \frac{A_1}{A_o}, \qquad (VII.18)$$

where A_o and A_1 are the beat amplitudes before and after the control pulse respectively, as in ref. [57].
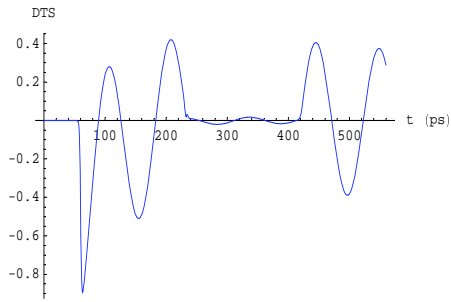
VII.3   Differential transmission signal (DTS) representing spin rotation in a GaAs dot by $\pi/2$ with pulse of $\sigma = 0.4$meV and $\Delta = \sigma$.
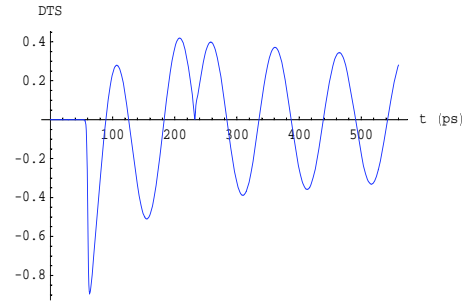
VII.4   Differential transmission signal (DTS) representing rotation of the spin in a GaAs dot by π with a resonant pulse of $\sigma = 0.4$meV.
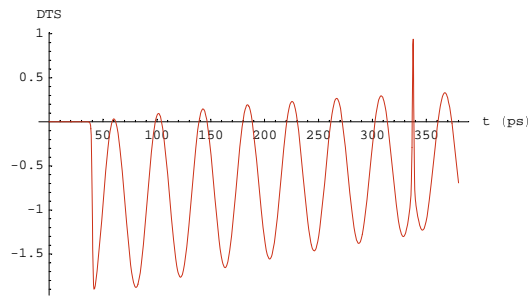
VII.5   DTS representing rotation of the spin in a InAs dot by π. The pulse is resonant with $\sigma = 0.8$meV.
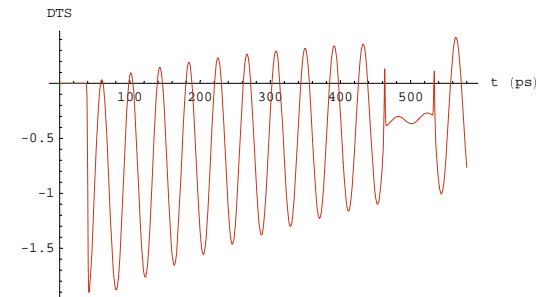
VII.6   DTS showing the rotation of the spin in a InAs dot by $\pi/2$. The pulse parameters are $\sigma = \Delta = 0.8$meV

F. Fidelity

1. Initialization

The initialization process described above ideally yields a 50% fidelity. However, the mechanism that undermines the fidelity of the initialization is the SGC, as mentioned above [42]. SGC is suppressed by making the Zeeman splitting larger [42, 41]. Our numerical simulations show that the fidelity of initialization is about 40% for GaAs, even for relatively large Zeeman splittings. Since the initialization is far from perfect anyway, we will not worry about SGC effects.

A more important issue is a possible uncertainty in the Rabi frequency, stemming from limited knowledge of the dipole matrix element between $|z\rangle$ and $|\mathcal{T}\rangle$. Deviation of the Rabi frequency from $\sigma/2$ will limit the generated polarization. In Section G. we discuss how to maximize the polarization by use of (adaptive) feedback loops.

Finally, valence band mixing will affect the spin polarization, by altering the selection rules. Again, a feedback loop that scans through the polarization of the laser may be employed, so that a true Λ-configuration is recovered. This, discussed in Section G., will also allow for correction due to valence band mixing in the subsequent control of the spin.

2. Rotation

The fidelity is given by [108, 110]

$$\mathcal{F} = \overline{|\langle\Psi|\widetilde{U}^\dagger U_{id}|\Psi\rangle|^2}, \tag{VII.19}$$

where Ψ is the initial state, $\widetilde{U}$ and U_{id} are the actual and ideal operations respectively and the average is to be taken over the whole Hilbert space. Clearly, for $U = U_{id}$, the fidelity obtains its largest value, 1, which means that the operation is perfect. If we define

$$I = \widetilde{U}^\dagger U_{id}, \tag{VII.20}$$

then the fidelity becomes (see Appendix A)

$$\mathcal{F} = \frac{1}{3} \sum_i |I_{ii}|^2 + \frac{1}{6} \sum_{i \neq j} |I_{ij}|^2. \tag{VII.21}$$

The purity of the operation is given by [110]

$$\mathcal{P} = \overline{\mathrm{Tr}(\rho_{out}^2)} = \frac{1}{3} \sum_i \mathrm{Tr} R_{ii}^2 + \frac{1}{6} \sum_{i \neq j} \mathrm{Tr} \left(R_{ii} R_{jj} + R_{ij} R_{ji} \right), \tag{VII.22}$$

where $R_{ij} = \widetilde{U} \rho_{ij} \widetilde{U}^\dagger$. This is a good measure for purity, since for a pure state $\rho^2 = \rho$, which is easily seen by writing $\rho = |\Psi\rangle\langle\Psi|$.

The fidelity of the operation deteriorates due to the following mechanisms: the decay of the trion state during the gate operation, the spin precession during the pulse action, and the spin dephasing. The dominant mechanism is the former; it is irreversible and will degrade the unitarity of the operation, with the effect being stronger for longer pulses and pulses closer to resonance. Obviously, the shorter the pulse the higher the fidelity; but there is a lower bound to how short a pulse may be, as there is an upper bound on pulse strength the system can accommodate. Fig. VII.8 shows the fidelity as a function of the pulse bandwidth. Smaller detunings correspond to larger rotation angles, Eq. (VII.17), so that the fidelity is lower for large rotation angles, and is close to perfect for small angles, as shown in Figs. VII.7 and VII.9 for GaAs and InAs dots respectively.

On the other hand, the precession of the spin vector during the action of the control pulse is a reversible evolution, and will not affect the purity of the operation. It will however cause a tilt to the axis of rotation, affecting the fidelity. In principle, this can be taken into account by choosing this alternate axis of rotation instead of insisting on rotations about z. In our case however, it does play a small role in the loss of fidelity, more so for longer pulses.

As in the initialization case, uncertainty in the Rabi frequency and valence band mixing will affect the fidelity of the rotation. In the next section we discuss how to overcome these effects using feedback loops. Once this process is carried out for initialization, the appropriate pulses will automatically be known for the rotation as well.

Fidelity

ϕ (π)

0.98
0.96
0.94
0.92

0.2 0.4 0.6 0.8 1
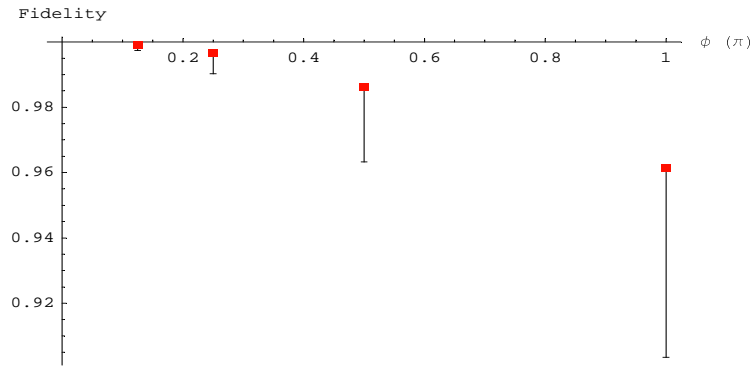
VII.7   Fidelity of the operation as a function of the angle of rotation for GaAs dots. Large angles correspond to pulses closer to resonance, yielding loss of fidelity due to (real) trion excitation. Here the bandwidth has been taken equal to 0.3 meV and the uncertainty in the laser electric field is 15%.

Fidelity

0.98
0.96
0.94

σ (meV)

0.3 0.4 0.5 0.6 0.7 0.8 0.9
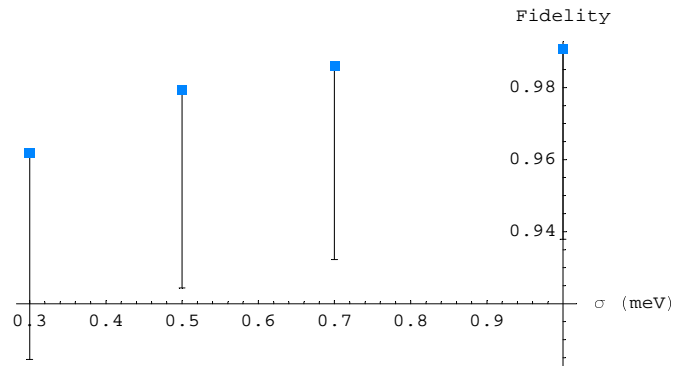
VII.8   Fidelity of the operation as a function of the pulse bandwidth for GaAs dots. Large bandwidth corresponds to fast pulses, and therefore smaller time intervals of trion excitation. Here the angle of rotation equals π. The uncertainty in the laser electric field is 15%.
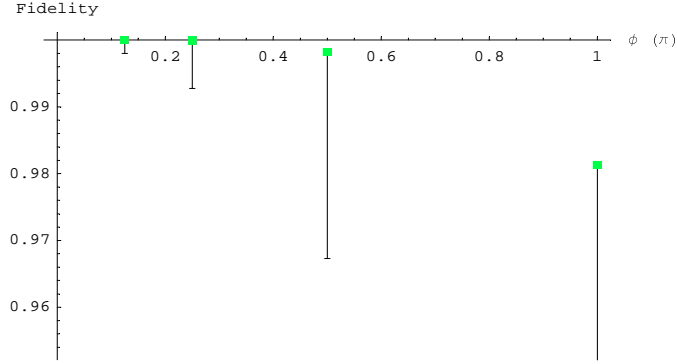
VII.9   Fidelity of the operation as a function of the angle of rotation for InAs dots. Large angles correspond to pulses closer to resonance, yielding loss of fidelity due to (real) trion excitation. Here the bandwidth has been taken equal to 0.8 meV. The uncertainty in the laser electric field is 15%.

G.   Overcoming errors with feedback loops

1.   Uncertainty in laser parameters

Experimentally, the Rabi frequency may not be exactly known if the polarization matrix element between $|z\rangle$ and $|\mathcal{T}\rangle$ has not been measured; one way to find the optimal value of the Rabi frequency is fixing the pulse duration and scanning the intensity until the response (spin polarization) is maximized. Actually, the theory can do better: even if the pulse duration is not precisely known, we can devise a feedback loop, which combined with the analyticity of our solution will yield the maximum polarization, i.e., will pick the pulse with $\Omega = \sigma/2$. By use of the evolution operator of Eq. (VII.14), we can find the trion population after the passage of the pulse. The truncated evolution operator for time t after the pulse and for resonant pulses takes the form in the $\{|\bar{z}\rangle, |z\rangle\}$ subspace

$$\Lambda(\Delta = 0) \simeq \begin{bmatrix} 1 & 0 \\ 0 & \cos(\frac{\Delta\theta}{2}) \end{bmatrix}, \tag{VII.23}$$

where $\Delta\theta = 2\pi\frac{\Omega}{\sigma}$ is the pulse area. Action of Λ on a mixed density matrix yields

$$\rho = \begin{bmatrix} 1/2 & 0 \\ 0 & (1/2)\cos^2(\frac{\Delta\theta}{2}) \end{bmatrix}. \tag{VII.24}$$
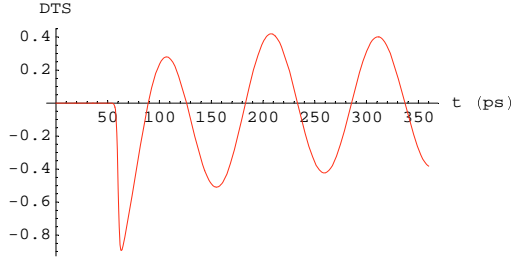
VII.10   Initialization using a sech pulse with $\sigma = 0.4$meV and $\Omega = \sigma/2$.
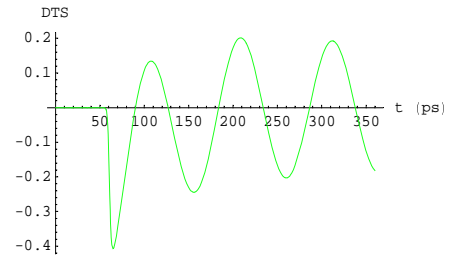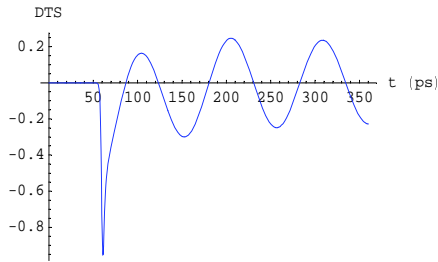
VII.11   Initialization with a pulse with $\sigma = 0.4$meV and $\Omega = 1.5\ \sigma/2$.

VII.12   Initialization with a pulse with $\sigma = 0.4$meV and $\Omega = 0.5\ \sigma/2$.

The feedback loop we propose consists of the laser, which is connected to the computer, which also records the measurements from each run, and a pulse-shaper. The pulse bandwidth is fixed but not precisely known. The initial value of the Rabi frequency (laser power) is also unknown, call it Ω_1. After the trion decays, the signal is proportional to the spin polarization. The maximum of the beats then is given by

$$P_1 = \frac{A}{2}\sin^2(\frac{\Omega_1}{\sigma}\pi), \tag{VII.25}$$

where A is some unknown constant related to the measurement process. The value P_1 is recorded and in the next run the Rabi frequency is doubled, $\Omega_2 = 2\Omega_1$. The next run will thus yield

$$P_2 = \frac{A}{2} \sin^2(\frac{2\Omega_1}{\sigma}\pi).$$
(VII.26)

The ratio is

$$P_1/P_2 = \frac{\sin^2(\frac{\Omega_1}{\sigma}\pi)}{\sin^2(\frac{2\Omega_1}{\sigma}\pi)} \Rightarrow \sqrt{\frac{P_2}{P_1}} = 2\cos\left(\frac{\Omega_2\pi}{2\sigma}\right) \Rightarrow \Omega_2 = \frac{\sigma}{2\pi}\arccos\left(\frac{1}{2}\sqrt{\frac{P_2}{P_1}}\right)$$
(VII.27)

Therefore, in the third run the Rabi frequency should be chosen to be

$$\Omega_3 = \frac{\pi\Omega_2}{\arccos\left(\frac{1}{2}\sqrt{\frac{P_2}{P_1}}\right)},$$
(VII.28)

which is the target value, $\sigma/2$, according to Eq. VII.27. An advantage of this scheme is that knowledge of neither the pulse duration nor the Rabi frequency are required. It is also an indirect way of determining the dipole matrix element between $|z\rangle$ and $|\mathcal{T}\rangle$.

2. Finite valence band mixing

In the presence of valence band mixing, the Hilbert space is no longer 3×3. We account here for mixing between the $|\frac{3}{2}\rangle$ ($|\frac{\bar{3}}{2}\rangle$) and the $|\frac{\bar{1}}{2}\rangle$ ($|\frac{1}{2}\rangle$) trions. Since in all cases the electrons are in the same orbital and in a spin singlet state, we list only the hole states:

$$|HH+\rangle = -\frac{1}{\sqrt{2}} |(X+iY)\uparrow\rangle$$
(VII.29)

$$|LH-\rangle = \frac{1}{\sqrt{6}} |(X-iY)\uparrow\rangle + \sqrt{\frac{2}{3}} |Z\downarrow\rangle$$
(VII.30)

$$|LH+\rangle = -\frac{1}{\sqrt{6}} |(X+iY)\downarrow\rangle + \sqrt{\frac{2}{3}} |Z\uparrow\rangle$$
(VII.31)

$$|HH-\rangle = \frac{1}{\sqrt{2}} |(X-iY)\downarrow\rangle,$$
(VII.32)

where $|X \pm iY\rangle$ and $|Z\rangle$ are the $\ell = 1$ spherical harmonics with $m = \pm 1$ and $m = 0$ respectively. The corresponding trion states will be denoted by $|H\rangle$ ($= |\mathcal{T}\rangle$), $|\bar{L}\rangle, |L\rangle, |\bar{H}\rangle$.

When valence band mixing is included, the valence Hamiltonian in the $\{|H\rangle, |\bar{L}\rangle, |\bar{H}\rangle, |L\rangle\}$ basis is

$$H = \begin{bmatrix} \epsilon_H & v & 0 & 0 \\ v^* & \epsilon_L & 0 & 0 \\ 0 & 0 & \epsilon_H & v \\ 0 & 0 & v^* & \epsilon_L \end{bmatrix}, \tag{VII.33}$$

where v is the coupling between heavy and light hole. The dot potential has been assumed such that the mixing between $|H\rangle$ ($|\bar{H}\rangle$) and $|L\rangle$ ($|\bar{L}\rangle$) is zero. An expression for v is given in Appendix B for a simple harmonic oscillator dot potential. To solve the eigenvalue equation, it helps to redefine the zero of energy by subtracting $\bar{\epsilon}/2 \equiv \frac{\epsilon_L + \epsilon_H}{2}$; then we get

$$H = \begin{bmatrix} -a & v & 0 & 0 \\ v^* & a & 0 & 0 \\ 0 & 0 & -a & v \\ 0 & 0 & v^* & a \end{bmatrix}, \tag{VII.34}$$

where $a = \frac{\epsilon_L - \epsilon_H}{2}$.

By diagonalizing within the blocks, the solution (known from the two-level system) is given by the following eigenvalues and eigenstates:

$$\lambda_\pm = \pm\sqrt{a^2 + v^2} \tag{VII.35}$$

$$C_{1,-} = \begin{bmatrix} \cos\frac{\phi}{2} \\ -\sin\frac{\phi}{2} \\ 0 \\ 0 \end{bmatrix} \equiv |H\bar{l}\rangle \tag{VII.36}$$

$$C_{1,+} = \begin{bmatrix} \sin\frac{\phi}{2} \\ \cos\frac{\phi}{2} \\ 0 \\ 0 \end{bmatrix} \equiv |\bar{L}h\rangle \tag{VII.37}$$

$$C_{2,-} = \begin{bmatrix} 0 \\ 0 \\ \cos \frac{\phi}{2} \\ -\sin \frac{\phi}{2} \end{bmatrix} \equiv |H\bar{l}\rangle \qquad (\text{VII.38})$$

$$C_{2,+} = \begin{bmatrix} 0 \\ 0 \\ \sin \frac{\phi}{2} \\ \cos \frac{\phi}{2} \end{bmatrix} \equiv |\bar{L}h\rangle. \qquad (\text{VII.39})$$

The angle ϕ is defined through

$$\cos \phi = \frac{a}{\sqrt{a^2 + v^2}} \qquad (\text{VII.40})$$

Restoring the zero of energy, we can write the Hamiltonian in the new basis, $\{|H\bar{l}\rangle, |\bar{L}h\rangle, |\bar{H}l\rangle, |L\bar{h}\rangle\}$, as

$$H = \begin{bmatrix} \frac{\bar{\epsilon}}{2} - \lambda & 0 & 0 & 0 \\ 0 & \frac{\bar{\epsilon}}{2} + \lambda & 0 & 0 \\ 0 & 0 & \frac{\bar{\epsilon}}{2} - \lambda & 0 \\ 0 & 0 & 0 & \frac{\bar{\epsilon}}{2} + \lambda \end{bmatrix}. \qquad (\text{VII.41})$$

If $\sigma+$ light is used, propagating along z and centered at the HH trions (with energy $\frac{\bar{\epsilon}}{2} - \lambda$) the trion states of higher energy can be ignored by frequency selectivity. In the presence of the mixing we will have a 4×4 Hamiltonian instead of the 3×3 from the previous sections, where mixing was ignored. In the $\{|z\rangle, |\bar{z}\rangle, |H\bar{l}\rangle, |\bar{H}l\rangle\}$ basis, where state $|H\bar{l}\rangle$ ($|\bar{H}l\rangle$) represents a state with largest contribution from the $|H\rangle$ ($|\bar{H}\rangle$) the total Hamiltonian, including the dipole interaction, is

$$H_4 = \begin{bmatrix} 0 & \omega_B & \Omega \cos \frac{\phi}{2} & 0 \\ \omega_B & 0 & 0 & \frac{1}{\sqrt{3}} \Omega \sin \frac{\phi}{2} \\ \Omega^* \cos \frac{\phi}{2} & 0 & \frac{\bar{\epsilon}}{2} - \lambda & 0 \\ 0 & \frac{1}{\sqrt{3}} \Omega^* \sin \frac{\phi}{2} & 0 & \frac{\bar{\epsilon}}{2} - \lambda \end{bmatrix}. \qquad (\text{VII.42})$$

From Eq. (VII.42) it is clear that when a $\sigma+$ 2π sech pulse is used, there is actually some error in the rotation scheme of the previous sections, due to an incomplete Rabi cycle involving the new state $|H\bar{l}\rangle$, and also due to some population transfer to the $|\bar{H}l\rangle$ state. Although this is going to be a very small effect (compared, for example, to the decay of the trion state during the pulse action), we can compensate for it by changing the polarization of the applied field and recover a 3×3 Λ-system, which will allow us to use our rotation scheme, as proposed in Section D. To find the target polarization, we assume elliptical polarization

$$c_x \hat{x} + i c_y \hat{y} \tag{VII.43}$$

and require

$$\langle \bar{H}\ell| \left(c_x \hat{x} + i c_y \hat{y} \right) |\bar{z}\rangle = 0. \tag{VII.44}$$

Solving (VII.44) for the c's along with the normalization condition $c_x^2 + c_y^2 = 1$, we find

$$c_x^o = \frac{\frac{1}{\sqrt{2}} \cos \frac{\phi}{2} - \frac{1}{\sqrt{6}} \sin \frac{\phi}{2}}{\left(\cos^2 \frac{\phi}{2} + \frac{1}{3} \sin^2 \frac{\phi}{2} \right)^{1/2}} \tag{VII.45}$$

$$c_y^o = \frac{\frac{1}{\sqrt{2}} \cos \frac{\phi}{2} + \frac{1}{\sqrt{6}} \sin \frac{\phi}{2}}{\left(\cos^2 \frac{\phi}{2} + \frac{1}{3} \sin^2 \frac{\phi}{2} \right)^{1/2}}. \tag{VII.46}$$

Then a three-level system is recovered, consisting of the states $|z\rangle, |\bar{z}\rangle$ and $|H\bar{\ell}\rangle$, and our rotation scheme may be carried out.

To determine the desired polarization, knowledge of ϕ, and thus c_x^o, c_y^o, is not necessary. Instead, a feedback loop can be devised, in the spirit of the one described in Subsection 1.

The Hamiltonian for arbitrary elliptical laser polarization, $c_x \hat{x} + i c_y \hat{y}$ is

given by

$$H = \begin{bmatrix} 0 & \omega_B & \Omega_+ & 0 \\ \omega_B & 0 & 0 & \Omega_- \\ \Omega_+^* & 0 & \frac{\bar{\epsilon}}{2} - \lambda & 0 \\ 0 & \Omega_-^* & 0 & \frac{\bar{\epsilon}}{2} - \lambda \end{bmatrix}, \tag{VII.47}$$

where

$$\Omega_+ = -\Omega\frac{(c_x + c_y)}{\sqrt{2}} \cos\frac{\phi}{2} - \Omega\frac{(c_x - c_y)}{\sqrt{6}} \sin\frac{\phi}{2} \tag{VII.48}$$

$$\Omega_- = \Omega\frac{(c_x - c_y)}{\sqrt{2}} \cos\frac{\phi}{2} + \Omega\frac{(c_x + c_y)}{\sqrt{6}} \sin\frac{\phi}{2}. \tag{VII.49}$$

Initially the density matrix is taken to be in a spin ensemble $\rho = \text{diag}(1/2, 1/2, 0, 0)$. After the pulse we have $\rho = \text{diag}(\frac{1}{2}\cos^2\frac{\theta_+}{2}, \frac{1}{2}\cos^2\frac{\theta_-}{2}, \frac{1}{2}\sin^2\frac{\theta_+}{2}, \frac{1}{2}\sin^2\frac{\theta_-}{2})$, where $\theta_\pm = \frac{2\pi\Omega_\pm}{\sigma}$. The signal then, ignoring SGC, will be

$$\begin{aligned} P &= \frac{A}{2}\left(\cos^2\frac{\theta_+}{2} - \cos^2\frac{\theta_-}{2}\right) \\ &= \frac{A}{4}(\cos\theta_+ - \cos\theta_-) \\ &= -\frac{A}{2}\sin\frac{\theta_+ + \theta_-}{2}\sin\frac{\theta_+ - \theta_-}{2}. \end{aligned}$$

Inserting the expressions for the angles $\theta_\pm$, we get

$$\begin{aligned} P &= \frac{A}{2}\sin\left(\frac{2\pi\Omega}{\sigma}c_y\left[\frac{1}{\sqrt{6}}\sin\frac{\phi}{2} - \frac{1}{\sqrt{2}}\cos\frac{\phi}{2}\right]\right)\sin\left(\frac{2\pi\Omega}{\sigma}c_x\left[\frac{1}{\sqrt{6}}\sin\frac{\phi}{2} + \frac{1}{\sqrt{2}}\cos\frac{\phi}{2}\right]\right) \\ &\equiv \frac{A}{2}\sin\left(\alpha_1\pi c\right)\sin\left(\alpha_2\pi\sqrt{1 - c^2}\right). \end{aligned} \tag{VII.50}$$

The feedback loop is designed as follows: First, we pick $c = c_x = 1/\sqrt{5}$ and the signal is

$$P_1 = \frac{A}{2}\sin\left(\frac{\alpha_1\pi}{\sqrt{5}}\right)\sin\left(\frac{2\alpha_2\pi}{\sqrt{5}}\right). \tag{VII.51}$$

For the second run, we choose $c \to 2c$ we get

$$\frac{P_2}{P_1} = \frac{\cos\left(\alpha_1\pi/\sqrt{5}\right)}{\cos\left(\alpha_2\pi/\sqrt{5}\right)}, \tag{VII.52}$$

which after some algebra becomes

$$\frac{P_2}{P_1} = \frac{\cos\left(\alpha_1 \pi/\sqrt{5}\right)}{\cos\left(\frac{\alpha_1 \pi}{2\sqrt{5}} + \sqrt{\frac{2\pi^2 \Omega^2}{5\sigma^2} - \frac{3\alpha_1^2 \pi^2}{20}}\right)}, \qquad \text{(VII.53)}$$

where

$$\alpha_1 = \frac{2\Omega}{\sigma}\left(\frac{1}{\sqrt{6}}\sin\frac{\phi}{2} + \frac{1}{\sqrt{2}}\cos\frac{\phi}{2}\right). \qquad \text{(VII.54)}$$

Equations (VII.53) and (VII.54) can be solved numerically and thus determine ϕ, from which the target polarization will be found from Eqs. (VII.45) and (VII.46), so that in the third run the ideal polarization will have been reached.

For small angle ϕ, i.e., small mixing the small-angle approximation may be employed to obtain an analytical solution for the polarization of the third run in terms of the signals from the first two runs. In this limit, we have for α_1

$$\alpha_1 \approx \frac{2\Omega}{\sigma}\left(\frac{\phi}{2\sqrt{6}} + \frac{1}{\sqrt{2}}\right), \qquad \text{(VII.55)}$$

and ϕ is then

$$\phi = \frac{\sqrt{30}\sigma}{\pi\Omega}\cot\left(\frac{2\pi\Omega}{\sqrt{10}\sigma}\right)\frac{P_1 - P_2}{P_1 + P_2}. \qquad \text{(VII.56)}$$

H.   Errors due to Incomplete Rabi Flop of Excitons

A crucial feature in our scheme is the complete Rabi flop of the trion with a 2π pulse. Rabi oscillations for excitons in quantum dots have been demonstrated experimentally [129], but they do exhibit distinct features compared to atoms. In Ref. [129] exciton population was measured as a function of the pulse area. For areas larger than π, the Rabi oscillations were shown to degrade considerably and the exciton was not flopped all the way back to the vacuum by a 2π pulse. This effect was seen by several groups [139, 152], and it was attributed to itinerant excitons, phonons, and coupling to wetting layer states [138]. Rabi oscillations between spins and trion states were recently demonstrated [56], and exhibit the same damping behavior. Our scheme should still work as a design for a proof-

of-principle experiment, but for a practical rotation this mechanism should be incorporated in the design, e.g. with pulse shaping techniques.

I.   Rotations about other axes

A full set of rotations about one more axes would allow for an arbitrary rotation when combined with the rotations about z. Using the heavy-hole trion state, we can obtain rotations about x using again RZ pulses, albeit a lot slower ones, by frequency selectivity. If, e.g., a pulse is slow enough to excite only one of the two spin states along x, then a 2π RZ pulse, otherwise exactly the same as above, will cause a rotation about x. Clearly, we would have to pay the price of slow pulses, which is exactly what we set off to avoid. Possibly use of higher trion states (e.g., light hole trions) and/or tilting the optical axis away from z may allow for more efficient rotations about axes other than z.

VIII.

Conclusions

In this chapter we summarize the main results presented in this dissertation and we give an outlook of future work.

A. Summary

Chapters II-IV contain background material needed to understand the chapters that follow.

Chapter II contains elements of basic semiconductor theory, of approximate bandstructure calculations, effective mass approximation and envelope function approximation for QDs. It introduces also the concepts of exciton, biexciton, and trion and briefly reviews quantum computation schemes with excitons and electron spins in dots. In III we give an elementary introduction of semiclassical and quantum optics, as needed for the development of the remaining chapters. In chapter IV, the nonlinear pump-probe experiment that measures the spin is explained and put in mathematical terms. We introduce the differential transmission signal (DTS) and explain its relation to the spin.

In Chapter V we present one of the main results of this dissertation, the full study of optical decoherence in the optically manipulated spin qubit in the quantum dot. An intriguing effect that arises is Spontaneously Generated Coherence (SGC). Understanding the decoherence mechanisms including SGC is

important in quantum information, both in the optical manipulation and initialization of the qubits. We present the theory of SGC, its effects on a pump-probe experiment, and the results of this experiment (performed by Prof. Steel's group in collaboration with us), which are in good agreement with our theoretical predictions.

In the same Chapter we introduce first the concept of Spontaneously Generated Coherence for a generic Λ system. Starting from a master equation, the derivation of the decay and decoherence equations is given step-by-step, and the SGC term is found to occur when the two transitions have parallel or antiparallel dipole matrix elements. We examine SGC first in the context of atomic physics, where it was initially predicted, and explain why its detection is challenging in atoms. It is subsequently explained how the conditions for SGC are met in the quantum dot. An intuitive explanation is given for the role of SGC in a pump-probe experiment, and finally the experiment itself is discussed. The experiment showed, in excellent qualitative agreement with the theory, that the presence of SGC induces a magnetic field-dependence to the amplitude and phase of the spin beats. This experiment, carried out by Duncan Steel's group in the University of Michigan in collaboration with our theory, constituted the first detection of SGC.

In Chapter VI we develop a general theoretical approach which unifies SGC, polarization entanglement, and two-pathway decay.

More specifically, SGC is reexamined in connection to other possible consequences of spontaneous emission in a Λ system, namely polarization entanglement, and two-pathway decay. We focus on a single system instead of an ensemble. Taking the viewpoint that spontaneous decay is governed by unitary quantum evolution when all subparts of the system are considered, we derive an expression for the state of the total system, including the photon wavepacket and the electron state. Depending on the couplings, which are functions of the emission direction and polarization, we found constraints for the various phenomena to occur. SGC is shown to be an effect complimentary to polarization entanglement, and using

this connection we established a continuous measure of SGC, in analogy to entanglement measures in quantum information theory. We also discuss the use of a quantum eraser to recover SGC from a two-pathway decay process, which opens up the possibility of SGC detection in atoms. We also propose detection of probabilistic SGC in a trapped ion. Finally, we examine SGC from a symmetry point of view and we explain the role of the common z axis of the quantum dots that constituted the ensemble in the SGC experiment.

A third major part of this thesis is presented in Chapter VII. In this part, we develop and propose a method for optical spin rotations about the growth axis in quantum dots by use of ultrafast circularly polarized Rosen-Zener 'sech' pulses.

In particular, use of ultrafast pulses allows for decoupling of the three-level system to 2+1 levels during the fast action of the pulse. Then, by using analytically solvable pulses for a two-level system, like the 'sech' pulses, the angle of rotation is obtained analytically as a function of the pulse parameters. We studied the fidelity of the operation by simulations to include the trion decay and unintended dynamics (such as spin precession). Besides decay mechanisms, unintended dynamics originating from valence band mixing and uncertainty in laser parameters also cause the operations to deteriorate. We take into account these undesirable processes and we devise adaptive feedback loops (containing a measurement device, a computer and a pulse shaper) in order to correct for these. We only assume knowledge of the pulse shape, not the laser parameters, and taking into account the analyticity of the solution, we show that the ideal pulse can be found after three runs of the feedback loop.

B. Future Directions

Quantum dots are still to be explored, especially in the context of optical transitions, coherent control, and possible applications in quantum technologies.

As a qubit, the spin in the quantum dot is very promising, but most of

the key DiVincenzo requirements [37] are yet to be shown. Initialization based on hole spin flip has been demonstrated with high fidelity [4], but it was too slow for practical uses. An ultrafast initializing scheme of high fidelity for the spin has not yet been demonstrated. One possible direction is using fast phonon relaxations, in resonance with transitions in the dots. Another possibility for initialization is looking into using the so-called anti-Zeno effect [73], in which decay is sped up by measurement.

Single-qubit rotations comprise a primary element of quantum computation. For universal quantum computation the full set of single-qubit rotations is necessary.[1] Extension of the ultrafast rotations proposed in this thesis to other axes should be addressed, possibly by use of energetically higher trion states and/or different optical axis. The problem of incomplete exciton Rabi flops is also open. The mechanism causing the Rabi oscillations to degrade should be taken into account in the design of the rotations, and pulse shaping methods may be investigated for its restriction.

The two-qubit controlled operations are also of great importance. Theoretical work has been done [107, 114] to that end, but a design closely related to an experimental demonstration will be a key step towards the implementations of controlled operations. Different geometries for coupled quantum dots, such as stacked or coplanar dots may be examined. In this context, there is a lot of work to be done regarding decoherence of the two qubits interacting with a common bath. As a concrete direction, the SGC effect for coupled quantum dots is a question of practical interest and a natural continuation of the work in this thesis.

Another interesting direction is design of quantum network architectures, addressing issues of transfer of quantum information, which is intimately related with optically controlled quantum dots, where the photons would serve as the flying qubits. In a similar spirit, hybrid systems for quantum information processing are also promising. Coupling of different quantum systems opens up the possibility

---

[1]Assuming we want to avoid using two-qubit operations to implement single-qubit rotations.

of exploiting the desirable features of each of them from a practical point of view for quantum information processing, and it encompasses the study of intriguing physics.

Appendix A.

Derivation of Expression for Fidelity for two-Dimensional Hilbert Spaces

The fidelity of an operation $\widetilde{U}$ is defined as

$$f_\Psi = |\langle\Psi|\widetilde{U}^\dagger U_I|\Psi\rangle|^2 \tag{A.1}$$

for a given initial state $|\Psi\rangle$, where U_I is the ideal operation. To find the actual fidelity, which is state-independent, we need to take an average over the whole Hilbert space:

$$f = \overline{|\langle\Psi|\widetilde{U}^\dagger U_I|\Psi\rangle|^2}. \tag{A.2}$$

Let us first define

$$I \equiv \widetilde{U}^\dagger U_I. \tag{A.3}$$

Also, the arbitrary initial state can be written as a superposition of the basis states:

$$\Psi = \sum_j c_j |j\rangle, \tag{A.4}$$

so that

$$f_\Psi = \sum_{ijkl} I_{ij} I_{lk}^* c_i^* c_j c_k^* c_l. \tag{A.5}$$

In the case of a 2×2 Hilbert space each of the c's can assume one of two values, c_+ and c_-.

It is useful to group the terms in five categories:

1. $\sum_i |I_{ii}|^2 |c_i|^4$

2. $\sum_{i \neq j} I_{ii} I_{jj}^* |c_i|^2 |c_j|^2$

3. $\sum_{i \neq j} I_{ij} I_{ij}^* |c_i|^2 |c_j|^2$

4. $\sum_{i \neq j} c_i c_j |c_j|^2 \times \left(I_{ij} I_{jj}^* + I_{ij} I_{ii}^* + I_{ii} I_{ij}^* + I_{ii} I_{ji}^* \right)$

5. $\sum_{i \neq j} (c_i^*)^2 (c_j)^2 I_{ij} I_{ji}^*$

Now we want to average the above terms; we parameterize in the following way:

$$c_+ = \cos\theta/2 \tag{A.6}$$

$$c_- = \sin\theta/2 \ e^{i\phi}, \tag{A.7}$$

where θ and ϕ are the polar and azimuthal angles respectively. The surface element is $\sin\theta d\theta d\phi$, which integrated gives 4π. We also note that

$$|c_\pm|^2 = \frac{1 \pm \cos\theta}{2}$$

Then we have for category (1), using the relation above:

$$\begin{aligned}
\overline{|c_\pm|^4} &= \frac{1}{4\pi} \int_0^{2\pi} d\phi \int_0^\pi d\theta \sin\theta \frac{(1 \pm \cos\theta)^2}{4} \\
&= \frac{1}{8} \int_0^\pi d\theta \sin\theta \left(1 + \cos^2\theta \pm 2\cos\theta \right) \\
&= \frac{1}{8} \int_{-1}^1 dx \left(1 + x^2 \pm 2x \right) \\
&= \frac{1}{4} \left(1 + \frac{1}{3} \right) \\
&= \frac{1}{3}
\end{aligned}$$

For the terms in (2) and (3):

$$
\begin{aligned}
\overline{|c_+|^2|c_-|^2} &= \frac{1}{2}\int_0^\pi d\theta \sin\theta \frac{(1+\cos\theta)(1-\cos\theta)}{4} \\
&= \frac{1}{2}\int_0^\pi d\theta \sin\theta \frac{(1-\cos^2\theta)}{4} \\
&= \frac{1}{8}\int_{-1}^1 dx\left(1-x^2\right) \\
&= \frac{1}{4}\left(1-\frac{1}{3}\right) \\
&= \frac{1}{6}
\end{aligned}
$$

The terms in (4) and (5) will vanish when averaged, due to the factors $e^{i\phi}$, which average to zero.

We thus have for the average fidelity:

$$
f = \frac{1}{3}\sum_i |I_{ii}|^2 + \frac{1}{6}\sum_{i\neq j}(I_{ii}I_{jj}^* + I_{ij}I_{ij}^*). \tag{A.8}
$$

As a check, when the operation is perfect, I is the identity matrix in two dimensions. The diagonal elements should then be equal to 1, which gives a perfect fidelity.

Now, it is useful to map the matrix elements of I to quantities that we simulate.

$$
\begin{aligned}
|I_{ii}|^2 &= |\langle i|\widetilde{U}^\dagger U_I|i\rangle|^2 = \langle i|\widetilde{U}^\dagger U_I|i\rangle\langle i|U_I^\dagger \widetilde{U}|i\rangle \tag{A.9} \\
&= Tr\left(\langle i|\widetilde{U}^\dagger U_I|i\rangle\langle i|U_I^\dagger \widetilde{U}|i\rangle\right) \\
&= Tr\left(\widetilde{U}|i\rangle\langle i|\widetilde{U}^\dagger U_I|i\rangle\langle i|U_I^\dagger\right) \\
&= Tr\left(\widetilde{U}\rho_i\widetilde{U}^\dagger U_I\rho_i U_I^\dagger\right)
\end{aligned}
$$

$$
|I_{ij}|^2 = |\langle i|\widetilde{U}^\dagger U_I|j\rangle|^2 = \langle i|\widetilde{U}^\dagger U_I|j\rangle\langle j|U_I^\dagger \widetilde{U}|i\rangle \tag{A.10}
$$

$$= Tr\left(\tilde{U}|i\rangle\langle i|\tilde{U}^\dagger U_I|j\rangle\langle j|U_I^\dagger\right)$$

$$= Tr\left(\tilde{U}\rho_i\tilde{U}^\dagger U_I\rho_j U_I^\dagger\right),$$

with $i \neq j$.

$$I_{ii}I_{jj}^* = \langle i|\tilde{U}^\dagger U_I|i\rangle\langle j|U_I^\dagger\tilde{U}|j\rangle \tag{A.11}$$

$$= Tr\left(\langle i|\tilde{U}^\dagger U_I|i\rangle\langle j|U_I^\dagger\tilde{U}|j\rangle\right)$$

$$= Tr\left(\tilde{U}|j\rangle\langle i|\tilde{U}^\dagger U_I|i\rangle\langle j|U_I^\dagger\right)$$

For concreteness, let us look at $I_{--}I_{++}^*$. We rewrite the operators $|+\rangle\langle-|$ and $|-\rangle\langle+|$ as:

$$|\pm\rangle\langle\mp| = \rho_x \pm i\rho_y - \frac{1}{2}(1 \pm i)\rho_z - \frac{1}{2}(1 \pm i)\rho_{\bar{z}} \tag{A.12}$$

$$\sum_{i\neq j} I_{ii}I_{jj}^* = 2\Re\left(Tr\left(\tilde{U}|+\rangle\langle-|\tilde{U}^\dagger U_I|-\rangle\langle+|U_I^\dagger\right)\right)$$

It is useful to define

$$\tilde{R}_j = \tilde{U}\rho_j\tilde{U}^\dagger \tag{A.13}$$

$$R_j^I = U_I\rho_j U_I^\dagger$$

Then

$$\sum_{i\neq j} I_{ii}I_{jj}^* = 2Tr(\tilde{R}_x R_x^I + \tilde{R}_y R_y^I$$

$$+\frac{1}{2}\tilde{R}_z R_z^I + \frac{1}{2}\tilde{R}_{\bar{z}} R_{\bar{z}}^I + \frac{1}{2}\tilde{R}_z R_{\bar{z}}^I + \frac{1}{2}\tilde{R}_{\bar{z}} R_z^I +$$

$$-\frac{1}{2}\tilde{R}_x R_z^I - \frac{1}{2}\tilde{R}_x R_{\bar{z}}^I - \frac{1}{2}\tilde{R}_y R_z^I - \frac{1}{2}\tilde{R}_y R_{\bar{z}}^I$$
$$-\frac{1}{2}\tilde{R}_z R_x^I - \frac{1}{2}\tilde{R}_z R_y^I - \frac{1}{2}\tilde{R}_{\bar{z}} R_x^I - \frac{1}{2}\tilde{R}_{\bar{z}} R_y^I)$$

Putting together all the above, we have

$$
\begin{aligned}
f \quad = \quad & \frac{1}{2}\, Tr\left(\tilde{R}_z R_z^I + \tilde{R}_{\bar{z}} R_{\bar{z}}^I\right) && \text{(A.14)}\\
& +\frac{1}{3}\, Tr\left(\tilde{R}_x R_x^I + \tilde{R}_y R_y^I + \tilde{R}_z R_{\bar{z}}^I + \tilde{R}_{\bar{z}} R_z^I\right)\\
& -\frac{1}{6}\, Tr\left(\tilde{R}_x R_z^I + \tilde{R}_x R_{\bar{z}}^I + \tilde{R}_y R_z^I + \tilde{R}_y R_{\bar{z}}^I\right)\\
& -\frac{1}{6}\, Tr\left(\tilde{R}_z R_x^I + \tilde{R}_{\bar{z}} R_x^I + \tilde{R}_z R_y^I + \tilde{R}_{\bar{z}} R_y^I\right)
\end{aligned}
$$

Appendix B.

Derivation of Valence Band Mixing

The Luttinger Hamiltonian in the $\{|\frac{3}{2}\frac{3}{2}\rangle, |\frac{3}{2}\frac{\bar{1}}{2}\rangle, |\frac{3}{2}\frac{1}{2}\rangle, |\frac{3}{2}\frac{\bar{3}}{2}\rangle\}$ basis is

$$
H_L \begin{bmatrix} P+Q & R & -S & 0 \\ R^\dagger & P-Q & 0 & S \\ -S^\dagger & 0 & P-Q & R \\ 0 & S^\dagger & R^\dagger & P+Q \end{bmatrix}, \tag{B.1}
$$

where

$$
P = \frac{\gamma_1}{2}(k_z^2 + k_x^2 + k_y^2) \tag{B.2}
$$

$$
Q = \frac{\gamma_2}{2}(-2k_z^2 + k_x^2 + k_y^2) \tag{B.3}
$$

$$
R = -\frac{\sqrt{3}}{2}\bar{\gamma}k_-^2 + \frac{\sqrt{3}}{2}\mu k_+^2 \tag{B.4}
$$

$$
S = \sqrt{3}\gamma_3 k_z k_-, \tag{B.5}
$$

$$
\bar{\gamma} = \frac{1}{2}(\gamma_2 + \gamma_3) \tag{B.6}
$$

$$
\mu = \frac{1}{2}(\gamma_3 - \gamma_2) \tag{B.7}
$$

and

$$k_x = -i\frac{\partial}{\partial x} \tag{B.8}$$

$$k_y = -i\frac{\partial}{\partial y} \tag{B.9}$$

$$k_z = -i\frac{\partial}{\partial z} \tag{B.10}$$

$$k_\pm = k_x \pm ik_y. \tag{B.11}$$

Combining the above, we find for R:

$$R = -\frac{\sqrt{3}}{2}\gamma_2(k_x^2 - k_y^2) + i\sqrt{3}\gamma_3 k_x k_y \tag{B.12}$$

$$S = -\sqrt{3}\gamma_3 k_z(k_x - ik_y). \tag{B.13}$$

The Hamiltonian for the dot is given by

$$H = H_L + V(z) + V_1(x) + V_2(y), \tag{B.14}$$

where the sum of the V's comprises the confinement potential of the dot. First we will ignore the mixing, i.e., we'll take $R = S = 0$. Then we have for the heavy and the light hole respectively:

$$H^H = H_x^H + H_y^H + H_z^H \tag{B.15}$$

$$H^L = H_x^L + H_y^L + H_z^L, \tag{B.16}$$

the Hamiltonian being separable in the three coordinates. The total energy is the sum of the three energies and the wavefunction is a product of the three wavefunctions. The x,y, and z parts of the Hamiltonian for the heavy hole are

$$H_z^H = -\frac{1}{2}(\gamma_1 - 2\gamma_2)\frac{\partial^2}{\partial z^2} + V(z) \tag{B.17}$$

$$H_x^H = -\frac{1}{2}(\gamma_1 + \gamma_2)\frac{\partial^2}{\partial x^2} + V_1(x) \tag{B.18}$$

$$H_y^H = -\frac{1}{2}(\gamma_1 + \gamma_2)\frac{\partial^2}{\partial y^2} + V_2(y), \tag{B.19}$$

while for the light hole we have

$$H_z^L = -\frac{1}{2}(\gamma_1 + 2\gamma_2)\frac{\partial^2}{\partial z^2} + V(z) \tag{B.20}$$

$$H_x^L = -\frac{1}{2}(\gamma_1 - \gamma_2)\frac{\partial^2}{\partial x^2} + V_1(x) \tag{B.21}$$

$$H_y^L = -\frac{1}{2}(\gamma_1 - \gamma_2)\frac{\partial^2}{\partial y^2} + V_2(y). \tag{B.22}$$

We define the in-plane HH and LH masses and those along the z direction:

$$m_z^H = \frac{1}{(\gamma_1 - 2\gamma_2)} \tag{B.23}$$

$$m_p^H = \frac{1}{(\gamma_1 + \gamma_2)} \tag{B.24}$$

$$m_z^L = \frac{1}{(\gamma_1 + 2\gamma_2)} \tag{B.25}$$

$$m_p^L = \frac{1}{(\gamma_1 - \gamma_2)} \tag{B.26}$$

We will assume the dot potential to be a harmonic oscillator with a different strength along each direction; we can therefore write down the energies and wavefunctions for the HH and LH.

$$\Upsilon^H(x, y, z) = \Psi^H(x)\Psi^H(y)\Psi^H(z) \tag{B.27}$$

$$\Psi^H(x) = \left(\frac{m_p^H \omega_x}{\pi\hbar}\right)^{1/4} e^{-m_p^H \omega_x x^2/2\hbar} \equiv C_x^H e^{-A_x^H x^2} \tag{B.28}$$

$$\Psi^H(y) = \left(\frac{m_p^H \omega_y}{\pi\hbar}\right)^{1/4} e^{-m_p^H \omega_y y^2/2\hbar} \equiv C_y^H e^{-A_y^H y^2} \tag{B.29}$$

$$\Psi^H(z) = \left(\frac{m_z^H \omega_z}{\pi\hbar}\right)^{1/4} e^{-m_z^H \omega_z z^2/2\hbar} \equiv C_z^H e^{-A_z^H z^2} \tag{B.30}$$

$$\Upsilon^L(x, y, z) = \Psi^L(x)\Psi^L(y)\Psi^L(z) \tag{B.31}$$

$$\Psi^L(x) = \left(\frac{m_p^L \, \omega_x}{\pi\hbar}\right)^{1/4} e^{-m_p^L \omega_x x^2/2\hbar} \equiv C_x^L e^{-A_x^L x^2} \tag{B.32}$$

$$\Psi^L(y) = \left(\frac{m_p^L \, \omega_y}{\pi\hbar}\right)^{1/4} e^{-m_p^L \omega_y y^2/2\hbar} \equiv C_y^L e^{-A_y^L y^2} \tag{B.33}$$

$$\Psi^L(z) = \left(\frac{m_z^L \, \omega_z}{\pi\hbar}\right)^{1/4} e^{-m_z^L \omega_z z^2/2\hbar} \equiv C_z^L e^{-A_z^L z^2} \tag{B.34}$$

A. Heavy Hole-Light Hole Mixing

To find the mixing between the heavy and light hole bands we have to find the matrix elements of R between $\Upsilon^L(x, y, z)$ and $\Upsilon^H(x, y, z)$. Note that the matrix elements of S and the part of R linear in the k's will vanish because of the parity of the wavefunctions. Then, we only need to find the matrix elements of:

$$R = -\frac{\sqrt{3}}{2}\gamma_2(k_x^2 - k_y^2) \tag{B.35}$$

We define

$$I_i = \langle \Psi_i^L | \Psi_i^H \rangle \tag{B.36}$$

$$R_x = \langle \Psi_x^L | \frac{\partial^2}{\partial x^2} | \Psi_x^H \rangle \tag{B.37}$$

$$R_y = \langle \Psi_y^L | \frac{\partial^2}{\partial y^2} | \Psi_y^H \rangle \tag{B.38}$$

Then we have for $\langle LH|R|HH \rangle$:

$$\langle LH|R|HH \rangle = \frac{\sqrt{3}}{2}\gamma_2 I_z \left(I_y R_x - I_x R_y\right) \tag{B.39}$$

The integrals are really simple and we just quote the answer:

$$I_i \;=\; C_i^L C_i^H \sqrt{\frac{\pi}{A_i^H + A_i^L}} \tag{B.40}$$

$$R_i \;=\; -2\sqrt{\pi}\,\frac{A_i^H A_i^L}{(A_i^H + A_i^L)^{3/2}}\, C_i^H C_i^L \tag{B.41}$$

Substituting the expression for the A's and using the relation $m_i^H \omega_i^H = m_i^L \omega_i^L$ we find for I_i

$$I_i \;=\; \sqrt{2}\,\frac{(\sqrt{m_i^H m_i^L})^{1/4}}{\sqrt{\sqrt{m_i^H} + \sqrt{m_i^L}}}. \tag{B.42}$$

For R_i we have

$$R_i \;=\; -\sqrt{2}\,\frac{(m_i^H \omega_i^H m_i^L \omega_i^L)^{5/4}}{(m_i^H \omega_i^H + m_i^L \omega_i^L)^{3/2}}. \tag{B.43}$$

$$R \;=\; -\sqrt{6}\gamma_2 \hbar \frac{\left(\sqrt{m_z^H m_z^L}\right)^{1/4}\left(\sqrt{m_p^H m_p^L}\right)^{1/4}}{\sqrt{\sqrt{m_z^H} + \sqrt{m_z^L}}\sqrt{\sqrt{m_p^H} + \sqrt{m_p^L}}}(m_p^H m_p^L)^{5/4} \times \tag{B.44}$$

$$\left(\frac{\left(\omega_x^H \omega_x^L\right)^{5/4}}{\left(m_p^H \omega_x^H + m_p^L \omega_x^L\right)^{3/2}} - \frac{\left(\omega_y^H \omega_y^L\right)^{5/4}}{\left(m_p^H \omega_y^H + m_p^L \omega_y^L\right)^{3/2}}\right).$$

We now use that $\omega_i^L = \sqrt{\frac{m_i^H}{m_i^L}}\,\omega_i^H$, which follows from the fact that heavy and light hole are subject to the same confining potential, and we also define a through $\omega_y^H = a\omega_x^H$ and R becomes

$$R \;=\; -\sqrt{6}\gamma_2 \frac{\left(\sqrt{m_z^H m_z^L m_p^H m_p^L}\right)^{1/4}}{\sqrt{\sqrt{m_z^H} + \sqrt{m_z^L}}\sqrt{\sqrt{m_p^H} + \sqrt{m_p^L}}}(m_p^H m_p^L)^{5/4} \times \tag{B.45}$$

$$\frac{\left(\sqrt{\frac{m_p^H}{m_p^L}}\right)^{5/4}}{\left(m_p^H + m_p^L \sqrt{\frac{m_p^H}{m_p^L}}\right)^{3/2}}(1-a)\hbar\omega_x^H$$

$$R = -\sqrt{6}\gamma_2 \frac{\left(\sqrt{m_z^H m_z^L m_p^H m_p^L}\right)^{1/4}}{\sqrt{\sqrt{m_z^H} + \sqrt{m_z^L}}\sqrt{\sqrt{m_p^H} + \sqrt{m_p^L}}} \frac{\left(m_p^H m_p^L \sqrt{\frac{m_p^H}{m_p^L}}\right)^{5/4}}{\left(m_p^H + m_p^L \sqrt{\frac{m_p^H}{m_p^L}}\right)^{3/2}}(1-a)\hbar\omega_x^H \quad \text{(B.46)}$$

$$R = -\sqrt{6}\gamma_2 \frac{\left(m_z^H m_z^L m_p^H m_p^L\right)^{1/8}}{\sqrt{\sqrt{m_z^H} + \sqrt{m_z^L}}\sqrt{\sqrt{m_p^H} + \sqrt{m_p^L}}} \frac{\left(m_p^H \sqrt{m_p^H m_p^L}\right)^{5/4}}{\left(m_p^H + \sqrt{m_p^H m_p^L}\right)^{3/2}}(1-a)\hbar\omega_x^H \quad \text{(B.47)}$$

We use the following values for the Luttinger parameters for GaAs:

- $\gamma_1 = 6.85$

- $\gamma_2 = 2.1$

- $\gamma_1 = 2.9$

and we get

$$R_{GaAs} = -0.1125(1-a)\hbar\omega_x^H \quad \text{(B.48)}$$

Bibliography

[1] Y. Akahane, T. Asano, B.-S. Song, and S. Noda, Nature (London) 425, 944 (2003).

[2] N. Akopian, N. H. Lindner, E. Poem, Y. Berlatzky, J. Avron, and D. Gershoni, B. D. Gerardot, and P. M. Petroff, Phys. Rev. Lett. 96, 130501 (2006).

[3] D. K. Armani, T. J. Kippenberg, S. M. Spillane, and K. J. Vahala, Nature (London) 421, 925 (2003).

[4] M. Atatüre, J. Dreiser, A. Badolato, A Högele, K. Karrai, A. Imamoglu, Science 312, 551 (2006).

[5] A. Bambini and P. R. Berman, Phys. Rev. A 23, 2496 (1981).

[6] M. Bayer, A. Kuther, A. Forchel, A. A. Gorbunov, V. B. Timofeev, F. Schäfer, J. P. Reithmaier, T. L. Reinecke, and S. N. Walck, Phys. Rev. Lett 82, 1749 (1999).

[7] M. Bayer, G. Ortner, O. Stern, A. Kuther, A. A. Gorbunov, A. Forchel, P. Hawrylak, S. Fafard, K. Hinzer, T. L. Reinecke, et al., Phys. Rev. B 65, 195315 (2002).

[8] C. H. Bennett, D. P. DiVincenzo, J. A. Smolin, and W. K. Wootters, Phys. Rev. A 54, 3824 (1996).

[9] R. E. Benner, P. W. Barber, J. F. Owen, and R. K. Chang, Phys. Rev. Lett. 44, 475 (1980).

[10] P. R. Berman, ed., Cavity Quantum Electrodynamics (Academic, San Diego, 1994).

[11] P. R. Berman, Lixin Yan, Keng-Hwee Chiam, and Ruwang Sung, Phys. Rev. A 57, 79 (1998).

[12] E. Biolatti, R. C. Iotti, P. Zanardi, and F. Rossi, Phys. Rev. Lett. 85, 5647 (2000).

[13] B. B. Blinov, D. L. Moehring, L.-M. Duan, and C. Monroe, Nature (London) 428, 153 (2004).

[14] F. Bloch, Phys. Rev. 70, 460 (1946).

[15] N. Bloembergen, Nonlinear Optics (World Scientific, Singapore, 1996).

[16] N. H. Bonadeo, G. Chen, D. Gammon, D. S. Katzer, D. Park, and D. G. Steel, Phys. Rev. Lett. 81, 2759 (1998).

[17] N. H. Bonadeo, J. Erland, D. Gammon, D. Park, D. S. Katzer, and D. G. Steel, Science 282, 1473 (1998).

[18] D. Bouwmeester, J.-W. Pan, K. Mattle, M. Eibl, H. Weinfurter, and A. Zeilinger, Nature (London) 390, 575 (1997).

[19] G. K. Brennen, C. M. Caves, P. S. Jessen, and I. H. Deutsch, Phys. Rev. Lett. 82, 1060 (1999).

[20] D. A. Broido and L. J. Sham, Phys. Rev. B 31, 888 (1985).

[21] T. A. Brun and H. Wang, Phys. Rev. A 61, 032307 (2000).

[22] D. A. Cardimona and C. R. Stroud, Jr., Phys. Rev. A 27, 2456 (1983).

[23] P. Chen, C. Piermarocchi, L. J. Sham, D. Gammon, and D. G. Steel, Phys. Rev. B 69, 075320 (2004).

[24] P. Chen, C. Piermarocchi, and L. J. Sham, Phys. Rev. Lett. 87, 067401 (2001).

[25] K. W. Chan, C. K. Law, and J. H. Eberly, Phys. Rev. Lett. 88, 100402 (2002).

[26] H. B. Chan, V. A. Aksyuk, R. N. Kleiman, D. J. Bishop, and F. Capasso, Science 291, 1941 (2001).

[27] G. Chen, T. H. Stievater, E. T. Batteh, X. Q. Li, D. G. Steel, D. Gammon, D. S. Katzer, D. Park, and L. J. Sham, Phys. Rev. Lett. 88, 117901 (2002).

[28] G. Chen, Ph.D. Thesis, University of Michigan (2002).

[29] J. Cheng, M. V. Gurudev Dutt, D. G. Steel, A. S. Bracker, D. Gammon, and L. J. Sham, Quantum Electronics and Laser Science 2003. QELS. Postconference Digest p. 2 (2003).

[30] J. I. Cirac, A. K. Ekert, S. F. Huelga, and C. Macchiavello, Phys. Rev. A 59, 4249 (1999).

[31] J. I. Cirac, P. Zoller, H. J. Kimble, and H. Mabuchi, Phys. Rev. Lett. 78, 3221 (1997).

[32] J. I. Cirac and P. Zoller, Phys. Rev. Lett. 74, 4091 (1995).

[33] C. Cohen-Tannoudji, J. Dupont-Roc, and G. Grynberg, Atom-Photon Interactions (Wiley Interscience, New York, 1992).

[34] E. U. Condon and G. H. Shortley, The Theory of Atomic Spectra, Cambridge University Press, Cambridge (1935).

[35] C. G. Darwin, Proc. Cambridge Philos. Soc. 27, 86 (1930).

[36] D. Deutsch and R. Jozsa, Proc. R. Soc. London A 439, 553 (1992).

[37] D. DiVincenzo, Fortschr. Der Physik 48, 771 (2000).

[38] G. Dresselhaus, Phys. Rev. 100, 580 (1955).

[39] L. M. Duan, M. D. Lukin, J. I. Cirac, and P. Zoller, Nature 414, 413 (2001).

[40] R. I. Dzhioev, V. L. Korenev, B. P. Zakharchenya, D. Gammon, A. S. Bracker, J. G. Tischler, and D. S. Katzer, Phys. Rev. B 66, 153409 (2002).

[41] M. V. Gurudev Dutt, Jun Cheng, Bo Li, Xiaodong Xu, Xiaoqin Li, P. R. Berman, D. G. Steel, A. S. Bracker, D. Gammon, Sophia E. Economou, Ren-Bao Liu, and L. J. Sham, Phys. Rev. Lett. 94, 227403 (2005).

[42] S. E. Economou, R. Liu, L. J. Sham, and D. G. Steel, Phys. Rev. B 71, 195327 (2005).

[43] J. M. Elzerman, R. Hanson, L. H. Willems van Beveren, B. Witkamp, L. M. K. Vandersypen, and L. P. Kouwenhoven, Nature 430, 431 (2004).

[44] A. K. Ekert, J. G. Rarity, P. R. Tapster, and G. M. Palma, Phys. Rev. Lett. 69, 1293 (1992).

[45] A. Ekert and P. Knight, Am. J. Phys. 63, 415 (1995).

[46] H.-A. Engel, V. Golovach, D. Loss, L. M. K. Vandersypen, J. M. Elzerman, R. Hanson, and L. P. Kouwenhoven, cond-mat/0309023 (2003).

[47] David Fattal, Kyo Inoue, Jelena Vučković, Charles Santori, Glenn S. Solomon, and Yoshihisa Yamamoto, Phys. Rev. Lett. 92, 037903 (2004).

[48] V. Fock, Z. Phys. 47, 446 (1928).

[49] R. P. Feynman, F. L. Vernon, Jr., and R. W. Hellwarth, J. Appl. Phys. 28, 49 (1957).

[50] K.-M. C. Fu, C. Santori, C. Stanley, M. C. Holland, and Y. Yamamoto, Phys. Rev. Lett. 95, 187405 (2005).

[51] D. Gammon, N. H. Bonadeo, G. Chen, J. Erland, and D. G. Steel, Physica E Low Dimensional Systems and Nanostructures 9, 99 (2001).

[52] C. W. Gardiner, Phys. Rev. Lett. 70, 2269 (1993).

[53] J. Gea-Banacloche, N. Lu, L. M. Pedrotti, S. Prasad, M. O. Scully, and K. Wodkiewicz, Phys. Rev. A 41, 369 (1990).

[54] N. Gisin, G. Ribordy, W. Tittel, and H. Zbinden, Rev. Mod. Phys. 74, 145-195 (2002).

[55] D. Goswami, Phys. Report 374, 385 (2003).

[56] A. Greilich, R. Oulton, E. A. Zhukov, I. A. Yugova, D. R. Yakovlev, M. Bayer, A. Shabaev, Al. Efros, I. A. Merkulov, V. Stavarache, D. Reuter, and A. Wieck, physics/0603020 (2006).

[57] J. A. Gupta, R. Knobel, N. Samarth, and D. D. Awschalom, Science 292, 2458 (2001).

[58] S. E. Harris, Phys. Rev. Lett. 62, 1033 (1989).

[59] S. E. Harris, J. E. Field, and A. Imamoğlu, Phys. Rev. Lett. 64, 1107 (1990).

[60] S. Hughes, Phys. Rev. Lett. 81, 33633366 (1998).

[61] A. Imamoğlu, D. D. Awschalom, G. Burkard, D. P. DiVincenzo, D. Loss, M. Sherwin, and A. Small, Phys. Rev. Lett. 83, 4204 (1999).

[62] A. Imamoğlu, H. Schmidt, G. Woods, and M. Deutsch, Phys. Rev. Lett. 79, 1467 (1997).

[63] D. F. V. James, P. G. Kwiat, W. J. Munro, and A. G. White, Phys. Rev. A 64, 052312 (2001).

[64] J. Javanainen, Europhys. Lett. 17, 407 (1992).

[65] B. E. Kane, Nature (London) 393, 133 (1998).

[66] K. Kheng, R. T. Cox, M. Y. d'Aubigné, F. Bassani, K. Saminadayar, and S. Tatarenko, Phys. Rev. Lett. 71, 1752 (1993).

[67] Z. Kis and F. Renzoni, Phys. Rev. A 65, 032318 (2002).

[68] A. A. Kiselev, K. W. Kim, and E. Yablonovitch, Phys. Rev. B 64, 125303 (2001).

[69] Y.-H. Kim, R. Yu, S. P. Kulik, Y. Shih, and M. O. Scully, Phys. Rev. Lett. 84, 1 (1999).

[70] P. L. Knight and L. Allen, Phys. Rev. A 7, 368 (1973).

[71] W. Kohn, Phys. Rev. 105, 509 (1957).

[72] M. Kroutvar, Y. Ducommun, D. Heiss, M. Bichler, D. Schuh, G. Abstreiter, and J. J. Finley, Nature (London) 432, 81 (2004).

[73] A. G. Kofman and G. Kurizki, Nature 405, 546 (2000).

[74] S. Lacey and H. L. Wang, Opt. Lett. 26, 1943 (2001).

[75] W. E. Lamb, Jr. and R. C. Retherford, Phys. Rev. 72, 241 (1947).

[76] M. A. Lampert, Phys. Rev. Lett. 1, 450 (1958).

[77] R. Leonhardt, W. Holzapfel, W. Zinth, and W. Kaiser, Chem. Phys. Letters 133, 373 (1987).

[78] R. B. Liu, W. Yao, and L. J. Sham, Phys. Rev. B 72, 081306 (2005).

[79] D. Loss and D. DiVincenzo, Phys. Rev. A 57, 120 (1998).

[80] E. Knill, R. Laflamme, and G. J. Milburn, Nature (London) 409, 46 (2001).

[81] A. Kiraz, M. Atatüre, and A. Imamoğlu, Phys. Rev A 69, 032305 (2004).

[82] R. Leonhardt, W. Holzapfel, W. Zinth, and W. Kaiser, Chem. Phys. Lett. 133, 373 (1987).

[83] X. Li, Y. Wu, D. Steel, D. Gammon, T. H. Stievater, D. Katzer, D. S. Park, C. Piermarocchi, and L. J. Sham, Science 301, 809 (2003).

[84] S. Lloyd, Phys. Rev. Lett. 75, 346 (1995).

[85] D. Loss and D. P. DiVincenzo, Phys. Rev. A 57, 120 (1998).

[86] B. Lounis, H. A. Bechtel, D. Gerion, P. Alivisatos, and W. E. Moerner, Chem. Phys. Lett. 329, 399 (2000).

[87] M. D. Lukin and A. Imamoğlu, Phys. Rev. Lett. 84, 1419 (2000).

[88] J. M. Luttinger, Phys. Rev. 102, 1030 (1956).

[89] X. Maître, E. Hagley, G. Nogues, C. Wunderlich, P. Goy, M. Brune, J. M. Raimond, and S. Haroche, Phys. Rev. Lett. 79, 769 (1997).

[90] L. Mandel and E. Wolf, Optical Coherence and Quantum Optics, Cambridge University Press (1995).

[91] S. L. McCall and E. L. Hahn, Phys. Rev. Lett. 18, 908 (1967).

[92] S. Menon and G. S. Agarwal, Phys. Rev. A 57, 4014 (1998).

[93] G. Messin, J. P. Hermier, E. Giacobino, P. Desbiolles, and M. Dahan, Opt. Lett. 26, 1891 (2001).

[94] P. Michler, A. Imamoğlu, M. D. Mason, P. J. Carson, G. F. Strouse, and S. K. Buratto, Nature (London) 406, 968 (2000).

[95] P. Michler, A. Kiraz, C. Becher, W. V. Schoenfeld, P. M. Petroff, L. Zhang, E. Hu, and A. Imamoğlu, Science 290, 2282 (2000).

[96] G. J. Milburn, Phys. Rev. Lett. 62, 2124 (1989).

[97] C. Monroe, D. M. Meekhof, B. E. King, W. M. Itano, and D. J. Wineland, Phys. Rev. Lett. 75, 4714 (1995).

[98] C. Monroe, Nature 416, 238 (2002).

[99] N. F. Mott and H. S. Massey, The Theory of Atomic Collisions (Oxford University Press, London, 1965).

[100] A. Nazir, B. W. Lovett, S. D. Barett, T. P. Spiller, and G. A. D. Briggs, Phys. Rev. Lett. 93, 150502 (2004).

[101] M. A. Nielsen and I. L. Chuang, Quantum computation and quantum information (Cambridge University Press, Cambridge, 2000).

[102] K. Nishibayashi, T. Okuno, Y. Masumoto, and H.-W. Ren, Phys. Rev. B 68, 035333 (2003).

[103] L. Pang, W. Nakagawa, and Y. Fainman, Applied Optics 42, 5450 (2003).

[104] Giovanna Panzarini, Ulrich Hohenester, and Elisa Molinari, Phys. Rev. B 65, 165322 (2002).

[105] M. Pelton, C. Santori, J. Vučković, B. Zhang, G. S. Solomon, J. Plant, and Y. Yamamoto, Phys. Rev. Lett. 89, 233602 (2002).

[106] M. Phillips and H. Wang, Phys. Rev. Lett. 89, 186401 (2002).

[107] C. Piermarocchi, P. Chen, L. J. Sham, and D. G. Steel, Phys. Rev. Lett. 89, 167402 (2002).

[108] C. Piermarocchi, P. Chen, Y. S. Dale, and L. J. Sham, Phys. Rev. B 65, 075307 (2002).

[109] M. B. Plenio, S. F. Huelga, A. Beige, and P. L. Knight, Phys. Rev. A 59, 2468 (1999).

[110] J. F. Poyatos, J. I. Cirac, and P. Zoller, Phys. Rev. Lett. 78, 390 (1997).

[111] J. Preskill, ph229 lecture notes, URL http://www.theory.caltech.edu/people/preskill/ ph229/#lecture.

[112] E. M. Purcell, Phys. Rev. 69, 681 (1946).

[113] H. Rabitz, R. de Vivie-Riedle, M. Motzkus, and K. Kompa, Science 288, 824 (2000).

[114] G. Ramon, Y. Lyanda-Geller, T. L. Reinecke, and L. J. Sham, Phys. Rev. B 71, 121305(R) (2005).

[115] E. I. Rashba, Sov. Phys. Semicond. 2, 1109-1122 (1960).

[116] M. Rontani, Ph.D. thesis, Modena, Italy (2000).

[117] N. Rosen and C. Zener, Phys. Rev. 40, 502 (1932).

[118] B. C. Sanders and G. J. Milburn, Phys. Rev. A 39, 694 (1989).

[119] C. Santori, D. Fattal, J. Vučković, G. Solomon, and Y. Yamamoto, Nature (London) 419, 594 (2002).

[120] H. Schmidt and A. Imamoğlu, Opt. Lett. 21, 1936 (1996).

[121] M. O. Scully and M. S. Zubairy, Quantum optics (Cambridge, 1997).

[122] A. Shabaev, A. L. Efros, D. Gammon, and I. A. Merkulov, Phys. Rev. B 68, 201305(R) (2003).

[123] J. Shah, Ultrafast Spectroscopy of Semiconductors and Semiconductor Nanostructures (Springer, Berlin, 1999).

[124] L. J. Sham, Phys. Rev. 150, 720 (1966).

[125] L. J. Sham and T. M. Rice, Phys. Rev. 144, 708 (1966).

[126] L. J. Sham, Quantum Mechanics 212A-C lecture notes (2002).

[127] P. W. Shor, SIAM J. Comput. 26, 1484 (1997).

[128] P. W. Shor, Phys. Rev. A 52, 2493 (1995).

[129] T. H. Stievater, X. Q. Li, D. G. Steel, D. Gammon, D. S. Katzer, D. Park, C. Piermarocchi, and L. J. Sham, Phys. Rev. Lett. 87, 133603 (2001).

[130] J. G. Tischler, A. S. Bracker, D. Gammon, and D. Park, Phys. Rev. B 66, 081310(R) (2002).

[131] F. Troiani, U. Hohenester, and E. Molinari, Phys. Rev. B 62, R2263 (2000).

[132] Q. A. Turchette, R. J. Thompson, and H. J. Kimble, Appl. Phys. B 60, S1 (1995).

[133] Thomas Unold, Kerstin Mueller, Christoph Lienau, Thomas Elsaesser, and Andreas D.Wieck, Phys. Rev. Lett. 92, 157401 (2004).

[134] K. J. Vahala, Nature (London) 424, 839 (2003).

[135] W. G. van der Wiel, S. De Franceschi, J. M. Elzerman, T. Fujisawa, S. Tarucha, and K. L. P., Rev. Mod. Phys. 75, 1 (2003).

[136] L. M. K. Vandersypen, M. Steffen, G. Breyta, C. S. Yannoni, M. H. Sherwood, and I. L. Chuang, Nature (London) 414, 883 (2001).

[137] F. Verluise, V. Laude, Z. Cheng, C. Spielmann, and P. Tournois, Optics Lett. 25, 575 (2000).

[138] J. M. Villas-Boâs, Sergio E. Ulloa, and A. O. Govorov, Phys. Rev. Lett. 94, 057404 (2005).

[139] Q. Q. Wang, A. Muller, P. Bianucci, E. Rossi, Q. K. Kue, T. Takagahara, C. Piermarocchi, A. H. MacDonald, and C. K. Shih, Phys. Rev. B, 72 035306 (2005).

[140] M. E. Ware, E. A. Stinaff, D. Gammon, M. F. Doty, A. S. Bracker, D. Gershoni, V. L. Korenev, S. C. Badescu, Y. Lyanda-Geller, and T. L. Reinecke, Phys. Rev. Lett. 95, 177403 (2005).

[141] V. Weisskopf and E. Wigner, Zeits. fur Phys. 63 (1930).

[142] H. M. Wiseman and G. J. Milburn, Phys. Rev. Lett. 70, 548 (1993).

[143] W. K. Wootters, Phys. Rev. Lett. 80, 2245 (1998).

[144] J.-H. Wu and J.-Y. Gao, Phys. Rev. A 65, 063807 (2002).

[145] W. H. Xu, J. H. Wu, J. Y. Gao, Phys. Rev. A 66, 063812 (2002).

[146] E. Yablonovitch, Phys. Rev. Lett. 58, 2059 (1987).

[147] Wang Yao, Ren-Bao Liu, and L. J. Sham, Phys. Rev. Lett. 95, 030504 (2005).

[148] T. K. Yee and T. K. Gustafson, Phys. Rev. A 18, 1597 (1978).

[149] P. Yu and M. Cardona, 'Fundamentals of Semiconductors', Springer (1995).

[150] Yuan Z., Kardynal B. E., Stevenson R. M., Shields A. J., Lobo C. J., Cooper K., Beattie N. S., Ritchie D. A., and Pepper M., Science 295, 102 (2002).

[151] H. P. Yuen, Phys. Rev. Lett. 51, 719 (1983).

[152] A. Zrenner, E. Beham, S. Stufler, F. Findeis, M. Bichler, and G. Abstreiter, Nature 418, 612 (2002).

[153] Valery Zwiller, Hans Blom, Per Jonsson, Nikolay Panev, Soren Jeppesen, Tedros Tsegaye, Edgard Goobar, Mats-Erik Pistol, Lars Samuelson, and Gunnar Björk, Appl. Phys. Lett. 78, 17 (2001).